UNIVERSITÀ' DEGLI STUDI DI TRIESTE

XVII CICLO DEL DOTTORATO DI RICERCA IN INGEGNERIA MECCANICA, NAVALE, DELL'ENERGIA E DELLA PRODUZIONE

OPTIMISATION'S TECHNIQUES OF HULL SHAPES USING CFD RANSE SIMULATIONS WITH LOW NUMBER OF CELLS

Settore scientifico-disciplinare: ING/IND-01

DOTTORANDO

ANDREA ANTONIO AGRUSTA

COORDINATORE

PROF. DIEGO MICHELI

SUPERVISORE DI TESI

PROF. IGOR ZOTTI

ANNO ACCADEMICO 2013/2014

Pochi sono coloro che possono dare del tu al mare

e quei pochi non lo fanno.

CONTENTS

LIST OF FIGURES

LIST OF TABLES

LIST OF SYMBOLS

α_q	Generic point in the domain
B	Hull beam
B_{MAX}	Maximum beam
B_{WL}	Waterline beam
b_1	Generic design variable
b_2	Generic design variable
C_F	Friction resistance coefficient
C_{F0}	Skin friction resistance coefficient
C_{PV}	Viscous pressure resistance coefficient
C_P	Pressure resistance coefficient
C_T	Total resistance coefficient
C_V	Viscous resistance coefficient
C_W	Wave resistance coefficient
$\check{C}_V$	Apparent viscous resistance coefficient
$\check{C}_W$	Apparent wave resistance coefficient
C_μ	Dimensionless constant
δ_{ij}	Kroneker delta
Δ	displacement
e	Dissipated energy per unit volume
ε	the turbulent dissipation rate
ΔE_{max}	Energy variation
$\overline{F_i}$	Volume forces
Fr	Froude Number
Fr_∇	Volumetric Froude number
H	Generic design variable
h_1	Generic design variable
K	Kinetic energy
k	Turbulent kinetic energy per mass unit
L	Hull length
$L_{bulb\_overbow}$	Bulb length over the stem
L_{OS}	Length over submerged
L_{OA}	Length over all
L_{WL}	Length at waterline
LCB	Longitudinal position of centre of buoyancy
λ	Scale factor
Φ	Potential of velocity
(M)	Froude coefficient
μ	Fluid viscosity
μ'	Module of bulk
μ	Viscosity of fluid
μ'	Bulk module

μ_t	Turbulent viscosity
p	Static pressure
Q	Intensity of source
$\overline{Q}$	Generic quantity
Re	Reynolds number
R_F	Friction resistance
R_{F0}	Skin friction resistance
R_P	Pressure resistance
R_{PV}	Viscous pressure resistance
R_T	Total resistance
R_{TM}	Total resistance in model scale
R_{T_VMAX}	Total resistance at maximum speed
R_{T_VCR}	Total resistance at cruising speed
R_V	Viscous resistance
$\check{R}_V$	Apparent viscous resistance
R_W	Wave resistance
$\check{R}_W$	Apparent wave resistance
ρ	Fluid density
$\hat{S}$	Source of the mass
s	Average deformation flow tensor
$\overline{S}$	internal work done by Reynolds stresses
$\overline{S}'$	internal work done by viscous stresses
$\overline{s}$	Average relative kinetic energy
$S_{\alpha q}$	source term
S	Wetted surface area
σ_{max}	Maximum bending stress
t	time
τ_{ij}	Viscous stress tensor
τ	Reynolds stress tensor
τ_w	Stress tensor on wall
T	temperature
$\tilde{u}$	Apparent length on x axis
u_i	Components of the velocity u of the water-air mixture
u_{max}	Maximum deflection
u_{all}	Allowable deflection
U	Velocity average component
U'	Floating quantities in the fluid
$\tilde{v}$	Apparent length on y axis
v	Velocity
v_t	turbulent velocity
v_x^+	Dimensionless velocity
V	Hull Velocity
V_M	Model scale velocity
V_S	Ship scale velocity
V_{CR}	Cruising speed
V_{MAX}	Maximum speed

∇	Moulded hull volume
$\widetilde{\omega}$	Apparent length on z axis
ζ	Height along z axis
y^{+}	First Centroid distance
Y_i	Initial beam of a frame
Y_m	Generic beam of a frame
z	Objective function

INTRODUCTION

Designing means innovating. In order to achieve an optimal hull you need to be able to analyze all possible solutions. The traditional design process entails the setting of the hull main parameters based on both statistics and personal experience. The hull is then tested and optimized through numerical techniques and/ or tank testing. The most important problem of the traditional ship design is the subjectivity of the results' goodness.

An innovative design process, instead, involves the analysis of all feasible solutions, i.e. of more different hulls matching with all the requirements of the project (input). After having explored the performances (output) the designer can decide which are the best hulls: at first collecting the upsides and then optimizing the performance through the numerical simulation of the impact related to each kind of modification. This process provides the mathematical certainty to improve something that is already close to optimality.

Some years ago this approach was difficult to achieve because of the exponential increase in time and costs, having to perform hundreds of experimental tests to reach the optimal result. In recent years, the techniques of numerical hydrodynamic CFD, allowing the computer to simulate the interaction between solids and fluids, have greatly contributed to reduce costs. The use of CFD software enables an definitely realistic simulation of hydrodynamic phenomena. These software allow the designer/ programmer to analyze several solutions, to assess various macro or micro modifications on the chosen hull in order to investigate the impact in terms of motion resistance, trim, seakeeping, comfort, and then to choose the most performant hull in relatively short times.

Computational Fluid Dynamics (CFD) is referred to methods and techniques able to simulate the dynamic behavior of fluids in complex physical problems. The use of numerical simulation in the hull design phase is necessary when there is the need to perform predictions and analysis of a high number of cases; then CFD allows to eliminate or reduce the necessity of numerous physical models to be experimentally studied.

For this reason CFD is extremely advantageous in the analysis of a given design: it allows different initial configurations to be considered in a relatively simple way compared to the experimental investigation, both for geometries and for boundary conditions. So the responses to variations of the relevant parameters may be evaluated with a good degree of confidence compared to the physical reality.

The numerical analysis can be performed through panel methods called BEM (Boundary Elements Methods), which are based on the potential flow theory, or through the use of viscous methods called RANS (or RANSE), which solve the averaged Navier-Stokes equations.

BEM methods are efficient and rapid; they allow different design solutions to be evaluated in a short time with the aid of modest computing resources. However, the results are approximate and the absence of analysis of the viscous fluid prevents the possibility to assess the resistance in a complete way.

Instead RANS methods allow accurate results to be obtained even in absolute terms so delivering to a designer much more information on the analyzed physical phenomenon.

By contrast they normally require computational domains with a high number of cells and therefore enormous amounts of data to be processed, consequently involving higher computation time as well as considerable hardware resources.

Recent years have seen an increasing use of mathematical algorithms for multi-objective optimization associated with 3D parametric modelers and then at CFD BEM potential solvers [1],[2],[3]. These applications typically allow you to find the optimal hull forms which, according to constraints set, generate the minimum wave resistance to one or more certain speeds [4],[5],[6].

Associating an optimization process to a viscous RANS solver allows instead, knowing a multitude of physical parameters in addition, to optimize the result by following more objectives. Particularly the viscous RANS solver, having the ability to assess the effect of friction, allows to optimize the hull shapes in order to reduce the total resistance.

In literature, it's possible to see some examples of multi-objective optimizations performed with viscous codes [7], [8], [9], but often they involve very simple cases [10], or they concern several cases solved with many hours of calculation, thus making the optimization not economic.

In fact until yesterday, an optimization process associated with CFD RANS simulations, though theoretically possible, was actually inconvenient because of the enormous amount of calculations to be performed to evaluate the goodness of hundreds of different solutions, making process too long and expensive. Sometimes to contain computation time, some optimization techniques based on mixed BEM / RANS solvers [11], [12] have been used.

The aim of this work was to associate a process of hull optimization based on the reduction of total resistance to progress with CFD RANS simulations, performed with a computational domain with low number of cells. This calculation domain derives from the accurate development of a standardized procedure that enables to run RANS simulations with a standard grid which, even if "coarse", ensures the accuracy of the result.

In fact, the secondary objective of this work was to minimize the number of computational cells in order to reduce the time and cost of simulations, preserving in any case adequate results. In this way viscous RANS simulations will be very attractive with respect to BEM potential methods also from the point of view of computing time.

The initial assumption has been to create a certain number of standard meshing set-up for some groups of hulls, to be identified by common parameters.

In order to optimize and standardize the process of reduction of the cells, several models of boats with available experimental results have been tested.

At the end of the work three different families of hulls have been achieved (Round Bilge Displacement Hull, Round Bilge and Hard Chine Semiplaning Hull (Single and Multi-Hull), Hard Chine Planing Hull) grouped by similarity of geometries and operating speed and therefore having in common an similar wave formation.

The optimization process here shown has been applied to an innovative semi-planing hard-chine hull with bulbous bow: the starting point was a basic hull that matching all the requirements of the project and, according to constraints set, it has been found the optimum hull geometry in order to reduce the total resistance at two different speed (cruise and maximum). At the end of the activity, the execution of tank tests on scale model was carried out to validate the results numerically obtained.

RESISTANCE

1.1 RESISTANCE

It is well known [13] that the total resistance is divided into the two classic components:

Total resistance R_T = Pressure resistance R_P + Friction resistance R_F

The total resistance breakdown is well explained in the fig.1.1:

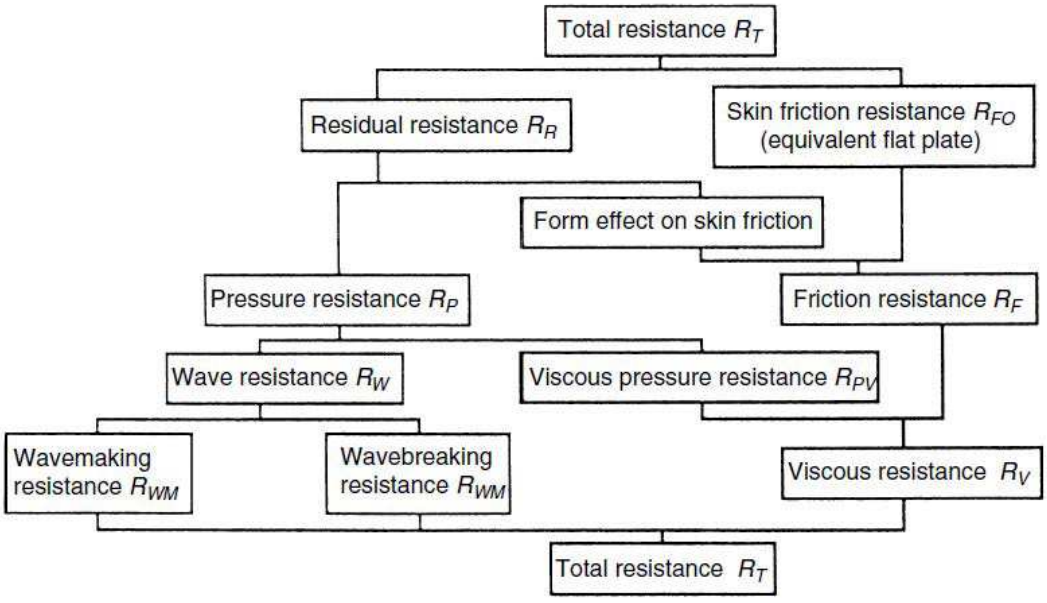

Fig. 1.1 - Breakdown of the total resistance *(Principles of Naval Architecture)*

In this components of resistance subdivision, it is assumed that there are no interactions between the components and that the energy required to the generation of waves is transformed in wave resistance component.

Actually the waves of a viscous system crash; when this happens, some of the energy moves from the wave system to the wake one. Wave breaking phenomena are observed also around the bows of large tankers.

The modification of these wavy flows on the surface also changes the intensity of the viscous component.

The wave system energy generated may be perceived even far away from the ship. Through the turbulent phenomena, the wake energy dissipates into thermal energy.

You can then write :

$$R_T = R_W + R_{PV} + R_F \qquad (1.1)$$

Where, considering that all the symbols used are in compliance with ITTC Symbols [14],:

• R_W: nominal wave resistance

• R_{PV} : viscous pressure resistance

This is the method which is nowadays used to split the components of the resistance.

By separating the effects of viscosity and wave formation, it can divide the total resistance also in another way:

$$R_T = R_V + R_W \qquad (1.2)$$

with:

• R_V: total viscous resistance: resistance met by a hull into a viscous fluid, whose free surface is assumed to be undeformed;

In dimensionless terms you can write:

$$C_T = C_V + C_W \qquad (1.3)$$

with:

$$C_V = C_V\,(Re) \quad \text{and} \quad C_W = C_W\,(Fr)$$

This defining method is however not satisfying for an experimental investigation; instead it seems more appropriate defining the "apparent" resistance $\check{R}_V$ and $\check{R}_W$, respectively linked with the mechanical energy dissipation measured in the wake and the energy flow related to the wave system.

In other words, instead of considering the physical causes generating resistance separately, we analyze separately the effects experimentally detectable. We can then write:

$$R_T = \check{R}_V + \check{R}_W \tag{1.4}$$

or in dimensionless terms:

$$C_T = \check{C}_V + \check{C}_W \tag{1.5}$$

with:

$$\check{C}_V = \check{C}_V\,(\mathrm{Re}, \mathrm{Fr})\ \check{C}_W = \check{C}_W\,(\mathrm{Re}, \mathrm{Fr}) \tag{1.6}$$

You can underline how the $\check{R}_V$ takes into account, in addition to the friction forces in the boundary layer and the formation of vortices, even local effects of wave formation - such as the breaking of the bow waves - while the $\check{R}_W$ takes into account the amount of energy carried by so-called "*free waves*", most evident at a certain distance from the hull. Such kind of waves are called "free" because, once generated, are not affected by the boundary conditions on the hull, and their propagation is governed only by Laplace equation and the boundary conditions at the free surface.

Starting from these assumptions, the apparent viscous resistance may be defined as the expression:

$$\tilde{R}_V = \rho g \int_{-b}^{b} \int_{\zeta}^{h} e\, dz\, dy \tag{1.7}$$

indicating with “e” the energy dissipated per unit volume, while the apparent wave resistance will assume the following expression:

$$\tilde{R}_W = \tfrac{1}{2}\rho g \int_{-b}^{b} \zeta^2 dy + \tfrac{1}{2}\rho \int_{-b}^{b} dy \int_{-h}^{0} (\tilde{v}^2 + \tilde{\omega}^2 + \tilde{u}^2) dz \tag{1.8}$$

Among the assumptions done, the following quantities can be defined:

$$u = \tilde{u} - V \qquad v = \tilde{v} \qquad \omega = \tilde{\omega} \tag{1.9}$$

1.2 WAVE RESISTANCE CREATION

At low speeds the wave resistance is modest and it increases as long as the speed; the C_W = f (Fr) coefficient also increases, together with crests and trough formation, reaching its maximum for Fr next to 0.45. For such value, the resistance may vary along with the speed through an exponent n = 4 or greater.

Increasing the speed the wave system changes, because the different wavy formations generated by the hull are made by varying the relative positions of the peaks and hollows. As speed changes, the resulting wave system strengthens or decays, generating C_W curve with humps and hallows. The designer will always try to choose the precise ship speed condition at which a minimum value of that rate will match.

Eggert (1939) [15] noted as the pressures produced on different parts of a hull reproduced the wavy profiles; computing the longitudinal components generated by the pressure forces on the vessel length, he showed that the resultant resistance value is very close to that total resistance one to which the component of friction has been removed.

1.3 WAVE SYSTEM EXPERIMENTAL ANALYSIS

The wave system analysis establishes a link between the deformation of the free surface and the flow, in order to determine the wave resistance by simple survey of such a surface. This model is justified from a potential flow motion on the entire control surface. It is completely consistent with the given definitions of the apparent wave resistance in real flow, with viscous wake limited to a region of space.

If you indicate with Φ the potential of a disturbance propagating in the x-direction with a constant speed V, in the mobile reference system already set, you can express the wave resistance using the integral extended to the surface $x = x_B$

$$\tilde{R}_W = \frac{1}{2}\rho g \int_{-b}^{b} \zeta^2 dy + \frac{1}{2}\rho \iint_B (\tilde{\Phi}_y^2 + \tilde{\Phi}_z^2 + \tilde{\Phi}_x^2) dy dz \qquad (1.10)$$

This relationship has been obtained, in linearized form, by Thomas Havelock (1934) [16] , but it results precise in the context of the potential motions theory. The challenge is to find the relationships between the potential functions and wave heights $\zeta(x, y)$. Then cinematic and dynamic boundary conditions should be imposed, valid on the free surface $z = \zeta(x, y)$.

It is assumed then that the waves are of small amplitude and an unlimited domain (free waves). The boundary conditions in a steady system become:

$$\begin{cases} g\zeta - V\tilde{\Phi}_x + \tilde{\Phi}_t = 0 \\ \zeta_t - V\zeta_x - \tilde{\Phi}_z = 0 \end{cases} \qquad for\ z = 0 \tag{1.11}$$

that, for *t=0,* in the body's coordinate system it can be also written:

$$\begin{cases} \tilde{\Phi}_x = \frac{y}{V}\zeta \\ \tilde{\Phi}_z = -V\zeta \end{cases} \tag{1.12}$$

Since the Laplace equation can be applied:

$$\nabla^2\tilde{\Phi} = 0 \tag{1.13}$$

searching for a general solution able to satisfy the boundary conditions and to provide the expression of the potential Φ for the solution of the problem.

Generally the function Φ is expressed by an integral of the type:

$$\tilde{\Phi}(x,y,z) = \int_{D_1} H_1(k,\theta,x,y,z)dk\ d\vartheta \tag{1.14}$$

from which, by replacing in the preceding equations, we get a relation like:

$$\zeta(x,y) = \int_{D_2} H_2(k,\theta,x,y,z)dk\ d\,\theta \tag{1.14}$$

and finally:

$$\tilde{R}_W = \int_{D_3} H_3(\theta)d\theta \tag{1.15}$$

It should be observed how in the final expression $\check{R}_W$ appears as a function of a single variable. This behavior is explained considering that, given the ship advance in calm water, only a single infinite number of waves - belonging to the double infinity of potential plane waves, the so called free waves, contributes to the resistance to motion.
For such waves there is a link between the wavelength and the propagation direction like:

$$F(k,\theta) = 0 \tag{1.16}$$

By replacing this relation in the expression of Φ and $\boldsymbol{\zeta}$, simplified expressions can be found:

$$\tilde{\Phi}(x,y,z) = \int_{D_1} J_1(\theta,x,y,z)d\theta \quad (1.17)$$

$$\zeta(x,y) = \int_{D_2} J_2(\theta,x,y)d\theta \quad (1.18)$$

moreover matching with the expressions derived from the previous more general ones, where it was decided $(x^2 + y^2) \rightarrow \infty$.

1.4 FLOW AROUND THE HULL

A complete description of the flow around the hull can be provided using the Navier-Stokes equations. Of course, the appropriate boundary conditions must be imposed, assuming that fluid is viscous and the presence of vortices and separation. This kind of problems, properly issued, can be solved through some techniques employing methods of discretization with finite volume.

Actually this hypothesis of solution is not realistic for ships. One of the reason why is that viscous phenomena study requires the formulation of very dense grids. The study of wave events, at a large-scale, (as the free surfaces, on which the waves develop, are very wide) requires instead the formation of less dense grids. The demand for very dense grids on the free surface would require a computing (and memory) capacity even beyond the current capabilities of actual calculus systems. It must also be remembered that the free surface is a part of the requested solution.

Simplifications are therefore required. The first one is to define regions with predominantly potential flow and regions with predominantly viscous flow. This hypothesis is comparable to the Froude's one which splits the total resistance in the friction component and in the residual component.

There are thus two different types of computations:

1. Computation of the flow in viscous system;
2. Computation of the flow in potential system.

It is necessary that the viscous flow is investigated both in the wake and in the boundary layer, while the potential one in the external surface areas where wave formation presence is prevalent.

The uniform flow involving the hull is considered as potential one, and then both viscosity and fluid particles rotation are neglected. In these areas Laplace equation can be applied.

The boundary conditions are those on the free surface, while near the boundary layer the actions taken into account are tangential ones.

Very often, assuming the boundary layer (i.e. layer's thickness) negligible, it is hypothesized the presence of tangential flow along the hull.
In viscous regions you can use boundary layer equations, because the boundary layer is considered to be thin.
Wake zones are studied through the Navier-Stokes equations.

1.4.1 Potential flow calculations

First of all it is appropriate to distinguish:

1. panels' methods without free surface;

2. panels' methods with free surface.

The easiest computing method is the one without free surface. It is assumed that the free surface does not change when the flow invests the hull. In practice this may be accomplished by the technique of double model, driven at great depths, where the floating waterline becomes a plane of symmetry and the speed orthogonal to that plane are zero.

If the flow that invests the object does not give rise to actions of lift, you can replace the object with a distribution of sources. These are distributed spread on the discretized hull surface. This surface's elements are called "panels". The boundary condition chosen is the condition of tangential flow to the ship's hull. This condition must be set at the center of the panel, at one specific point called "control point".
The simplest shape assumed for the panel is the quadrangular one, on which a uniform distribution of constant intensity strength is placed.
This implies that the distribution of sources is as stepped one (step function) more than a continuous kind of distribution.
This methodology, applied first by Hess & Smith [17], approximates the double hull shape (mirror hull) with a N high number of flat panels. On each panel you stand a uniform distribution of sources/sinks of unknown intensity Q.

It can be written2 the expression for the potential function $\Phi(x, y, z)$ as a sum due to each potential functions of the single elements. The speed induced on an arbitrary control point, outside of the object, can be expressed by the functions of influence of the individual panels.
The influence function of each single panel is unique, but the uniqueness can be integrated over the whole panel. Therefore, the speed induced in an arbitrary control point can be expressed as a linear function of the *N* intensities of Q_i source.
The boundary conditions are then applied, requiring that the flow is tangential to each control point. This involves *N* conditions for *N* panels.

The system solution allows to determine the intensity *Qi* of individual panels sources. Then you can determine the speed at each point of the vessel's hull and also outside of the hull itself, by deriving potential function $\Phi(x, y, z)$ along the chosen direction. It is noted that panels' size reduce the computational accuracy of the derivatives, since the derivatives should be calculated as the difference of values measured between two panels.

Once speeds are known, pressure values are derived using the Bernoulli theorem. Of course, it is important to point out the consequences of the simplifications made by these methods.
First of all the assumption of perfect fluid, without viscosity, requires that the object resistance is null (D'Alembert's paradox). Furthermore there is no separation of flow around the hull (no vortex formation).
The free surface remains undisturbed, for which also the wave resistance is equal to zero.
For these reasons, the results so obtained are used only to determine the relative validity values about alternative proposals chosen to optimize a hull qualitatively, before the execution of expensive tests.
In the 1977, a calculation method with the free surface implementation was developed by Dawson [18].
They can also be used to indicate and to identify possible improvements performed on the hull, showing the distributions of pressures or foreseeing the trends of speeds.

Typical cases:

1. alternative choices between different types of bulbous bow;
2. distributions of pressure about alternative solutions of the hull's shapes;
3. development of the streamlines (for the positioning of appendages);
4. alternative choices of the stern's shape in order to accommodate appendages or pads;
5. distributions of pressure around the stern area near of the propellers.

1.4.2 Computing in viscous field

The main solutions of the flow in a viscous field make use of the Navier-Stokes equations. The solution of these equations is rather onerous under the computational point of view, even if calculation techniques using simplified procedures are available, now.

You can define areas in which there is a flow separation, compute the wake components - such as axial, radial and tangential - and assess the performance of the flow and specific speed components in hull's areas where the shapes are very troubled, and much more.

CFD RANSE SIMULATIONS

2.1 COMPUTATIONAL FLUID DYNAMICS

The Computational Fluid Dynamics is the study of methods, techniques and algorithms able to simulate the dynamic behavior of fluids in complex physical problems.

This numerical simulation consists in the elaboration of sophisticated mathematical models describing the temporal evolution of the fluid through its fundamental fluid dynamic parameters: speed, pressure, temperature, density.

The use of numerical simulation in the design phase becomes necessary where there is the need to perform predictions and analysis of a high number of cases of study; CFD therefore allows to eliminate, at least in the initial stages, the execution of various prototypes.

In practice, this virtual simulation tool is able to provide answers that are quite consistent with reality, with times and costs significantly reduced compared to what is necessary to achieve the physical experimentation.

This is in fact one of the main reasons which makes the CFD an extremely advantageous mean in the design analysis: it allows to perform, in a relatively simple manner and, in any case, always simpler than real investigation, parameterizations for different initial configurations , for both geometries and boundary conditions allowing to evaluate the performances of the resistance components in operating conditions close to the physical reality.

Another great advantage of CFD is its independence to the scale factor: this enables - especially in the shipbuilding industry - the elimination of the problems - sometimes very

significant, difficult and expensive - of viewing the fluid dynamic parameters in the simulation of real prototypes.

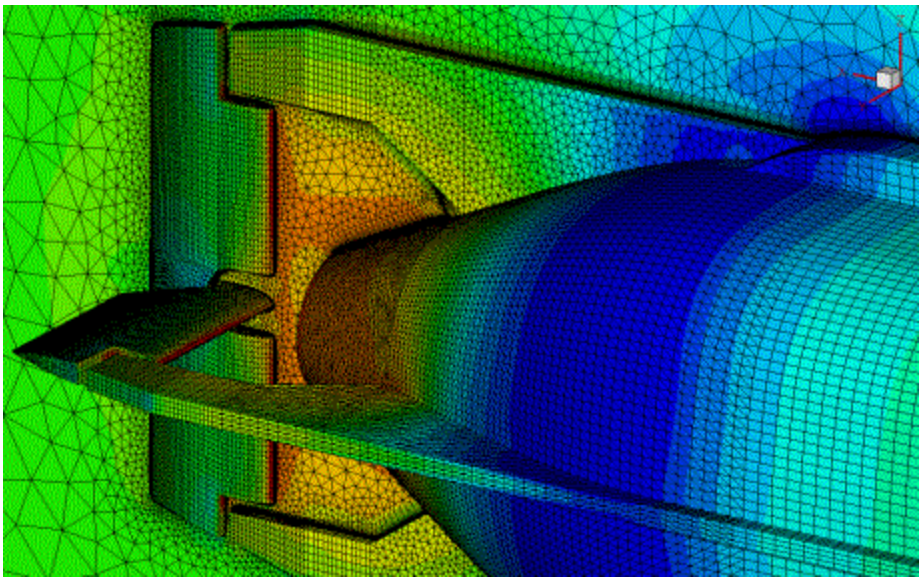

Fig. 2.1 - Rudders of a submarine - CFD & Volume Mesh *(Courtesy of CD-Adapco)*

The geometric model to analyze is accomplished by defining the surfaces surrounding the domain of fluid to be tested; while in the structural analysis programs the object to be outlined by a mesh is the solid portion of it, in the fluid dynamic analysis what matters is the whole domain unless the object itself, which, in this case, acts as a boundary for the fluid.
The direct resolution of the Navier-Stokes equation is practically possible only in the case of laminar flows, and for simple geometries (spheres, flat sheets).
The turbulent flows encountered in real applications require the use of a turbulence model and, because of the high computational cost involved, they need numerical techniques to reach the solution. In this case, you use the Navier-Stokes equations in Reynolds average formulation (called RANS or RANSE: Reynolds Average Navier-Stokes Equations), which require the use of additional equations (such as the turbulence model k-ε) to solve the problem [19].
In many cases also other equations- in addition to the Navier-Stokes ones or to the turbulence model equations - must be solved simultaneously.

They may include those related to the concentration of different kinds (multicomponent flow), chemical reactions (reagent flows), thermal radiation, etc.. More complex problems require modeling of additional phenomena, as in case of two-phase flows (i.e. gas / liquid) or in case of non-Newtonian fluids.

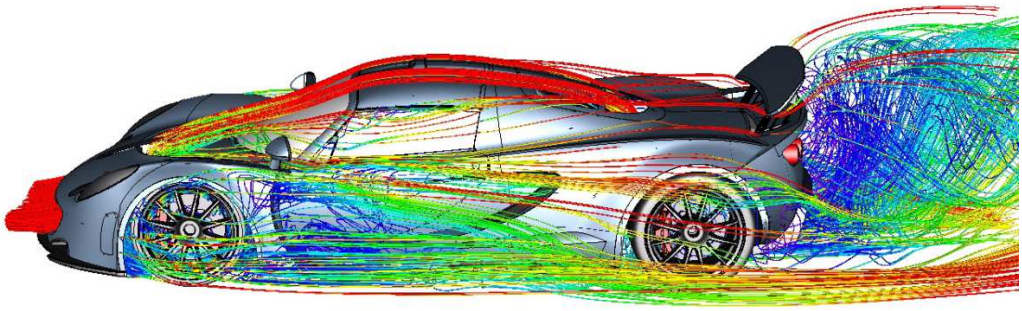

Fig. 2.2 - CFD streamlines analysis of a speeding car (Courtesy of CD-Adapco)

2.2 CONCEPT OF CONTINUOUS

Obviously, in order to process a continuous, you must first understand what is meant by "continuous". The classical meaning of continuous defines it as a region of space whose characteristics are defined by mathematically functions - which are all defined for each point of the domain and limited for each in a sufficiently small range of the point considered. But how it can be applied to fluids? In the common experience that definition would be accurate, but since some centuries it is well known that matter is not "full" but it is instead made up of a finite number of particles, which are in turn constituted by other particles.

Even without dealing with the “infinitely small”, it is very common the concept of atom or molecule. This behavior leads to deny the very statement of "continuous". This is also demonstrated by a "virtual" experiment.

If you take a sample of continuous, for example a glass of water, its mass is one of its fundamental characteristics able to describe it. You define mass density the mass included in a given space divided by the volume of that space.

Assuming that the fluid examined has a constant density in the space, if it varies arbitrarily the volume considered, the density should always have the same value.

This is not true when you tend to increase smaller volumes (in reality this effect is always present even for large volumes but it is considered negligible).

This behavior is due to the fact that the volume varies with continuity, while the mass is made up of particles occupying the given volume. These particles will vary in a discrete manner, since they are always defined as a sum of finite particles. This implies that a characteristic quantity of the fluid, in this case, would not be represented by a continuous function, but by a discrete one, as shown in the figure below:

:

This phenomenon, as already mentioned, is significant when the size of the volume taken into consideration is sufficiently small to allow the physical quantities of interest to undergo variations related to their real molecular constituents.
Therefore in order to use the concept of continuous, the average aspect of the state variables was introduced. This implies that the theory is valid only if you look at the continuous at a sufficiently large size to neglect the molecular discontinuity.
This is highly plausible for most of the common interest physical phenomena related with marine engineering, in which an average characteristic of the particles around a certain point can be evaluated.
This hypothesis is not in contrast to the concept of infinitesimal then used in all subsequent mathematical treatment. This is due to the fact that the present research work is interested in the physical phenomena of orders of magnitude much greater than the molecules' size of the fluid or solid to be investigated.
Thanks to this concept of infinitesimal spatial average, some physical quantities belonging to fluid mechanics - such as the above-mentioned mass density, pressure, energy density and many others - take place.

They are all characteristics that can be expressed through appropriate functions varying in space and time in a continuous manner, with the expression:

$$\rho\ (x, t) \tag{2.1}$$

ρ, for example, means the value of the density at the instant *t* which identifies an infinitesimal volume around the point featured by the vector x position.

2.3 CFD CODE OPERATION

The typical approach of a CFD code requires to discretize the fluid domain in elementary cells, so as to obtain a calculation grid (also called mesh), on which you can apply the methods of iterative resolution in order to solve the Navier-Stokes or Euler equations.
Modern codes are made up of three main elements: a pre-processor, a solver and a post-processor.
The preprocessor is a user interface in which you enter the data of the problem. These data are then processed in a form suitable for the solver.
The task of the operator during the step of pre-processing includes:

• definition of the geometry of the domain of interest;
• generation of computational grid: subdivision of the domain in a certain number of sub-domains smaller cells;
• selection of the physical phenomenon that needs to be modeled;
• defining the properties of the fluid;
• definition of the boundary conditions which must be satisfied;

The solution of the problem (speed, pressure, temperature, etc ..) is given in correspondence with each cell. The solution accuracy depends on the number of grid cells. It is clear that the smaller the cell size, the better the viewing details of the performance of the flow, since the higher the resolution and the more you can appreciate details.
But the greater the number of cells used, the greater will be the computation time and / or the computing power required. It will be up to the expert user finding the right compromise between the desired accuracy and the computational cost for the solution, then. A correct meshing is often not uniform: the mesh will be denser where you have greater variations and/or where there are most interesting areas.

This analysis phase is certainly the most crucial and delicate one: often much of the time taken to address the issue is devoted to the domain definition and to the mesh generation.

The pre-processor also allows the user the access to libraries of materials for the most common fluids, and it enables to retrieve models of particular physical and chemical processes (turbulence models, models for the motion of bodies, models for the generation of waves, combustion models).
Dealing with the solver, there are various techniques of numerical solution. In this work, two techniques have been taken into account: the RANSE one and the potential one.

The steps involved by the solver are essentially the following:
• approximation of the fluid unknown variables with some functions;
• discretization achieved by the replacement of the approximate forms in the equations governing the fluid, and further mathematics handling;
• solutions of algebraic equations.

The CFD codes contain discretization techniques suitable for the transport phenomena, convection (transport due to fluid flow) and diffusion, as well as for the source terms and temporal variation. The basic physical phenomena are quite complex and non-linear, so it is necessary an iterative approach.

2.4 CALCULATION MODELS IN VISCOUS FIELD

The viscous calculation models solve the equations of mass conservation and momentum in an approximate way, with an accuracy level depending on the characteristics of the model and the computing resources.

According to the study concerned, additional equations are solved, such as the balance of energy and the thermal exchanges.

In the present work, there are two different fluid that invests the body, air and water. It means that there are some perturbations on the interface surface between the two fluids, for this reason it's necessary to place an additional equation which takes into account specifically the presence of the two fluids ("multi-phase" model). For such kind of problems, it is often adopted the model called VOF (volume of fluid) [20].

2.4.1 Equation of mass conservation

The equation of mass conservation, or equation of continuity, within a defined control volume, is given by the following relation:

$$\frac{\partial \rho}{\partial t} + \rho \frac{\partial u_i}{\partial x_i} = \hat{S} \qquad (2.2)$$

where $\hat{S}$ in this case represents the source of the mass (in the study carried out $\hat{S}$ = 0), ρ is the fluid density and u_i represent the components of the velocity u of the water-air mixture. The previous formula applies in the case of both compressible and incompressible fluids.

In this last case the first term on the first member of equation vanishes and the equation becomes:

$$\frac{\partial u_i}{\partial x_i} = 0 \qquad (2.3)$$

This last equation is the one solved in the present study because both fluids are considered incompressible.

2.4.2 Equation of momentum conservation

The equation of momentum conservation expresses the equality between the instantaneous variation of the momentum and the sum of the forces acting on the single fluid particle. Assuming a constant density (incompressible fluid), the equation written in differential form, is given by:

$$\rho \frac{\partial u_i}{\partial t} + \rho \cdot u_j \frac{\partial u_i}{\partial x_j} = \frac{\partial \tau_{ij}}{\partial x_j} - \frac{\partial p}{\partial x_i} + \overline{F}_i \tag{2.4}$$

where p is the pressure, τ_{ij} is the viscous stress tensor, which is the component of the deviation of the Cauchy tensor ($\tau = \sigma\text{-}pI$) and F_i represents the volume forces acting on the body. The equation of momentum conservation is supplemented by the relation between the velocity field to the stress one, that for a fluid with a Newtonian behavior is:

$$\tau_{ij} = \mu \left(\frac{\partial u_j}{\partial x_i} + \frac{\partial u_i}{\partial x_j} \right) + \left(\mu' - \frac{2}{3}\mu \right) \left(\frac{\partial u_i}{\partial x_i} \right) \delta_{ij} \tag{2.5}$$

where δ_{ij} is the Kronecker delta, μ is the fluid viscosity and μ' is the module of bulk (generally negligible for very densier fluids). Considering the incompressible fluid, you may neglect the second term at the right-hand side getting the following relation:

$$\tau_{ij} = \mu \left(\frac{\partial u_j}{\partial x_i} + \frac{\partial u_i}{\partial x_j} \right) \tag{2.6}$$

Placing this constitutive relation in the equation of momentum conservation you will get the Navier-Stokes equations for incompressible fluids:

$$\rho \frac{\partial u_i}{\partial t} + \rho \frac{\partial (u_j u_i)}{\partial x_j} = \mu \nabla^2 u_i - \frac{\partial p}{\partial x_i} + \vec{F}_i \tag{2.7}$$

2.4.3 Turbulence

As already mentioned above, the behavior of water around the hull of a vessel assumes, normally, turbulent character. In the boundary layer the flow velocity changes rapidly from zero to the undisturbed flow value. As soon as a fluid particle moves inside the boundary layer, it begins to rotate due to velocity gradient in this area: the speed in the upper part of this area is greater than the one next to the hull. This phenomenon generates swirling motion (rotational motion), or movements with a "not equal to zero" vorticity.
At a certain distance from the bow the boundary layer becomes turbulent, and the particles become strongly distorted because of the random and irregular turbulence nature (it is an instability of the velocity field). The transition from laminar flow to turbulent one occurs for Reynolds numbers placed in the range between 10^5 and 10^6 (critical Reynolds number, Re_{cr}) and it is a function of the surface roughness and of the presence of turbulence in the stream away from the hull.

Identifying a specific Reynolds number at the transition point is quite complex. The transition may take place not at one point but in an area of the hull: this is due to the irregularity of the transition ("spottiness"). Typically, the transition starts in some random points, where the Reynolds number is equal to Re_{cr}. These starting points of turbulence develop more rapidly towards the stern until the entire keel is surrounded by the turbulent flow.
The complex phenomenon of transition from laminar to turbulent concerns the instability of the velocity field.
The transition from laminar to turbulent flow implies a change in the shape of the boundary layer velocity profile. The turbulent velocity profiles are quite flat, they have a high velocity gradient in proximity of the wall and they produce boundary layer thickness larger than the one of laminar flow.

The components of the velocity, for example, assume the following formulation:

$$U = U(x) + U'(x,t) \tag{2.8}$$

where $U(x)$ is the velocity average component and $U'(x, t)$ represents the floating quantities in the fluid.

An analytical approximation of the turbulent motion can be given by expressing the velocity and pressure as the sum of an average component and an oscillating one. These fluctuations are constrained within a range of values, in terms of frequency and amplitude. This turbulent kinetic

energy spectrum can be evaluated using statistical tools from which we can derive a number of formulations for the equations of mass and momentum conservations.
The most widely used of these ones is known as the "Reynolds averaging", and is the basis of the RANSE equations ("Reynolds-averaged Navier-Stokes Equations").

The average is a time average over a period long enough to let the separate measurements give the same result. Some procedural complexities can be achieved when the conditions imposed are not stationary.

So averaging a generic quantity *Q* means:

$$\overline{Q} = \frac{1}{\Delta t}\int_{t1}^{t2} Q dt \tag{2.9}$$

Where *t* is a great value compared to any temporal dimension included in the *Q* variation.

2.4.4 Reynolds equations

The Navier-Stokes equations are the mathematical formalization of three physical principles to which the fluids have to obey:

• the principle of conservation of mass: continuity equation;
• the second principle of dynamics: balance of the momentum;
• the first principle of the thermodynamics: energy balance.

Considering a turbulent incompressible viscous flow, where all dimensions are constant, the equations which govern the fluid motion are the momentum and continuity ones:

$$\frac{\partial v}{\partial t} + (v \cdot \nabla)v = -\frac{1}{\rho}\nabla p + \nu\nabla^2 v \tag{2.10}$$

$$(\nabla \cdot v) = 0 \tag{2.11}$$

Taking into consideration the following mathematical relationship valid for every vector u:

$$\nabla \cdot (uu) = \nabla u \cdot u + (\nabla \cdot u)u \tag{2.12}$$

The equation of continuity, applied to the velocity vector of an arbitrary incompressible flow, becomes:

$$\nabla \cdot (vv) = \nabla v \cdot v + (\mathrm{v} \cdot \nabla)v \tag{2.13}$$

which provides the following equation of the momentum:

$$\frac{\partial v}{\partial t} + \nabla \cdot (vv) = -\frac{1}{\rho}\nabla p + \nu \nabla^2 v \tag{2.14}$$

The instantaneous velocity and pressure can be decomposed as a sum of an average physical quantity and a fluctuating one:

$$v(x,t) = \overline{v}(v,t) + v'(x,t) \tag{2.15}$$

$$p(x,t) = \overline{p}(v,t) + p'(x,t) \tag{2.16}$$

By applying an operation of averaging to both members of the equation you can obtain:

$$\frac{\partial \overline{v}}{\partial t} + \nabla \cdot \left(\overline{vv} + \overline{v'v'}\right) = -\frac{1}{\rho}\nabla \overline{p} + \nu \nabla^2 \overline{v} \tag{2.17}$$

From which:

$$\frac{\partial \overline{v}}{\partial t} + (\overline{\mathrm{v}} \cdot \nabla) \cdot \overline{v} = -\frac{1}{\rho}\nabla \overline{p} + \nu \nabla^2 \overline{v} - \nabla(\overline{v'v'}) \tag{2.18}$$

In it, the stress tensor of Reynolds appears:

$$\tau = \rho \cdot \overline{v'\, v'} \tag{2.19}$$

It therefore indicates the tensor of the correlations of the fluctuating velocity, it is symmetric and it has six independent components. Substituting this formulation into the previous equation and applying the average to the equation of continuity you can obtain the Reynolds equations, valid for an arbitrary incompressible turbulent flow:

$$\frac{\partial \overline{v}}{\partial t} + (\overline{\mathrm{v}} \cdot \nabla) \cdot \overline{v} = -\frac{1}{\rho}\overline{p} + \nu \nabla^2 \overline{v} - \frac{1}{\rho}\nabla \cdot \tau \tag{2.20}$$

$$\nabla \cdot \overline{v} = 0 \tag{2.21}$$

$$\nabla \cdot \tau = \left\{\frac{\partial}{\partial x_1} + \frac{\partial}{\partial x_2} + \frac{\partial}{\partial x_3}\right\} \begin{pmatrix} \tau_{11} & \tau_{12} & \tau_{13} \\ \tau_{21} & \tau_{22} & \tau_{23} \\ \tau_{13} & \tau_{23} & \tau_{33} \end{pmatrix}^T = \left\{\sum_{i=1}^{3} \frac{\partial \tau_{1i}}{\partial x_i} + \sum_{i=1}^{3} \frac{\partial \tau_{2i}}{\partial x_i} + \sum_{i=1}^{3} \frac{\partial \tau_{3i}}{\partial x_i}\right\}$$

(2.22)

The equation of average flow continuity is the same as of the instantaneous flow's one and it is achieved by replacing the instantaneous velocity with the average one. As a result, you get:

$$\nabla \cdot v - \nabla \cdot v = \nabla \cdot (v - v) = \nabla \cdot v' = 0 \tag{2.23}$$

where you can see that the field of fluctuating velocities has the same kinematic features of the field of instantaneous ones.

The equation of the average momentum, unlike the equation of the instantaneous momentum, has within it the stress tensor of Reynolds. In conclusion, you obtain a system of four scalar at partial differential equations, in ten unknowns terms consisting of the three average speeds, the average pressure and the six floating speeds independent of the Reynolds stress tensor.

The usefulness of the models of turbulence lies in the fact that they associate the Reynolds stress tensor to average velocities and they have the main aim to close the previous equation. They therefore provide only the average values of the variables which describe the turbulent flow.

2.4.5 Turbulent stress algebraic models

Dealing with the issue of the equations' closing, it is taken into account the process of cascade through which, starting from the larger turbulent vortices, the energy is finally moved to the molecular motion able to convert it into heat.

It is therefore clear that the turbulent flow increases the average flow dissipation.

These observations lead to assume a parallelism between Reynolds stresses and viscous ones on which the Boussinesq model is based:

$$\tau = \frac{2}{3}\rho k I - 2\mu_t \overline{S} \tag{2.24}$$

where

$$k = \frac{1}{2}\overline{v'v} \tag{2.25}$$

is the turbulent kinetic energy per mass unit, μ_t is the turbulent viscosity, and *s* indicates the average deformation flow tensor. You can notice how the expression of τ of the Boussinesq model allows to switch from six to two unknown terms, i.e. k and μ_t.

It's also important to underline that the turbulent stress Boussinesq model is similar to the Stokes one for viscous stress. As it was observed that the larger turbulent flows are the ones interacting with the mean flow, indicating respectively with v* and t* an appropriate speed scale and an appropriate time scale of the vortices, you can assume that:

$$\mu_t = \rho v_t = \rho C^* v^{*2} t^* \tag{2.26}$$

If you also take into account the fact that turbulent flow largest vortices contain most of its kinetic energy, the previous relation becomes:

$$\mu_t = \rho C_\mu k t^* \tag{2.27}$$

Where the dimensionless constant C_μ should be determined experimentally. Replacing this last relation you get the model of turbulent viscosity:

$$\tau = \frac{2}{3}\rho k I - 2\rho C_\mu k t^* \overline{S} \tag{2.28}$$

where you can see the need to model at least two turbulent quantities, one of which is the turbulent kinetic energy.

The Boussinesq model is used in 80% of the numerical simulations of turbulent flows; the two most important alternatives to this model are nonlinear algebraic models of Reynolds stresses and some models based on the solution of the differential equations of Reynolds stresses transport.

2.4.6 Two equations models

In the last two decades the models with two equations have found great success in the research. Such kind of models provide the solution of two independent differential equations - thus not only the turbulent kinetic energy, as it occurs in one equation models - but also the turbulent length scale.
One can say that the models with two equations are quite complete, that is, they can be used to predict the properties of a given turbulent flow without knowing in advance the turbulent structure itself.

The starting point for all models in two equations is the Boussinesq approximation.

In fact, the turbulent kinetic energy transport equation is the fundamental equation of the methods based on algebraic models of Reynolds stresses. It describes the performance of the same energy in the average flow. So, before going on to the description of the models, it is necessary to define the average kinetic energy and the flow deformations. The average kinetic energy per mass unit K of a turbulent flow is given by the sum of the energy of the average motion $\overline{k}$ and turbulent kinetic energy *K*:

$$K = \frac{1}{2}\overline{v \cdot v} = \frac{1}{2}\left(\overline{\overline{v} \cdot \overline{v} + 2\overline{v} \cdot v' + v'v'}\right) = \overline{k} + k \tag{2.29}$$

The speed of instant deformation of a fluid is defined as:

$$K = \frac{1}{2}\left(\nabla v + (\nabla v)^{\mathrm{T}}\right) \tag{2.30}$$

which, distinguishing its average and fluctuating portion, becomes:

$$K = \frac{1}{2}(\nabla\,\overline{v} + (\nabla\,\overline{v})^{T}) + \frac{1}{2}(\nabla\,v' + (\nabla\,v')^{T}) = \overline{S} + S' \tag{2.31}$$

This formulations is the equation of the kinetic energy equation of the average motion, obtained by multiplying the Reynolds equation for the average speed and dividing by two.

The seven terms in this equation are:
1. the kinetic energy local variation of the average motion;
2. the kinetic energy spatial variation of the average motion;
3. the average flow transportation due to the average pressure;
4. the average flow transportation due to Reynolds stresses;

5. thea verage kinetic energy transportation due to viscous stresses;
6. the internal work done by Reynolds stresses;
7. the internal work done by viscous stresses.

Subtracting to the Navier-Stokes equation the Reynolds equation and multiplying for the fluctuating speed scarily and then performing the average, you obtain the turbulent kinetic energy equation:

$$\frac{\partial k}{\partial t} + (\overline{v} \cdot \nabla) \cdot k = -\frac{1}{\rho}\nabla \cdot \left(\overline{p'v'} + \frac{1}{2}\overline{\rho(v' \cdot v')v'}\right) + v\nabla^2\overline{k} - \frac{1}{\rho}\tau \cdot \overline{S} - \varepsilon \tag{2.32}$$

where

$$\varepsilon = 2v\,\overline{S' \cdot S'} \tag{2.33}$$

The seven terms in the equation are:

1. the local variation of turbulent kinetic energy;
2. the spatial variation of turbulent kinetic energy;
3. the turbulent flow transportation due to the fluctuating pressure;
4. the turbulent flow transportation due to Reynolds stresses;
5. the turbulent kinetic energy transportation due to viscous stresses;
6. the internal work done by Reynolds stresses;
7. the internal work done by viscous stresses.

Notice that the work done by Reynolds stresses is present, although with a changed sign, in both equations of the kinetic energy: in turbulent flows its value is positive, while in the other is negative. This is the result of the kinetic energy transfer mechanism from the average motion to turbulent flow, which causes a production of turbulent kinetic energy at the expense of the average motion one. Instead, the work of the viscous stresses on the turbulent flow is always negative because of the turbulent kinetic energy conversion in the temperature increase of the fluid.

2.4.7 k-epsilon model

The k-ε the model is one of the best known and most widely used, especially in the industrial field, for turbulent flows simulations thanks to its strength, its efficiency and also because in several cases it is able to provide enough realistic predictions. It features by two differential equations to be modeled: one for the turbulent kinetic energy *k* and the other for the turbulent dissipation rate ε.

This model was born when Chou, in 1945, proposed the exact modeling of the ε equation. According to his formulation the turbulent viscosity, the turbulent length scale and the dissipation were linked by the relation*:*

$$\mu_t \approx \rho k^2 / \ \varepsilon, l \ \approx k^{3/2} / \ \varepsilon \tag{2.34}$$

The turbulent kinetic energy equation can be rewritten in the form:

$$\frac{\partial k}{\partial t} + (\overline{v} \cdot \nabla) \cdot k = P - \varepsilon + D + v\nabla^2 k \tag{2.35}$$

with

$$P = 2C_\mu k t^* \overline{s} \cdot \ \overline{s}\ , \varepsilon = 2v\ \overline{s' \cdot s'}\ , D = -\nabla\left(\frac{1}{2}\overline{p'v'} + \frac{1}{2}\overline{(v' \cdot v')v'}\right) \tag{2.36}$$

These three quantities represent respectively the production of turbulent kinetic energy, the speed of dissipation of turbulent kinetic energy and turbulent diffusion of *k*.

The time scale for the *k-ε* the model is:

$$t^* = \frac{k}{\varepsilon} \tag{2.37}$$

Placing this relation both in the Reynolds stresses expression and in the production one, you get:

$$\tau = \frac{2}{3}\rho k I - 2\rho C_\mu \frac{k^2}{\varepsilon}\overline{S} \tag{2.38}$$

$$P = 2C_\mu \frac{k^2}{\varepsilon}\overline{s} \cdot \overline{s} \tag{2.39}$$

The final quantity remaining to be modeled is the turbulent diffusion. It is supposed an analogy between the turbulent diffusion mechanisms and molecular once; the expression of transportation model due to the Reynolds stresses is thus :

$$\frac{1}{2}\overline{p'v'} + \frac{1}{2}\overline{(v' \cdot v')v'} = -\frac{v_t}{\sigma_k}\nabla k \tag{2.40}$$

It is therefore possible to get the final form of the turbulent kinetic energy equation:

$$\frac{\partial k}{\partial t} + (\overline{v} \cdot \nabla)k = 2C_\mu \frac{k^2}{\varepsilon}\overline{s} \cdot \overline{s} - \varepsilon + \nabla \cdot \left[\left(\frac{v_t}{\sigma_k} + v\right)\nabla k\right] \tag{2.41}$$

While the turbulent kinetic energy transportation equation *k* derives from an exact formulation, the dissipation rate transportation equation derives from considerations of empirical nature. The final form of the standard dissipation rate equation is:

$$\frac{\partial \varepsilon}{\partial t} + (\overline{v} \cdot \nabla)\varepsilon = C_{\varepsilon 1}\frac{\varepsilon}{k}P - C_{\varepsilon 2}\frac{\varepsilon^2}{\mathrm{k}} + \nabla \cdot \left[\left(\frac{v_t}{\sigma_\varepsilon} + v\right)\nabla \varepsilon\right] \tag{2.42}$$

The values of the constants are determined from the average values derived from the experimental data regression of many types of turbulent flows; they are:

$$C_\mu = 0.09\ , \sigma_k = 1.00\ , \sigma_\varepsilon = 1.30\ , C_{\varepsilon 1} = 1.44\ , C_{\varepsilon 2} = 1.92$$

2.4.8 Wall functions

In the wall functions you can proceed identifying two zones: one nearest to the wall, where the flow is laminar and the other in the farthest layer from the walls, where the flow is turbulent, instead.

The nearest layer to the wall is the viscous sub-layer, where the flow is simulated as if it was laminar one, while the outer layer is the completely turbulent region, where the flow is simulated as if it was turbulent. There is also a connection zone, called mixing region, which is neglected.

From these considerations, the motion field closer to the wall is simulated by solving the boundary layer equations, known as *wall functions*, while the turbulent part is simulated by solving the turbulence models equations at a suitable distance from the walls.

If you define the dimensionless velocity as:

$$v_x^+ = \frac{\overline{v}_x}{v_\tau} \tag{2.43}$$

Where *x* indicates the direction parallel to the walls. The wall functions for the laminar underlayer, are:

$$v_x^+ = y^+ \tag{2.44}$$

$$k^+ = A_k y^{+2} \tag{2.45}$$

$$\varepsilon^+ = 2A_k \tag{2.46}$$

(A_k depends on the flow field characteristic).

The distribution of the dimensionless speed parallel to the wall, in the logarithmic region, is:

$$v_x^+ = \frac{1}{\kappa}\ln(y^+) + C = \frac{1}{\kappa}\ln(y^+) + \ln(E) = \frac{1}{\kappa}\ln(Ey^+) \tag{2.47}$$

where k=0.41 and E=9

If you assume that in the turbulent boundary layer the pressure gradients along the walls are small, a local turbulent kinetic energy equilibrium occurs.

In this hypothesis, turbulent and viscous diffusive contributions can be neglected, compared to the production and dissipation so that they balance.

By the transportation equation of *k* is then:

$$P - \varepsilon = 0 \Rightarrow 4C_\mu \frac{k^2}{\varepsilon} = \varepsilon \Rightarrow S^* = \frac{1}{2\sqrt{C_\mu}} \tag{2.48}$$

in which it is placed

$$S^* = k\overline{S}/\varepsilon \tag{2.49}$$

Remembering that in the turbulent layer the stress on the wall coincides with the turbulent one, you will achieve:

$$\tau_w = 2\rho C_\mu k s^* \Rightarrow k^+ = \frac{1}{\sqrt{C_\mu}} \tag{2.50}$$

At the end it is obtained , in a simple way, that:

$$\varepsilon^+ = \frac{1}{ky^+} \tag{2.51}$$

2.4.9 Multiphase model

To perform the study of wave resistance is necessary to consider the interaction between the two fluids, air and water. This is made possible thanks to the use of a multiphase model.
Solving a further equation able to describe the phases' distribution in the calculation domain, previous equations are reformulated according to the mixture of the two fluids.
In this specific case, the presence of an interface surface between two homogeneous areas will take place.
The waves generated from the boat moving in the fluid domain will be calculated as a "ripple" in the interface zone between the two phases.
The model that best meets the computation needs in such kind of issue is the VOF ("Volume of fluid").

The VOF model is the one which considers two or more immiscible fluids: in those cases the interface between the fluids is the real unknown term of the problem.
The VOF can model two or more immiscible fluids by solving a single set of conservation of momentum equations, and then by tracing the volume fraction of each of the two fluids through the entire domain.

However, such kind of multiphase model has several limitations, among which the main ones are:

- the continuity equations and conservation of the momentum equations must be solved in a serial way and not simultaneously within the same iteration;
- only one phase can be compressible;
- It is not compatible with all models of turbulence.

In VOF formulating you consider the volume fraction of the *q-th* phase in the point. The sum of the volume fractions of all phases must be equal to 1 in each point of the domain α_q.

Analytically, the following relation is valid:

$$\sum_{q=1}^{n} \alpha_q = 1 \tag{2.52}$$

Where *n* is the number of phases included in the fluid domain (*n* = 2 in the following study). The pressure and velocity fields are shared between the phases and they represent the weighted values on the volume fraction of each phase (they are, as already mentioned, relative to the mixture).

For example, if the *k-th* fluid volume fraction within a cell is defined by a coefficient α_q, then there are three possible conditions:

- $\alpha_q = 0$ in the considered point the q-th fluid is not present
- $\alpha_q = 1$ the q-th fluid is the only one present
- $0 < \alpha_q < 1$ in the considered point there is a mixture of fluids

For the *k-th* phase the balance equation appears as follows:

$$\frac{\partial \alpha_q}{\partial t} + v_i \cdot \frac{\partial \alpha_q}{\partial x_i} = \frac{S_{\alpha q}}{\rho_q} \tag{2.53}$$

where $S_{\alpha q}$ to the second member is a source term which, in the case study, assumes the value equal to zero.

The VOF equation is not solved for the "primary phase"; indeed the volume fraction of this, within each cell, will be evaluated from time to time.

The properties shown in the transportation equation are determined by the presence of the component phases in each control volume. In a two-phase system like this, if these are named *k* and *h*- and if volume fraction of *h* must be drawn - the density in each cell is given by:

$$\rho = \alpha_h \cdot \rho_h + (1 - \alpha_h) \cdot \rho_k \tag{2.54}$$

There are similar formulations also for other properties (such as viscosity).

2.5 NUMERICAL GRID

Next step to the numerical scheme is the choice of space-time discretization necessary to describe the problem itself. In the past times, also for this purpose several different techniques have been employed. They often appeared to be constrained to the numerical discretization method chosen.

Almost all grids or meshes used must comply with some basic criteria determining the mathematical form. The first criterion is that of completeness: a mesh must completely cover the computational domain of interest.

The second criterion is called *no-overlapping*: part of two constitutive elements of the mesh should never occupy simultaneously the same region of space.

It is fair to say that in computational fluid dynamics, there are some exceptions to these general rules. An example is the "Chimeras" mesh in which the condition of no-overlapping is not respected. There are also other methods known as *meshless* wherein the feature of completeness is not observed: such as, for example the SPH methods (smooth particle hydrodynamic).

In the modern CFD, meshes may be classified in many different ways: according to elements' typologies characterizing them, according to the spatial dimension, etc. but undoubtedly one of the main used is being structured or not. Mesh featuring also constrains the solution method used.

The meshes therefore are divided into:

Structured: They are those in which, you can uniquely identify each point of the domain - at least a block- through a *n*-number of indices, representing the entire domain.

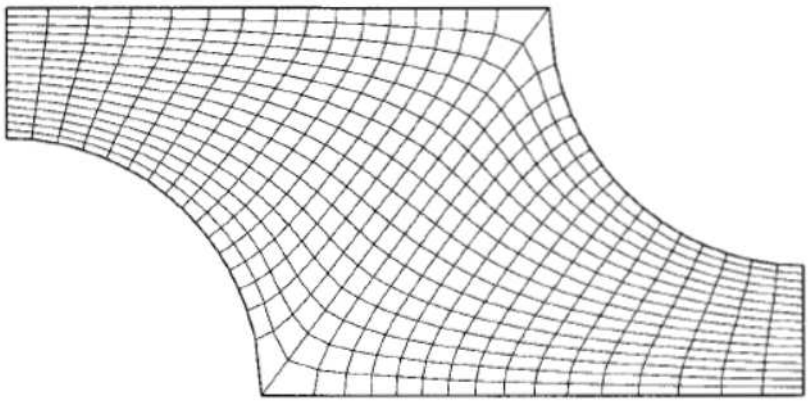

Fig. 2.3 – Example of structured mesh

This typology is undoubtedly the oldest one, and each discretization methodology can be applied to it. In the past, it was the increased use mesh and many sophisticated techniques were adopted for its construction. They enabled to build meshes around sufficiently complex domains. These meshes allow to obtain rather high quality cells but they lack in their extreme mathematical complexity of their construction above all depending upon the complexity of the domain examined. Despite this, the structured meshes had a considerable use, also thanks to the improvement of *chimera* techniques, which allow the application of this type of meshes even in domains of some complexity, thanks to the overlapping.

Non-structured: The most modern approach is focused to unstructured mesh. They are able to support cells of any type of element, together with a great automation and ability to discretize even extremely complex domains. This type of mesh often lacks in quality.

Another trouble of such mesh is both algorithmic complexity in its creation, and in the larger size of the data structures composing it. Today's largest commercial codes use such kind of mesh with some variants increasing the quality and speed of meshing: the famous *Cartesian* mesh or polyhedral one

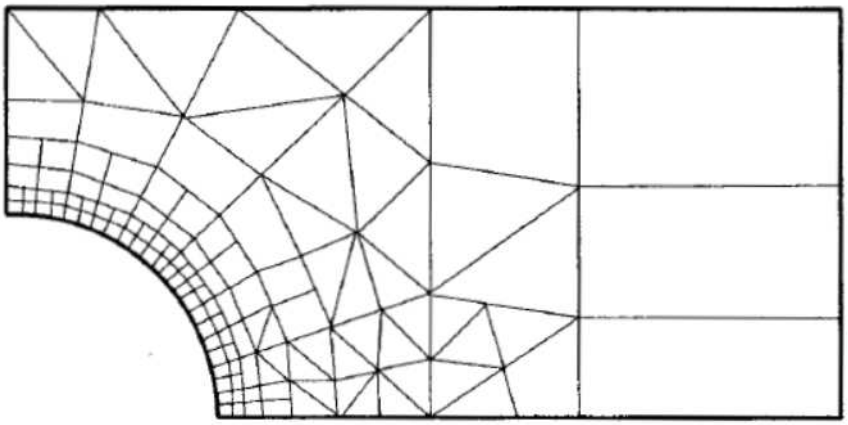

Fig. 2.4 – Example of non-structured mesh

2.6 SOLVING CRITERIA

The different methodologies used in the CFD, in order to be applied and to ensure that the calculation will be successful, must provide some criteria of existence.

The main and most important criteria are:

• *Convergence*: This property sets out the capability of the numerical scheme to ensure an exact solution when the calculation distance of the points tends towards zero.

• *Consistency*: is the ability of the numerical scheme to produce an algebraic relations set equal to starting equations when spacing tends to zero.

• *Stability*: is the capacity of the method of not amplify any mistakes potentially present in the solution, but making them close to zero while process iterations increase.

These three criteria are the foundation of the numerical discretization of a differential equations system. However, a major issue arises.

While the latter two criteria can be mathematically demonstrated for most of the approaches used nowadays, the convergence criterion is absolutely not demonstrable. The non-demonstrability lies in the fact that the convergence compares the obtained solution to the real

one, which, however, is unknown from the outset. For this reason, in the overwhelming majority of cases, this property can't be mathematically ensured.

Often, because of this difficulty you can refer to the Lax theorem [21],[22] which states that, for a linear problem, it is sufficient to ensure both the stability and consistency to guarantee the convergence automatically. Unfortunately the equations related to the CFD are often of non-linear kind, so the theorem is not applicable. Therefore it is claimed that the chosen scheme ensures the existence of both two criteria plus a number of additional criteria able to define it a very reliable method, although not mathematically certain.

Therefore the additional criteria are:

• *Conservation:* is the property of the scheme to ensure that if a given physical quantity shall be preserved during the evolution of the problem, the scheme ensures that conservation also at the numerical level.

• *Limitation*: thanks to this property, in every step of the solution the variables remain still limited to their field of existence. A clear example is given by the coefficient of pressure in the stagnation point that has to be physically limited to 1. A good numerical scheme ensuring the limitation, is conceived in such a way as to avoid the exceeding of this value because of numerical errors.

• *Realisability:* is the capacity of a scheme to maintain its stability properties even in presence of physical phenomena which have not been taken into account by the model. An example is the turbulence, which, even not solved, should not generate too high instability in the examined system.

• *Accuracy*: is the ability to provide a solution as similar as possible to reality, the least possible affected by the choice of the mesh or by the approximations of the scheme. Often this feature is guaranteed trough the famous *mesh-depending* where increasingly dense mesh are used gradually, until you get a solution no longer dependent on the mesh itself.

As already mentioned, all of these properties are essential to any numerical scheme used. Some properties can be guaranteed in mathematical form, but usually the most of them are tested through simulations on particular domains, on which or the analytical solution is already known or numerous experimental tests have been carried out, and you can make a code validation on which. That's the new frontier of testing able to provide results capable to validate (or to create) more and more precise numerical models.

2.7 STAR CCM + ®

In this research, the software chosen to perform simulations is CD-Adapco Star CCM + [23]. It is a commercial code (CFDC) of multipurpose computational fluid dynamics ranging across a broad spectrum of fluid dynamics, from the combustion to multiphase flows.
It allows to create unstructured mesh based on hexahedrons, polyhedrons and tetrahedrons, then giving the chance to make mesh extrusions and to apply prismatic layers. As in other software of this kind, it is possible importing meshing files from other software.

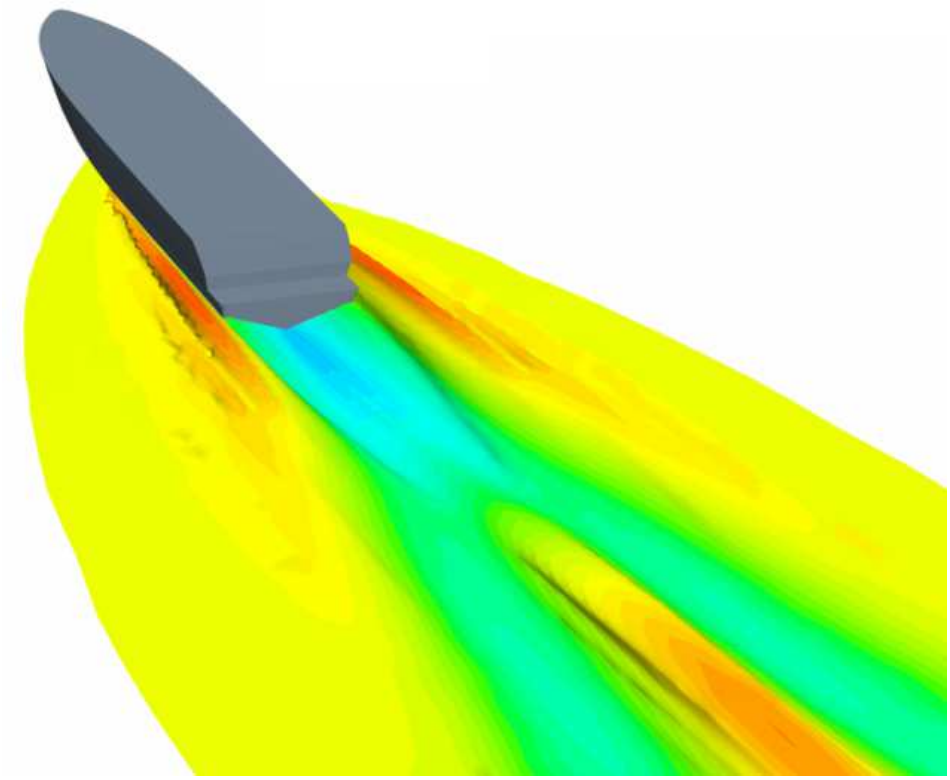

Fig. 2.5 - Planing simulation with Star-CCM + (Courtesy of CD-Adapco)

As for the highlights regarding the shipbuilding industry, it should be underlined that the program allows the computation in a perfect flow, both laminar and turbulent one, and in addition, it enables the motions' calculation and then of the trim using the 6-DOF form.
Moreover, trough a specific physical model, the transition phase from laminar to turbulent flow can be taken into account, too.

It has an intuitive user interface and it gives you access and data of interest viewing already during the processing of the same. Star CCM + is based on the finite volume method, which began as a special formulation of finite differences once.

It consists of several steps:

• integration of the problem equations on all finite control volume of the domain;

• discretization with the replacement of the problem integral equation terms with a series of finite difference approximations, with a consequent transformation of integral equations in a system of algebraic equations;

• solution of algebraic equations through an iterative method.

The first step - that is the integration into the control volume - distinguishes the finite volume method from other all CFD techniques.

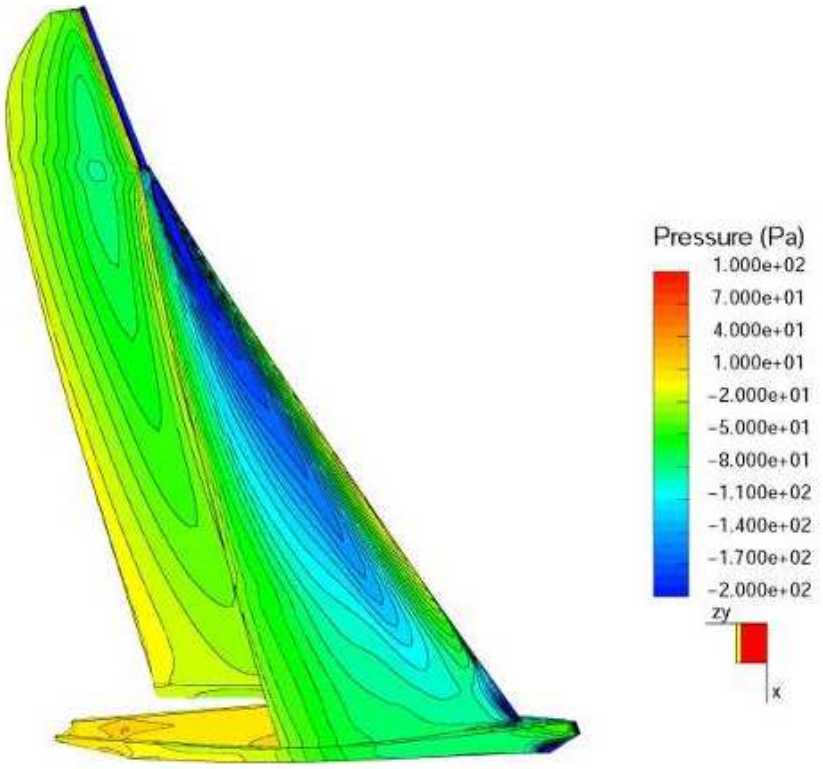

Fig. 2.6 - Sail system Analysis - Star CCM + (Courtesy of CD-Adapco)

2.7.1 Graphic interface and shipbuilding industry use

The user interface of Star-CCM +, although incredibly rich in tools, appears to be simple and intuitive. In the left side of the screen you can find typical "tree" design with pull-down menus

and submenus, and on the right side you have one or more windows displaying images or diagrams of the physical phenomenon under study.

To prepare a physical model you start by building a control volume and by importing the geometry of the hull to be tested (for example in *.iges* format). Through one repairing tool, you can fix any matching problems of surfaces. After that you can subdivide the hull in several areas (REPRESENTATION / SHELL menu); at this point from the menu CONTINUE/MESH you can choose the characteristics of meshing (base size, condensation in areas of interest, anisotropy). Once this is done, you can generate at first surface mesh and then the volume ones, through the appropriate commands on the toolbar. At this point, through the menu CONTINUE / PHISYCS it is possible to set the characteristic quantities of the phenomenon in question i.e. degrees of freedom (from DFBI menu), speed, mono or multi-phase mixture (water/air), generation of waves due to disturbance of the free surface. Also, in case of simulation with free model, you can reset a "ramp-time" in which the simulation begins with a fixed model and then the model is progressively left free to move.

Instead, from the menu SCENES you can set some views and/ or diagrams of the control volume and of what is going inside: you can for example choose to display the wave formation generated by the ship or the only mesh. From MONITORS menu you can set and monitor the physical quantities that you want to measure (and to diagram them through the menu PLOTS): for example, you can ask the software to measure sink, trim, lift and drag.

At this point, once defined the characteristic times and the value of the time step, you can launch the computation through the RUN command. At this stage, it is expected a saw-tooth trend of the diagram of RESIDUALS, to witness that the process works correctly, and that it is reaching convergence.

It's important to note that, step by step, Star-CCM + allows you to display the results of the phenomena examined, even during the computation. It also allows you to change the input values without stopping the calculation, which from that moment on will be calibrated on the new input. In the fig.2.7.3 it’s possible to see a typical screenshot of the Star-CCM+’ interface.

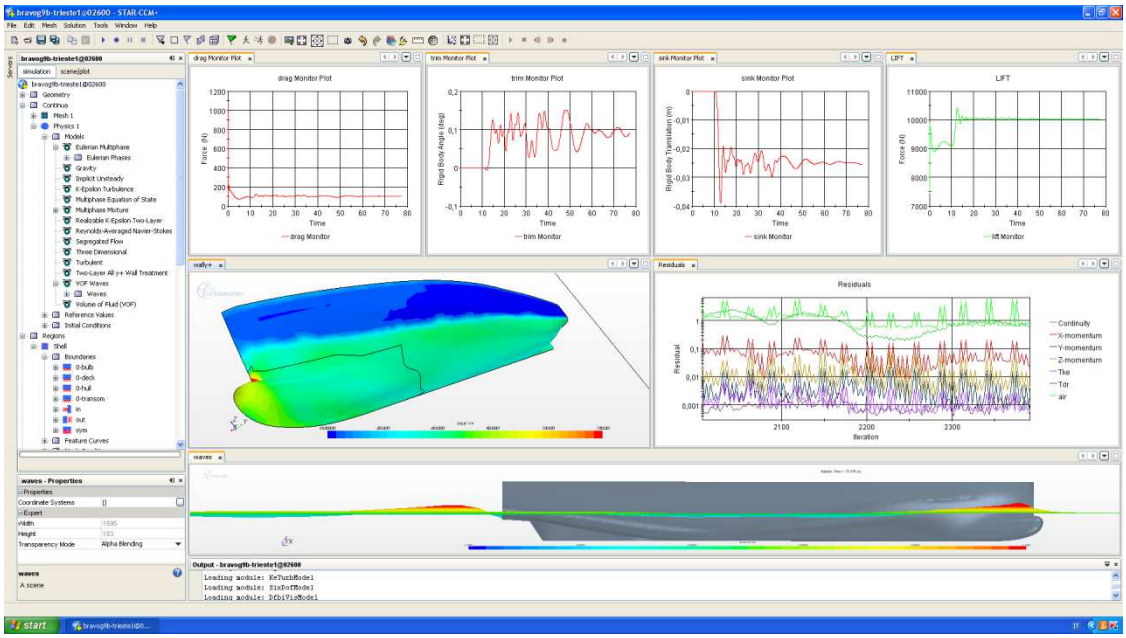

Fig. 2.7 - Star CCM + - Typical Screenshot of the graphic interface: on the left the characteristic drop-down menus, in the upper right corner notice respectively the graphs of DRAG, TRIM, SINK and LIFT; In the middle left area a perspective view of the boundary layer factor Wall Y +, middle right RESIDUALS trend showing the convergence of calculation; below a longitudinal view of the hull in motion.

DEVELOPMENT OF A METHODOLOGY FOR SIMULATIONS WITH LOW NUMBER OF CELLS

3.1 SIMULATION DATABASE AND METHODOLOGY ADOPTED

The aim of this work was to minimize the number of computational cells in order to reduce time and cost of simulations, preserving in any case adequate results. The simulations were performed with the software STAR CCM +, using the VOF method with deformable free surface and k-epsilon turbulence model.

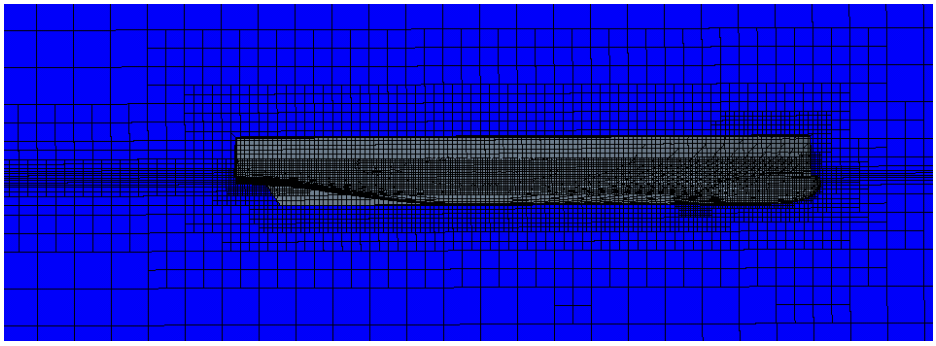

Fig 3.1 - Volume mesh thickened only where needed

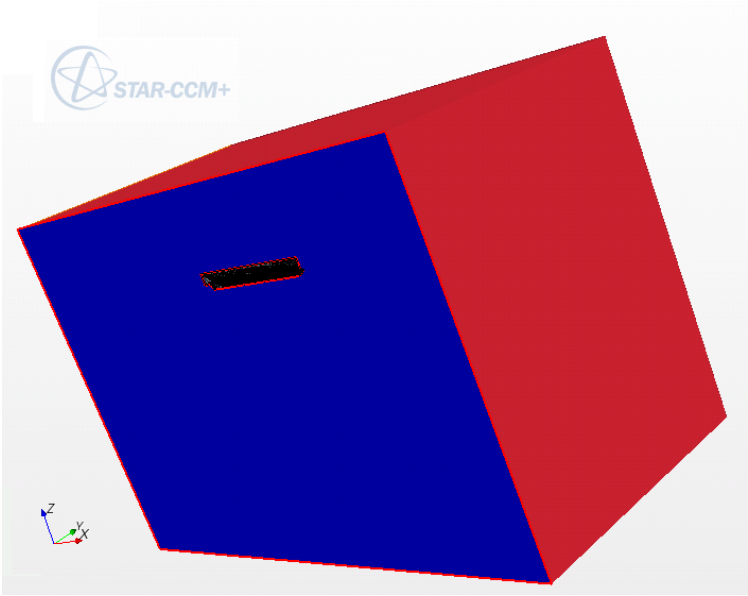

Fig. 3.2 - Volumetric control – Star CCM+

The computational domain used is made up of unstructured mesh to localized thickening (fig. 3.1). The created volume meshes are anisotropic, that is with the three typical sides of different lengths (and therefore the shape mesh is a parallelepiped and not a cube).

This, combined with correct thickening of meshing only on the necessary areas (boundary layer, eventual bulbous bow, the area of floating, triangular area of wake), allows to obtain a volumetric mesh model fairly "light".

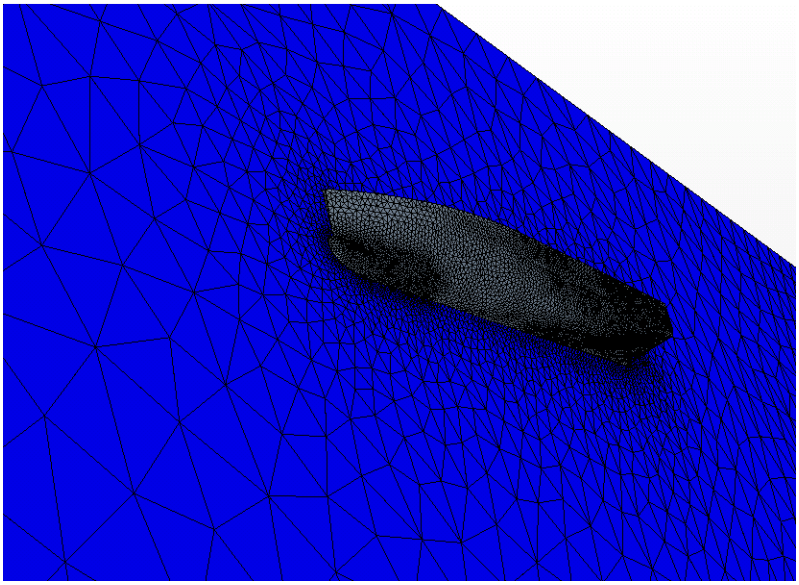

Fig. 3.3 - Surface meshing

To assess the possibility to reduce computing cells and to standardize a meshing procedure and analysis as much as possible, several simulations were performed on 41 different hulls of various geometries and with a range of operating speeds strongly different each other [24],[25]. Each type of hull simulation was performed at several speeds and different loading conditions, generating about 1250 cases of study database [26], divided in different groups (table n.3.1).

Table n.3.1 Hull database

HULLS	CONDITIONS	
15 displacement hulls	From 2 to 5 conditions of displacement and trim for each tested hull	From 8 to 10 speeds tested for each case
10 semi-planing hulls		
10 planing hulls		
6 semi-planing multihulls		

3.2 PHYSICAL CONDITIONS

To ensure close adherence to reality (as well as with the experimental cases taken as benchmarks) the calculations are carried out in three degrees of freedom to consider the ship advancing free to heave along the *z* axis and to assume trim rotations about the *y* axis.
The degrees of freedom inherent sway (translation along the *y* axis), yaw (rotation around the *z* axis) and roll (rotation around the *x* axis) were inhibited since they are not considered relevant for a ship advancing in calm water.
To speed up the calculations and to simultaneously facilitate comparisons with experimental data it was decided to proceed with the simulations in a hypothetical model scale. The resistance and the dynamic trim are evaluated during the phase of uniform rectilinear motion of the hull.

3.3 SURFACE AND VOLUME MESH

For the hull surface mesh, a different grid density is used for each area to maintain an adequate resolution of the involved geometries with an accurate representation of geometric details [27], though minimizing where possible, the number of elements, for instance in flat surfaces or where the curvature is large. In fig. 3.4 is possible to see the effect of the density gradient of the surface mesh in the bulbous area of the hull SL36 (see paragraph 4.1.5).

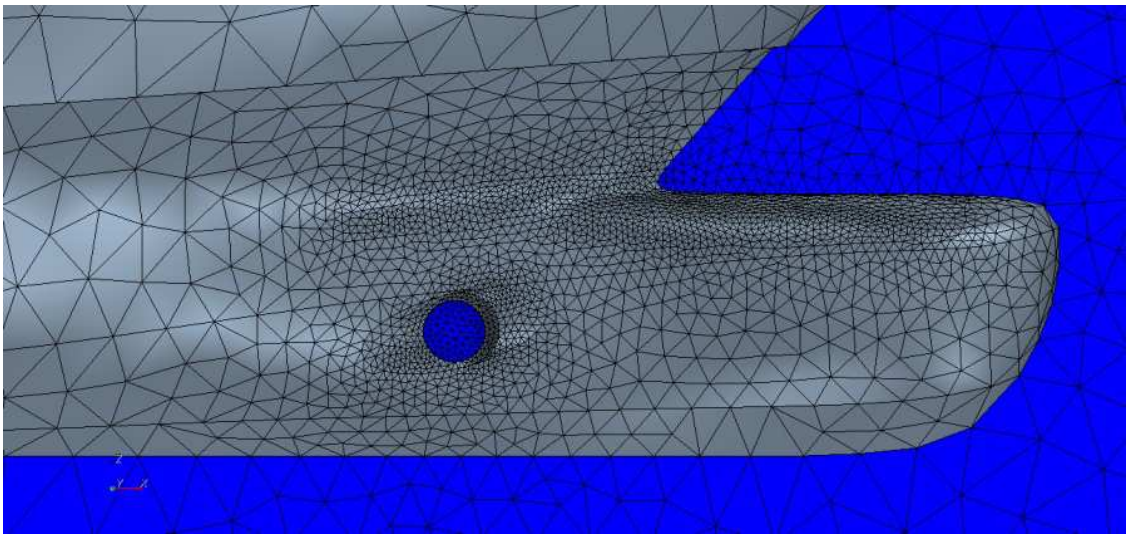

Fig.3.4 - Effect of hull surface mesh gradient

It was decided to use a coarse basic volume-mesh thickening through appropriate volumetric-controls only in areas of interest.

In particular, volumetric-controls of mesh thickness were created:

- around the hull
- around the upper portion of the hull
- near the free surface, in order to capture the wave pattern with adequate resolution.

As far as the free surface is concerned, a first volumetric control is created around the entire surface, with a higher anisotropic condensation along the z axis, to evaluate the geometry of the wave pattern without increasing too much the number of cells; a second volumetric control was created in the triangular area where we expect the wake. (fig. 3.5)

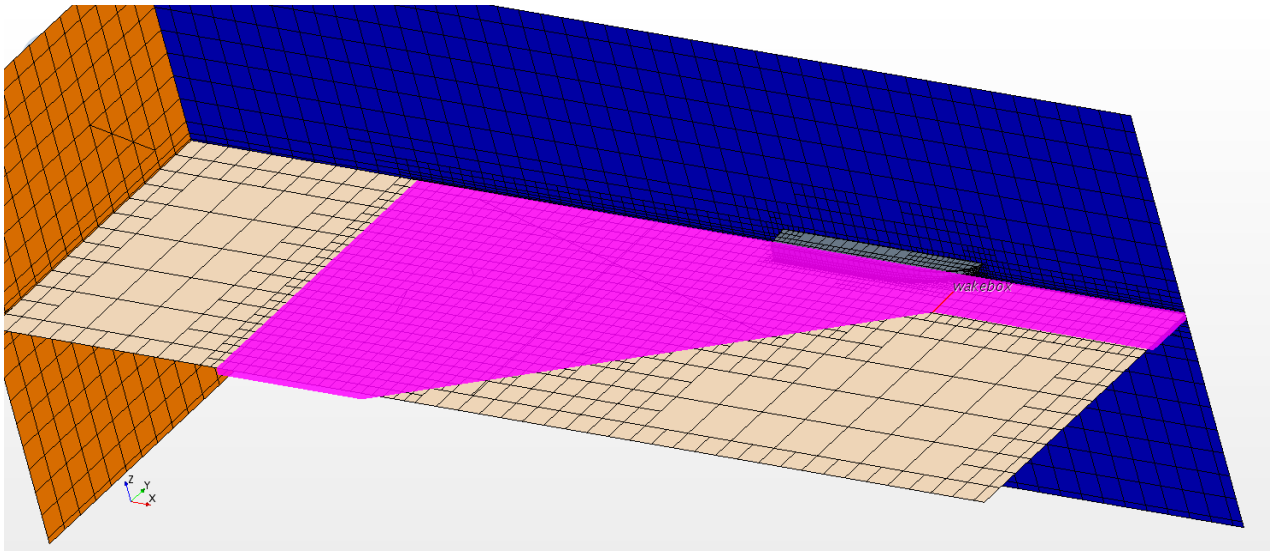

Fig.3.5 - Volume mesh: triangular volumetric control for wake analysis

3.4 FAMILIES OF HULLS

After having evaluated several solutions trying to catalog database simulations data, it was assessed that it is not possible the use of a single domain standard for all types of boats tested, at the expense of the inadequacy of the results of some of them, or worse at the expense of the divergence of other.

At the beginning it was decided to try to divide the hull groups only in relation of their similar Froude number's range. This allowed a standardization of physical set-up of the simulation but it wasn't so useful at it seemed at first because it was impossible to define an automated meshing system with a lot of different hulls (with or without immersed transom, with or without round bilge, with an high block coefficient and with a low one , etc..). Then, it was tried to divide the hulls families by similar geometry (i.e. round bilge shaped, hard-chine shaped, monohulls, multihulls, etc..).

This method proved immediately more effective for automated mesh standardization since it was capable to divide the hulls of the same group in about the same regions (eg. Transom, bottom, side, bulb, etc..), defining a mesh thickness and a mesh gradient for each surface. However this solutions didn't allow to create a standard grid because this solution was dependent on the boat speed too, particularly for the thickness of the boundary layer and for the mesh resolution able to capture the wake.

Therefore it was decided to divide the hulls not simply basing on the speed range OR on geometries but according to the geometrical differences AND to the same speeds range [28].

In fact, to outline the meshing procedure it was decided to consider three different hull families:

1) round bilge displacement hulls;

2) semi-planing hulls with round bilge or with chine; both for mono-hull and multi-hulls;

3) hard chine planing hulls.

Each of these families is featured by a similar geometry and by the same Froude number range. So a different type of grid is optimized to identify the peculiarities of the particular flow behavior typical of the family.

3.5 TYPES OF COMPUTATIONAL DOMAINS

Defined *L* as the length of the model, the computational fluid domain chosen is about

- 3.5-4*L* long
- 2.5*L* wide and
- 2*L* high (fig 3.6)

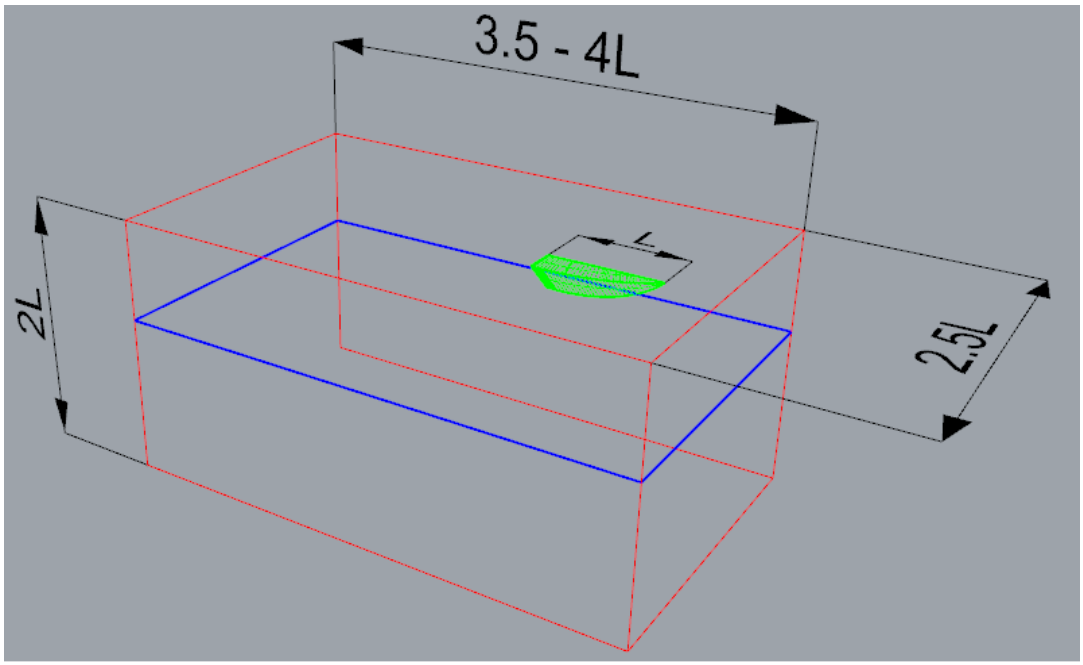

Fig.3.6 - Typical dimensions of computational domain

The volumetric controls mesh-size has different characteristics for each of the three families.
The peculiarities of the mesh are different depending on the characteristics of the vessels typical of each family. This, added to the difference in the magnitude of the measured phenomena, means that the computational domain requires a number of cells quite different depending on the family of the examined hull.
In fact, the features concerning phenomena acting on the hulls of each family are of different orders of magnitude. Particularly, considering the displacement boats, there will be very little changes of longitudinal trim as well as slamming linked to the generation of low pressure fields on the bottom but several gradients quite difficult to map. Also the wake produced by the boat motion will be developed on the vertical direction, in absolute terms, but it will have an extremely complex profile, with a multitude of peaks and small size hollows to be properly captured by the computing grid.
As for planing boats, higher longitudinal dynamic trim angles will occur. They are associated with raising phenomena definitely not negligible and caused by very high pressure on the hull bottom; instead, the wake will all be at the stern area of the boat, leaving its side almost completely dry; on the other hand there won't be small peaks and secondary hollows to catch but high and extensive waves with an easier profile.

This shows that the optimal meshing for a displacement hull consists in a densier mesh refinement strip near to the waterline level, in order to catch small and complex profile of waves. Instead for a planing boat it is necessary to adopt a less dense volumetric control but with greater thickness, also reasonably inclined to ensure that, once the boat has found its dynamic equilibrium trim, it does not spill out from the mesh, causing problems of solution stability.

3.6 BOUNDARY LAYER

For a proper computing convergence and especially for a correct evaluation of the frictional drag, it is essential to accurately model the area around the hull where the boundary layer is present.
Therefore it was decided to use particular volume meshes with prismatic shape. The boundary layer is well captured by the package of prismatic cells around the hull. It is very important to assess the total thickness of the package, the number of cells present in the package, the

thickness of each single cell and the possible gradient, that will be increasing moving away from the hull surface).

To be properly evaluated, the boundary layer must be completely contained within the package and the area of high velocity gradient must be captured exclusively into the first prismatic cell tangent to the hull.

The meshes optimized for planing hulls, provide three layers of prism meshes with a positive thickness gradient to 1.5.

For displacement hulls, from 5 to 8 layers of prism meshes with intermediate gradient of 2 are chosen (fig.3.7). Similarly, models for semi-planing hulls are midway between the other two.

The number and thickness of the prism layer, must also be consistent with the wall function and $y+$, which must always take values between 30 and 100 (fig.3.9) .

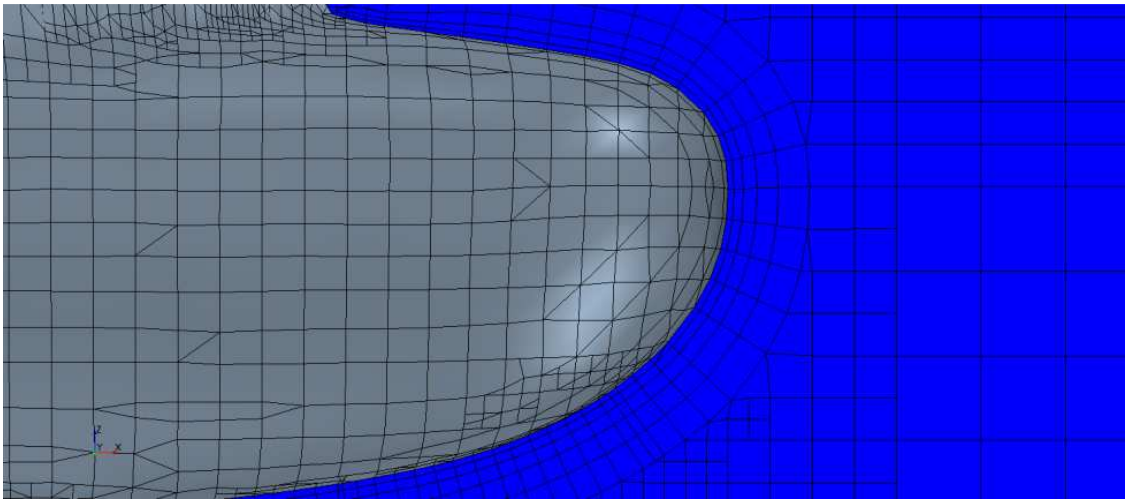

Fig. 3.7 - Prism layers on a bulbous bow (full displacement hull)

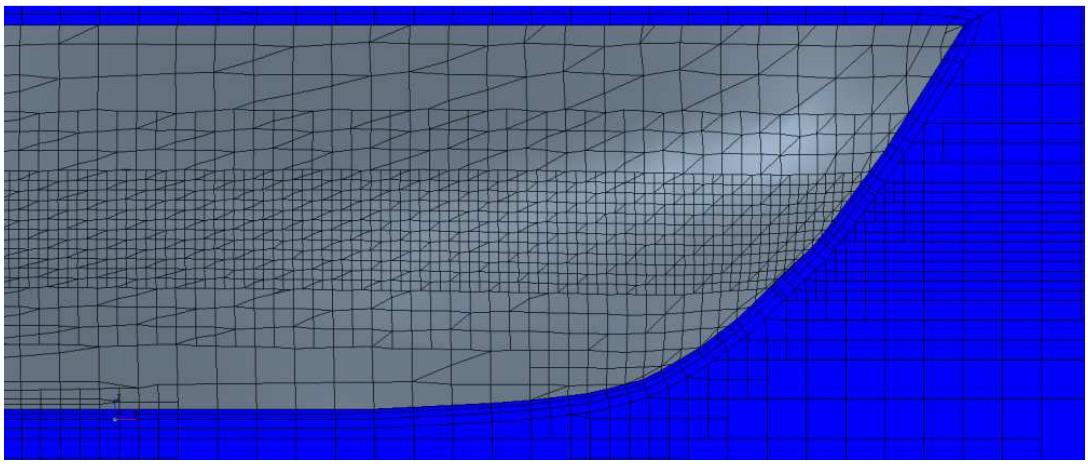

Fig. 3.8 - Prism layers on a bow (planing hull)

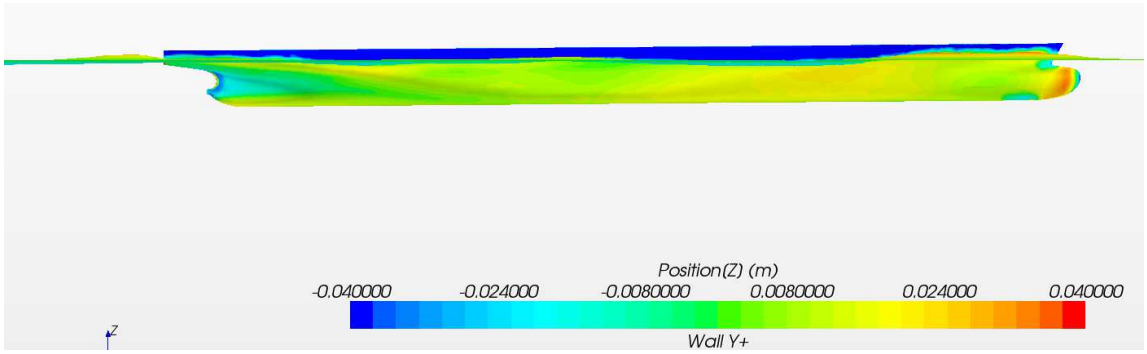

Fig.3.9 - Contours of Wall Y+ on KCS hull

3.7 COURANT NUMBER AND TIME STEP

The Courant number represents the ratio between the time step and the cell time. For “cell time” it is intended the time a fluid particle takes to pass through the smallest cell. For a correct physical analysis the number of Courant must always be less than 1 to ensure the right resolution of the behavior of the fluid in all the cells.

The implicit unsteady method allows the possibility to use the so called "fast transient" method. To further accelerate computational time, in this case is uses a time step higher than relative time of the cell, consequently with an higher order of magnitude of Courant number. This "fast-transient" method is valid only for that kind of motion simulations tending to converge in a correct way and which are not cyclic (for example the method is valid for resistance in calm water but it is not valid for seakeeping). In fact, the “fast transient” method loses the physical meaning of the solution during the transient calculation of each time step, while the calculated value at the end of each time step is trusted. In fact, normally the Courant number lies within the interval [0;1], in this case lies within the interval [1;10].
In this way, the computer time is strongly reduced. Obviously, this simplification is feasible only for cases that may be considered steady, as the calculations of resistance in calm water and the dynamic trim optimisation.

3.8 CONVERGENCE OF SIMULATIONS

To evaluate the resistance of a displacement hull, to analyze the pressure field on the bottom and to assess the generated wave pattern, computational models with domain of about 2 million cells are typically required.

After having identified the thickening required for each family type hull (all each other connected to a basic size of the base cell of about 20% of the length of the boat), it has been carried out to enlarge the cells gradually, thus reducing their total number, ensuring the convergence of the simulation and then consequently finding the limit of grid independence beyond which the simulation loses its physical meaning.

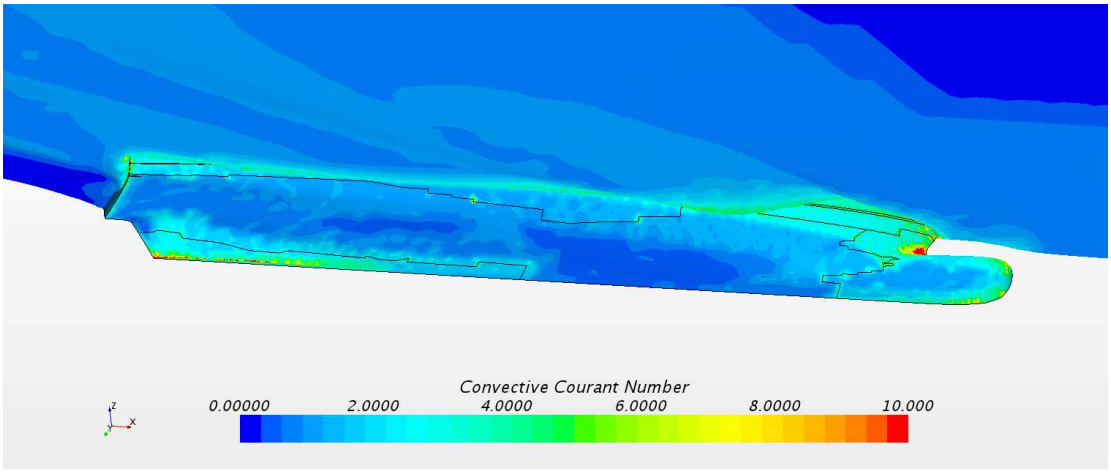

Fig. 3.10 - Contours of Courant number on a the hull and on the free surface

The convergence is tested using analysis of residual diagrams stationarity (fig.3.11) and it is achieved by means of degrees of freedom gradual release of trim and sink in order to allow the simulation settling even with low numbers of cells. In the procedure used, the first 2 physical seconds of motion have been developed with only one degree of freedom (advance in *x* axis). Afterwards it was released the possibility of rotation around the y axis (trim angle), not in a pulsed way, but in a gradual one to an additional two seconds of simulations, and only afterwards it was released the third degree of freedom related to the vertical raising.

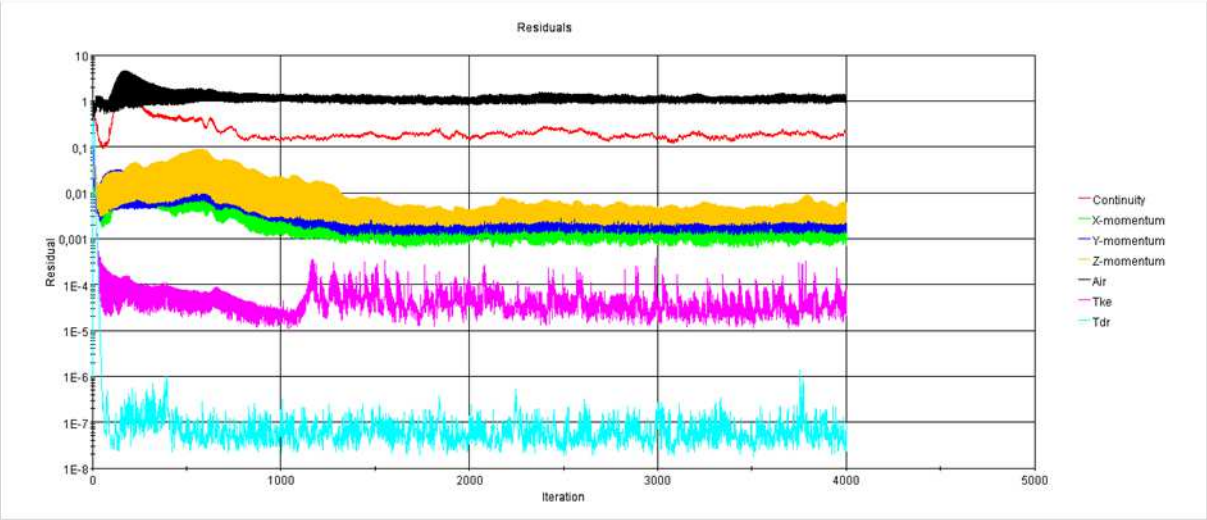

Fig. 3.11 - Residual analysis

The proper simulation convergence is evaluated both regarding the equations of continuity that in relation to the boundary conditions related to the management of turbulence models, particularly (having performed, in the second phase of the research, the optimizations focused to reduce the total resistance).

By testing grid convergence, it has turned out from the methodology applied in this study that domains of approximately 400,000 cells may be already adequate .

As far as the calculation models for semi-planing hulls are concerned, generally they are based on domains with at least 800,000 cells; in this case a model with approximately 280,000 cells has been used.

Finally, it is known that the domain representations for viscous flow of planing boats are lighter and require less cells than for displacement hulls. Also in this case a drastic reduction has been shown as possible leading from standard models of about 500,000 cells to models of 80,000 cells (table 2).

In order to validate the reduction cells procedure, tested on 1250 different cases, about 5% of these cases were selected in a random way and they have carried out through conventional procedure with a very high number of cells with use of computer center (about 4 million cells on displacement hull, twice plus of standard case) to check correspondence of the outcome. It is observed a discrepancy variable between 1 and 2.5%, but always in observance of the curves trend of the measured resistance.

Table 3.2. Comparison between standard domains size and case studies domains size

Hull type	Cell numbers		Percentage of reduction
	Standard domains	Case studies	
Displacement	2M	400k	80%
Semi-planing	800k	280k	65%
Planing	500k	80k	84%

3.9 CONCLUSIONS

Summarizing, 3 standard domains (plus a variant one for multihull) have been developed. They were featured by a preset volumetric control to run simulations in scale model on displacement boats, semi-planing and planing ones. It has been turned out that the abovementioned standard grids, in which to insert the 3D hull shape without readapting the mesh thickness, are quite functional: they lead to a proper convergence and they have a very small discrepancy (~ 1.5%) compared with calculations at high resolution and, however, a good approximation in absolute value compared to benchmark values from the literature and / or measured experimentally (see Chapter 4). It has also been noted that needing to use the grids to compare two or more of these solutions, they give a comparative result with an error margin below 1%, making it then particularly useful to such kind of of simulation, rapid in the early stages of the project. This validates the possibility to use this kind of simulations in a case of numerical optimization with a consequent good reliability of the results.

STANDARDIZATION OF THE PROCEDURE TO REDUCE THE NUMBER OF CELLS: PECULIAR CASE STUDIES

The cells' reduction procedure was standardized and strengthened also through some benchmark points with data found in literature and/or experimental results (tank testing). According to this, few examples of the results obtained with several boats, belonging to three families of hulls investigated, are shown.

As can be seen, despite the extreme diversity of boats the absolute results obtained are very respectable; also in cases where the discrepancy between simulation and experimentation tends to increase, however, the trend and the resistance curve shape are observed. This means that, in case of comparative analysis, errors potentially present in the analysis, being of the same sign and of equal magnitude, are deleted (within a tolerance of about 1.5%).

4.1 FAMILY 1 – ROUND BILGE DISPLACEMENT HULL

4.1.1 KCS Containtership bare hull

One of the first hulls on which the standard procedure with a low number of cells was tested was the displacement ship Kriso KCS containership. This hull was chosen because it has been

the subject of numerous numerical studies [29]. In additions, experimental results were made available.

Before starting to evaluate the use of the procedure, some tests on the KCS ship with 2.5 million of cells domain were performed, correctly convergent with tolerances of about 1.5% compared to the data available in literature. In order to reduce the number of cells and to obtain a mesh of 400k cells, a scale factor λ = 63.20 was chosen, which is twice of that traditionally used (λ=31.60). This was the first hull tested and the method was still to refine. However, an adequate shape of the C_R curve has been found also in the present CFD application, with an average error of only 7% as shown in table 4.1.

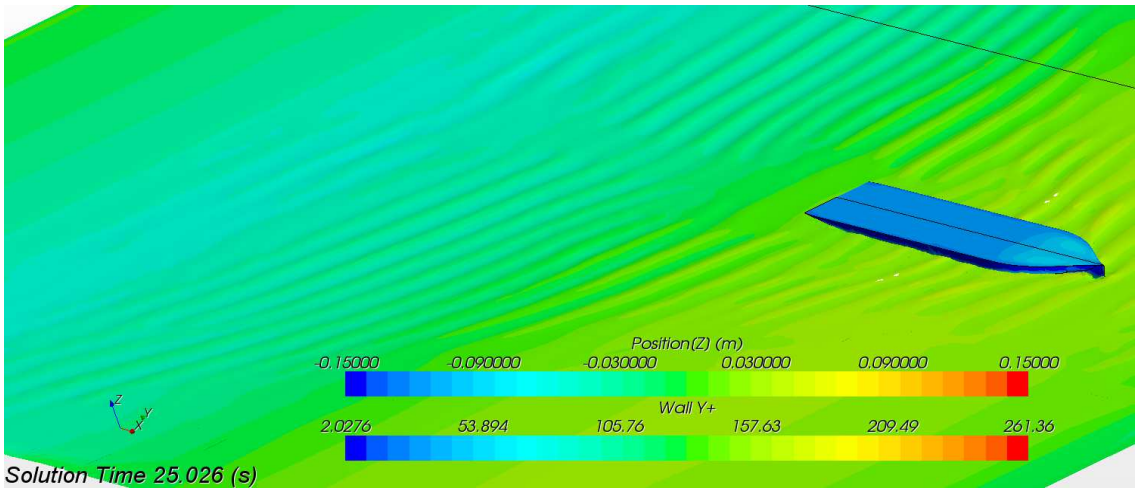

Fig. 4.1 - KCS at Fr 0.14

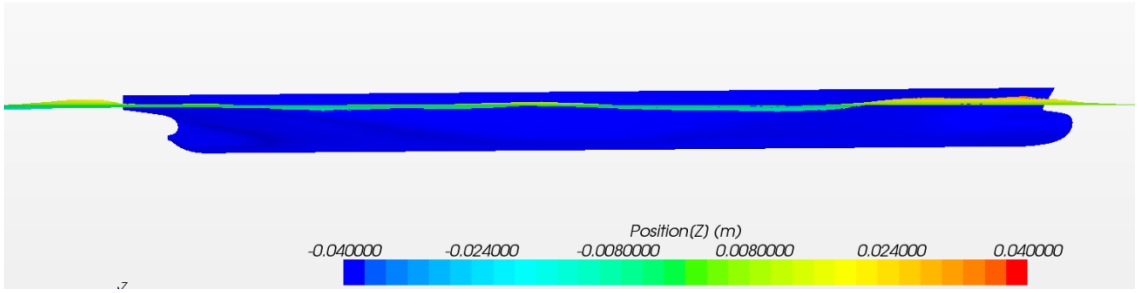

Fig. 4.2 - KCS at Fr 0.14 – wave pattern

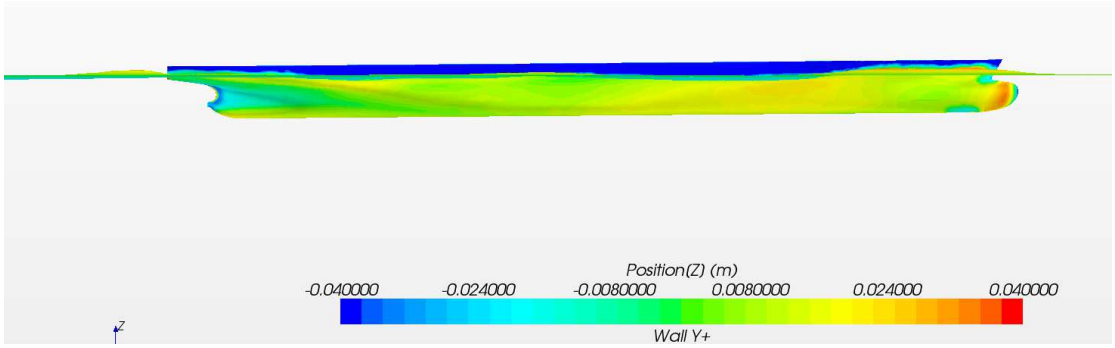

Fig. 4.3 - KCS at Fr 0.26 – wave pattern

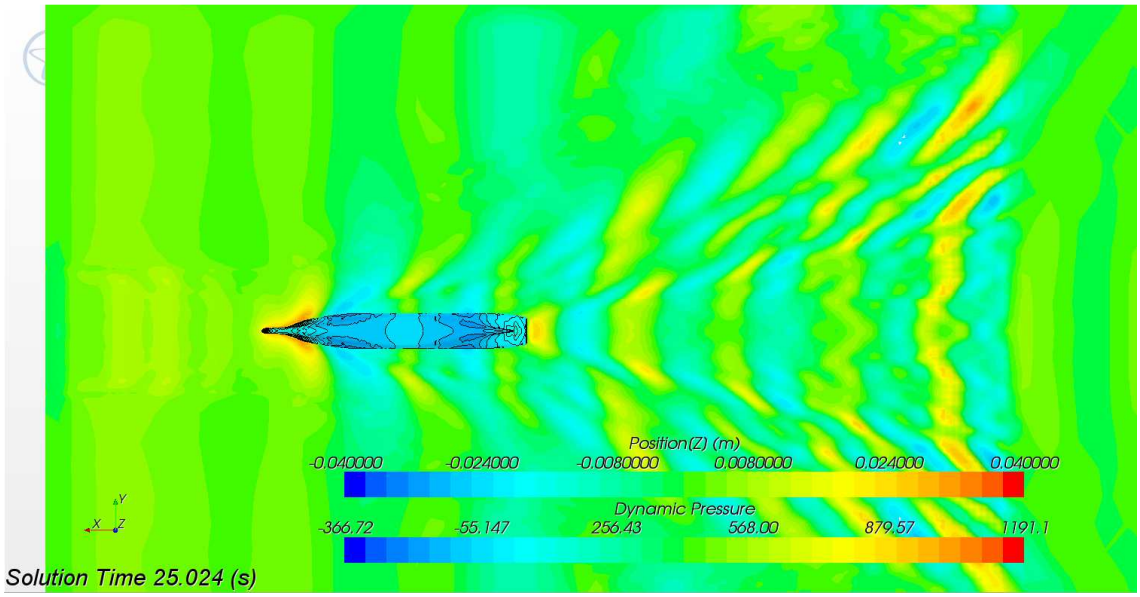

Fig. 4.4 - KCS at Fr 0.26 – wake analysis

Table 4.1 Comparison between public KCS data and CFD calculations

Run	Fr	10^3 C_R KCS	10^3 C_R CFD	C_R CFD / C_R Tank %
1	0.08	0.50	0.47	-6%
2	0.12	0.61	0.51	-16%
3	0.13	0.65	0.62	-5%
4	0.15	0.72	0.75	3%
5	0.18	0.68	0.62	-8%
6	0.19	0.61	0.54	-11%
7	0.21	0.61	0.57	-5%
8	0.23	0.70	0.67	-4%
9	0.25	0.91	0.85	-6%
10	0.28	1.30	1.35	4%

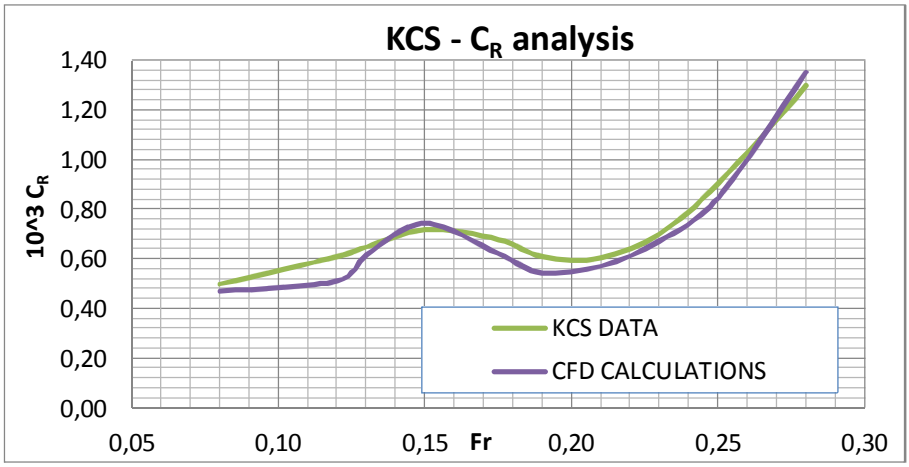

Fig. 4.5 - C_R comparison between public KCS data and CFD calculations

4.1.2 Round bilge bare hull SL42

As for the family of displacement boats, numerous simulations on different hulls have been carried out; as a first example the results obtained on the SL42 bare hull are provided below.

This is a 42metre motor-yacht hull, full displacement hull with round bilge and bulbous bow (see fig. 4.6 and 4.7).

For this hull tank test results performed at University of Naples are available [30].

Regarding this hull, we were able to get an optimized model of about 320k cells, which led to good results, reducing the average difference between CFD and tank test to 4.8% (table 4.2, fig.4.10).

Fig. 4.6 - SL 42 at 16kn – Profile view

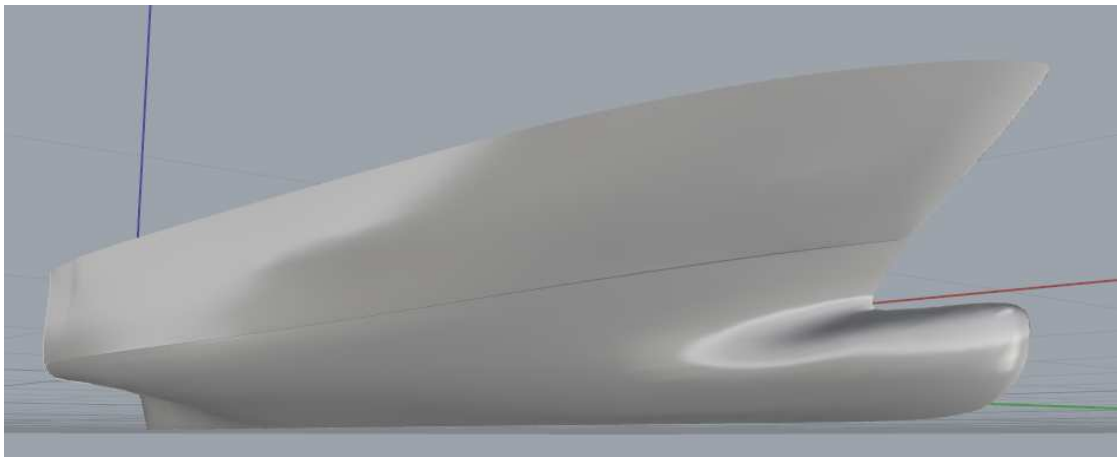

Fig 4.7 - Perspective view of SL42 bare hull.

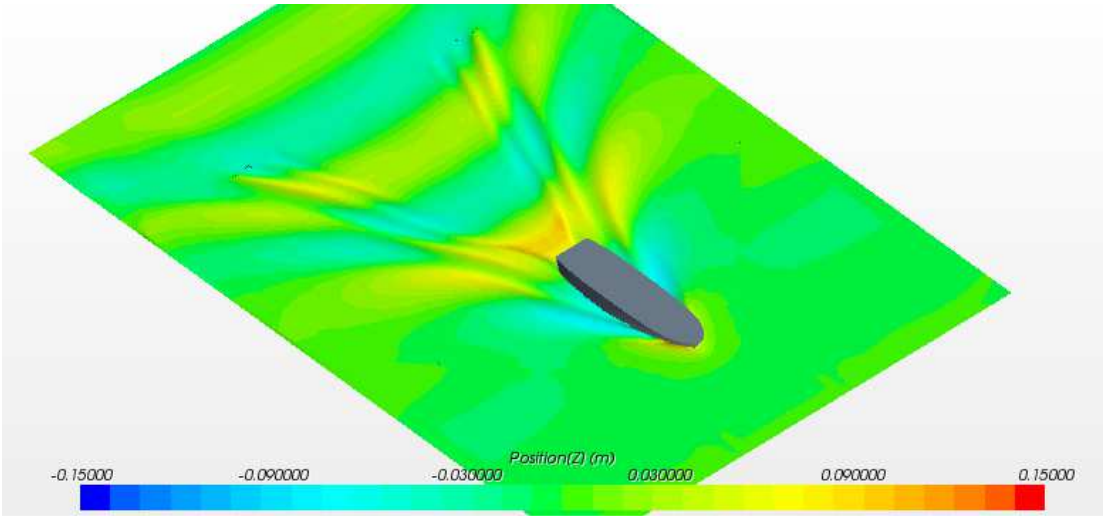

Fig 4.8 SL 42 – Wave pattern at 16kn - perspective view

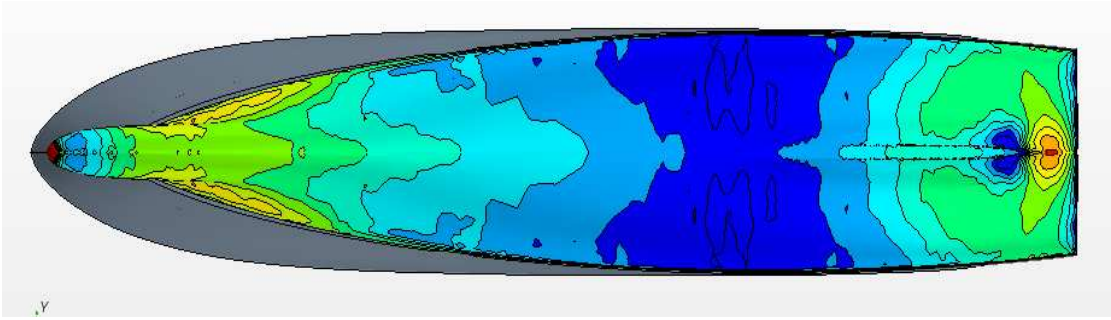

Fig 4.9 SL 42 –Pressure field on the bottom at 16kn

Table 4.2 Comparison between SL42 bare hull tank test and CFD calculations

Fr	10^3 C_R Tank	10^3 C_R CFD	C_R CFD / C_R Tank %
0.2	0.82	0.828	0.90%
0.25	0.763	0.732	-4.00%
0.28	0.764	0.711	-6.90%
0.3	0.821	0.769	-6.40%
0.35	0.918	0.86	-6.30%
0.38	1.048	0.978	-6.70%
0.41	1.237	1.184	-4.30%

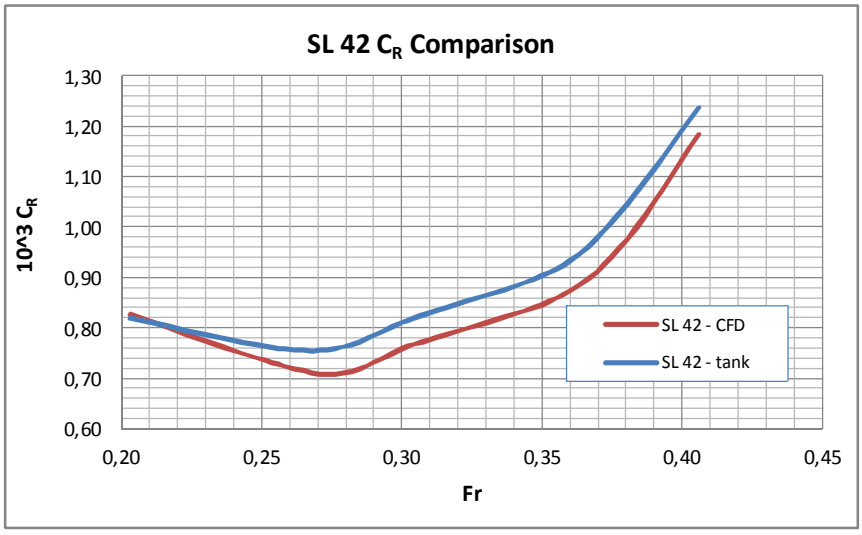

Fig 4.10 - C_R comparison between SL42 CFD calculations and tank test performed at Naples

4.1.3 AP1-40 Round bilge hull

Several other simulations were performed on a displacement hull with slim bow without bulbous called Ap1-40. This hull is a motor yacht of 40 metre and tank test results performed in University of Trieste are available [31]. These simulations, with a computational domain of approximately 350k cells created through the standardized procedure, led to resistance values different from those measured in the towing tank on average by 2.8% (fig. 4.13).

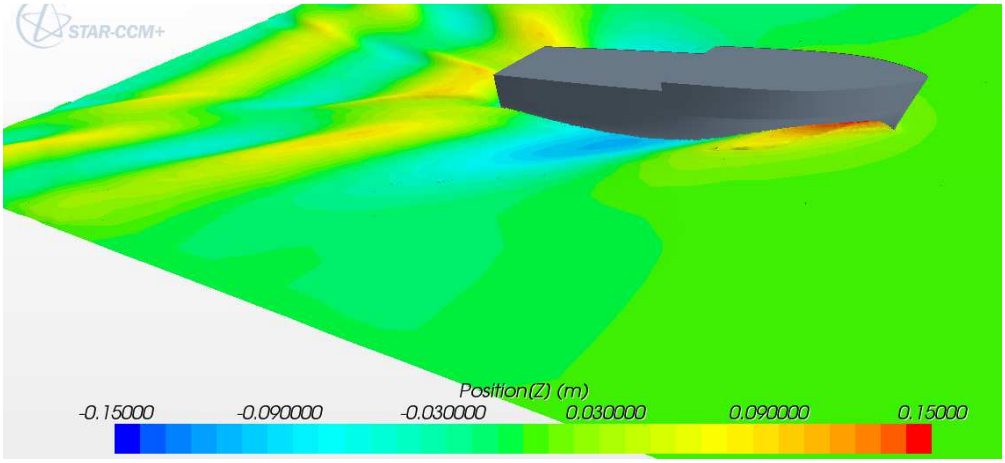

Fig 4.11 - AP1-40 during navigation at Fr 0.30

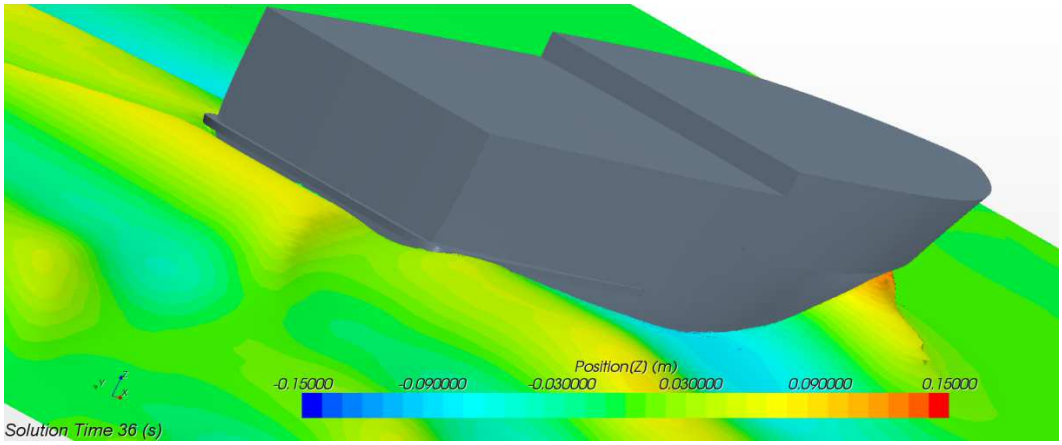

Fig 4.12 - AP1-40 view from stern

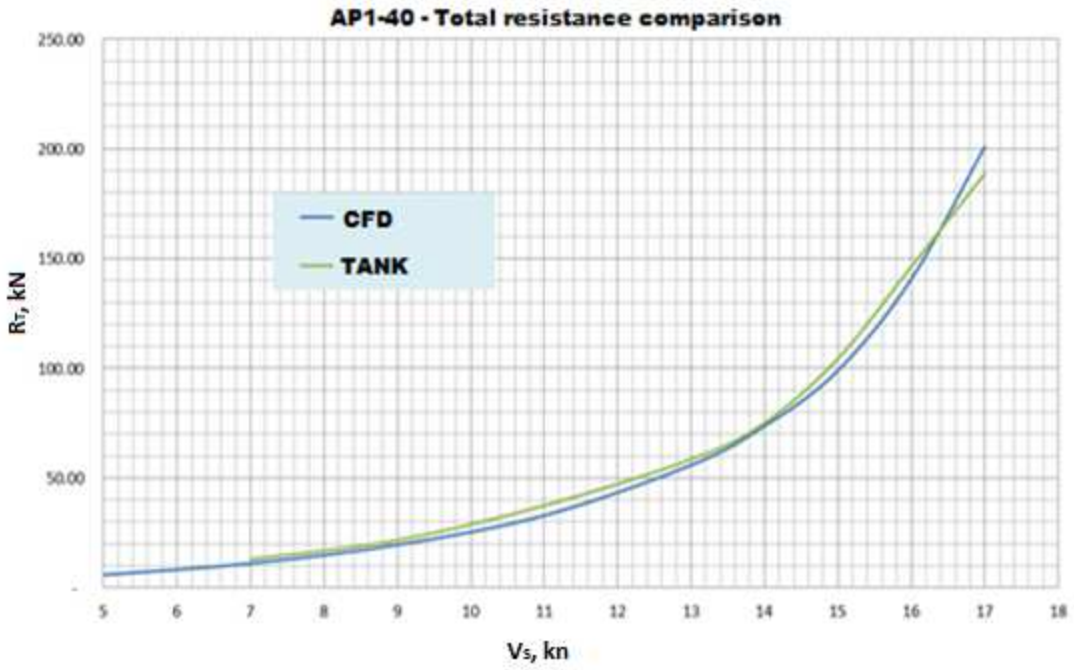

Fig 4.13 - Comparison of resistance curves of AP1-40 hull

4.1.4 Ap2-40 Round Bilge hull with bulbous bow

.Also the ap2-40 hull was tested. It was quite geometrically similar to its sister ap1-40 but it was equipped with bulbous bow. Also in this case tank test results performed in University of Trieste are available [32]. The results were very good in this case too, with average error of about 2% compared to the tank test one (fig. 4.15).

For this hull, just for an example it has been shown the trim angle in order to emphasize how the physical correspondence of the simulation with low number of cells is however verified (fig. 4.16). In the fig. 4.17, 4.18, 4.19 is possibile to see the dynamic pressure coefficient at Fr 0.3.

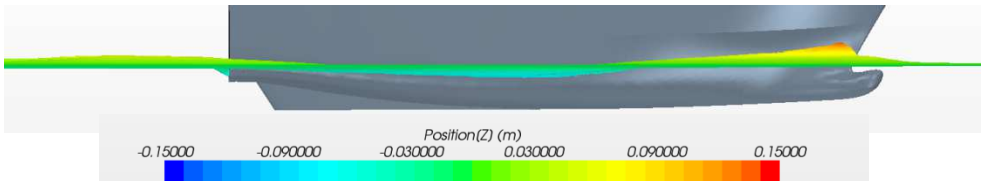

Fig 4.14 - AP2-40 hull , view profile at Fr 0.3

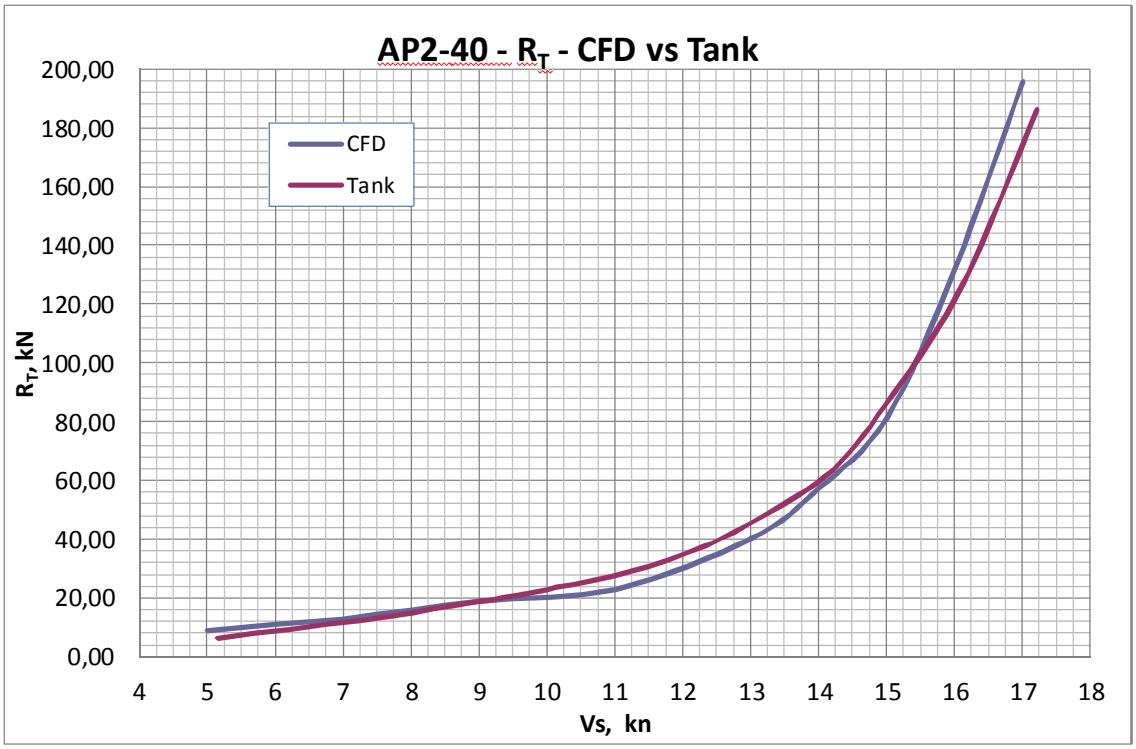

Fig 4.15 - Total resistance curves of AP2-40 hull

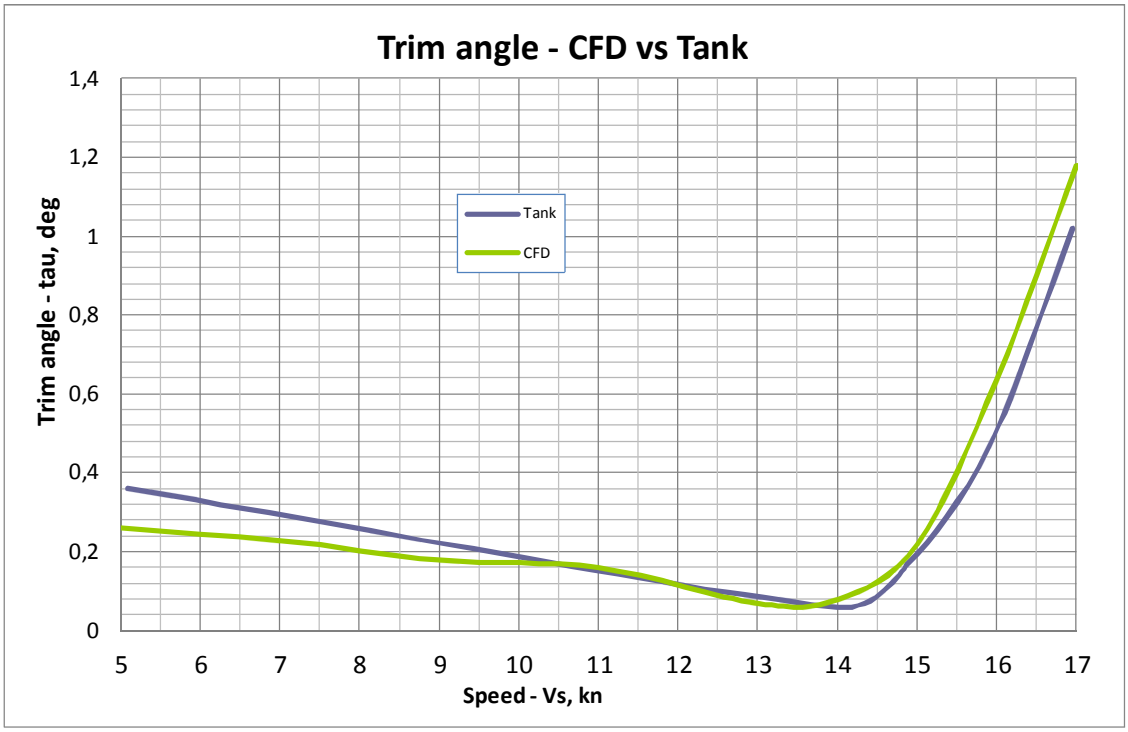

Fig 4.16 - Trim angle for the AP2-40 hull

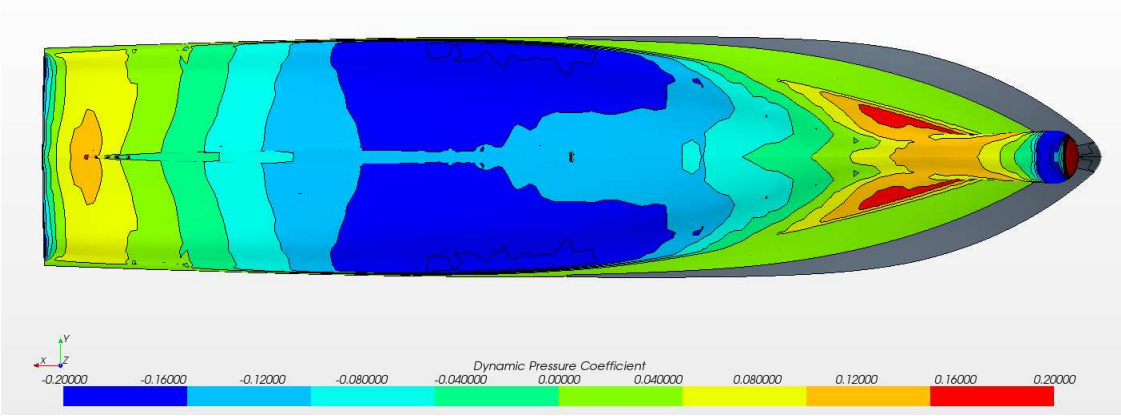

Fig 4.17 - Dynamic pressure on the bottom of the AP2-40 hull at Fr 0.3

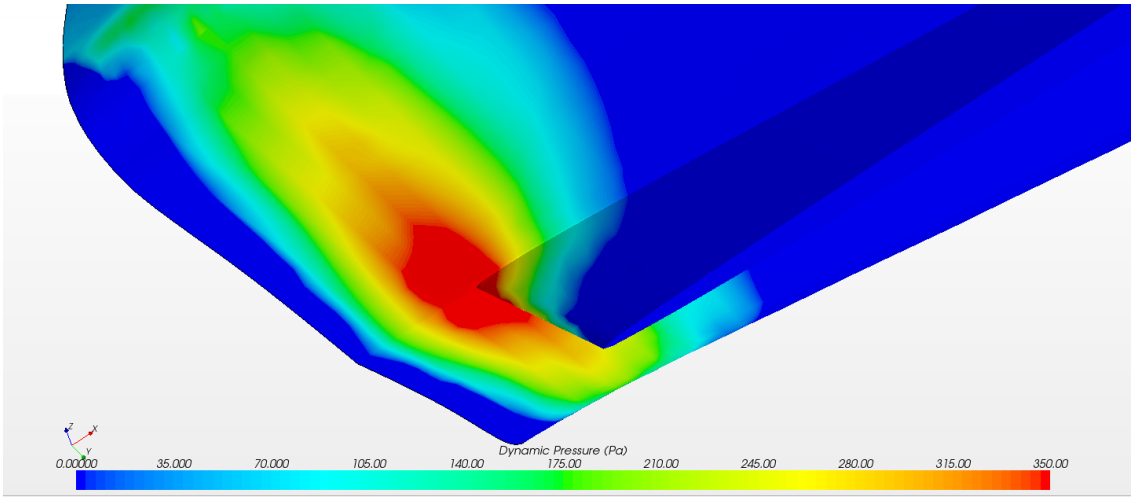

Fig 4.18 - Dynamic pressures on the stern (trim wedge area) AP2-40 hull at Fr 0.3

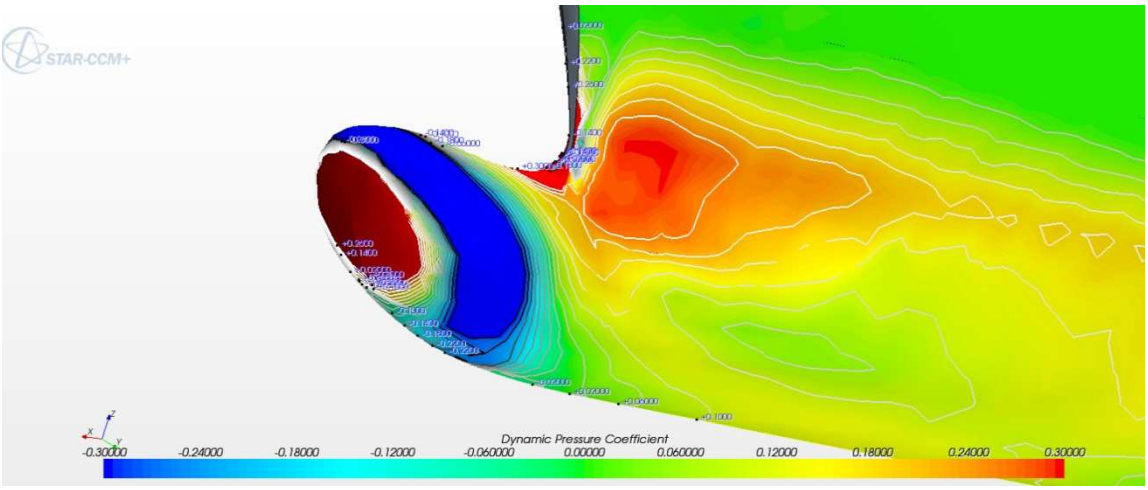

Fig. 4.19 - Dynamic pressure on the bulbous bow for the AP2-40 hull at Fr 0.3

4.1.5 SL 36 full appended hull

Some simulations have been performed trough the standard procedure adopted on a complex displacement hull for a maxi-yacht, for which the experimental results from a towing tank were available. The hull has a bulbous bow and a stern skeg. All the hull appendages, such as rudder, brackets, 0-speed fin stabilizers, bow thruster tunnel, have been considered.

Despite this complexity, we were able to get an optimized model of about 380k cells, which led to excellent results, reducing the average error up to 2.8% (table 4.3, fig. 4.22).

Also in this case, in order to validate the procedure, the results related to the trim are shown. The tank results performed in University of Naples are available [33] for bare hull and for appended hull but with the addition of the intruder. Instead, the hull tested in CFD is the appended one but without intruder: the trim angle results are in fact much more similar to those of bare hull just because there isn't the bow-down effect due to the intruder (fig.4.23).

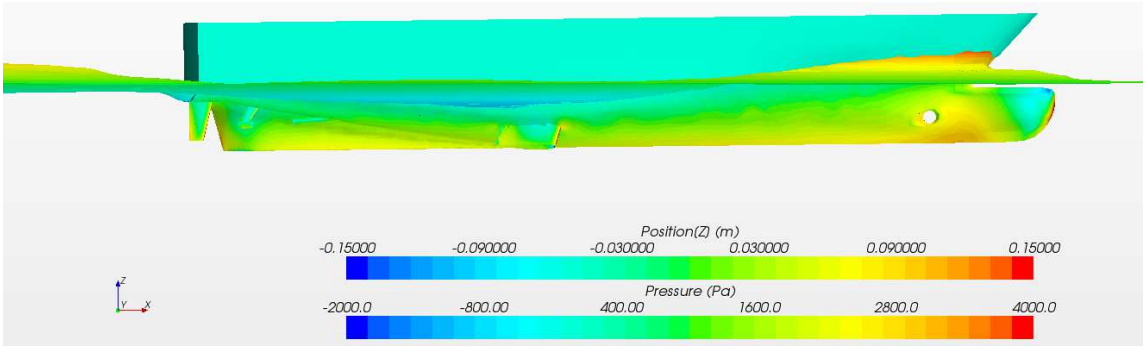

Fig 4.20 - SL 36: wave pattern and pressure field, profile view at Fr 0.28

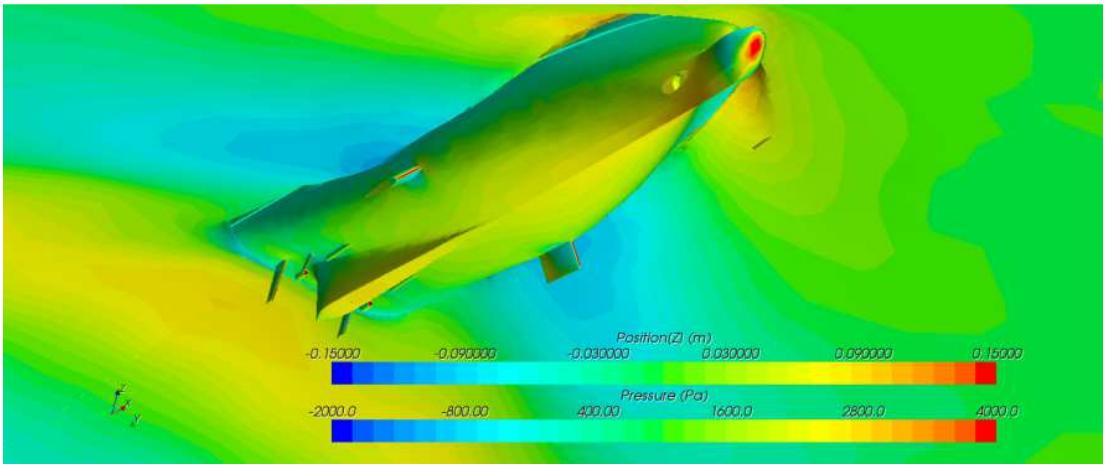

Fig. 4.21 - SL 36: wave pattern and pressure field, bottom view at Fr 0.28

Table 4.3 Comparison between SL36 tank test and CFD calculations

SL 36			
Fr	**10^3C_R tank**	**10^3 C_R CFD**	**C_R CFD / C_R tank %**
0.30	3.75	3.59	-4.3%
0.41	10.50	10.11	-3.7%
0.44	13.18	12.93	-1.9%
0.47	14.75	14.97	1.5%

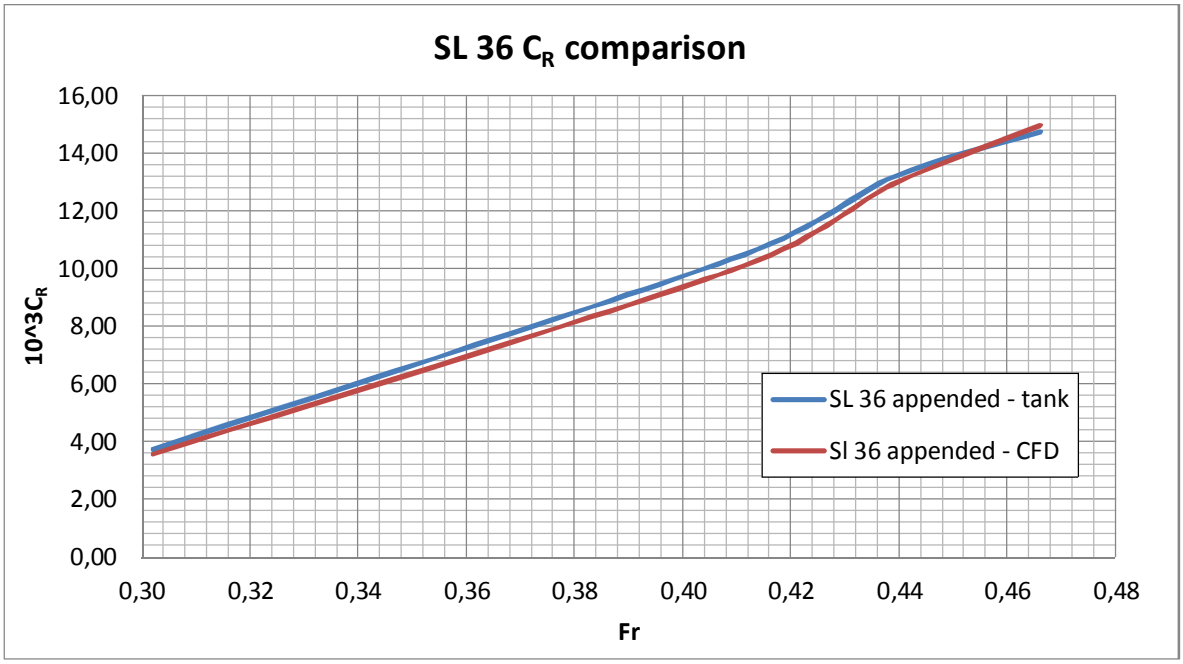

Fig. 4.22 - C_R comparison between SL36 tank test and CFD calculations

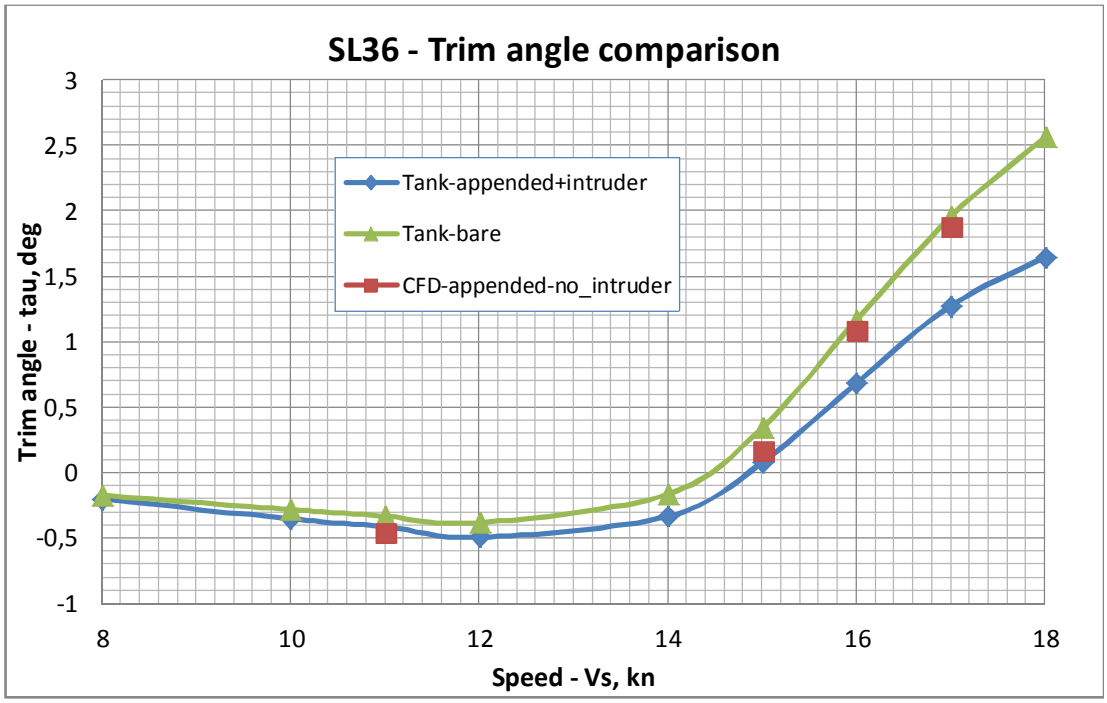

Fig. 4.23 - Dynamic trim comparison between SL36 tank test and CFD calculations

4.2 FAMILY 2 - ROUND BILGE SEMIPLANING HULL (SINGLE AND MULTI-HULL)

4.2.1 NPL series

For the semi-displacement and semi-planing family numerous tests on hulls belonging to the NPL series (fig. 4.24), also studied by other researchers [34],[35],[36], were carried out simulating the behavior of almost all models of the series. Performing tests in the same model scale of the tank experiments, the meshes employed in the computations for this type of hulls do not exceed in any case 270-280k. As an example, the results obtained with y_B=5.41 and y_B=6.25 models are provided below. The main data of the models are available in table 4.4 and 4.5.

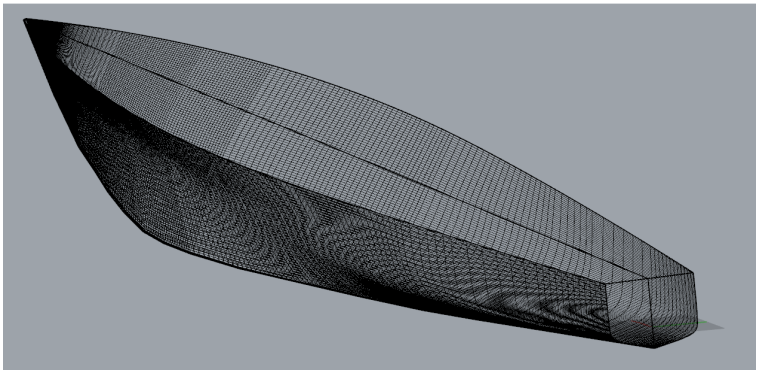

Fig. 4.24 - 3D model construction of the NPL 5.41.

Tables 4.4 and 4.5 Geometrical characteristics of NPL hulls

NPL 5.41	
L, m	3,84
B, m	0,71
L/B	5,41
∇, m^3	0,20
S, m^2	2,40
(M)	6,90

NPL 6.25	
L, m	3,84
B, m	0,61
L/B	6,25
∇, m^3	0,17
S, m^2	2,08
(M)	6,90

In the following figure (Fig. 4.25) it's possible to see the typical wave pattern for the model the model 5.41. The residual resistance results are given in table 3. They show that, though using a low number of computational cells, the shape of the C_R curve has been found also in CFD, with an average error of 5.8% (table 4.6, fig. 4.27, 4.28, 4.29).

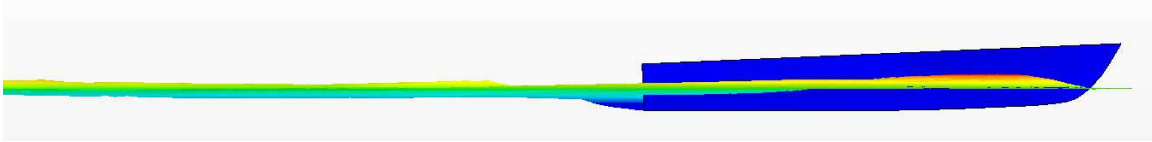

Fig. 4.25 - Wave pattern of NPL 5.41 at Fr 0.79

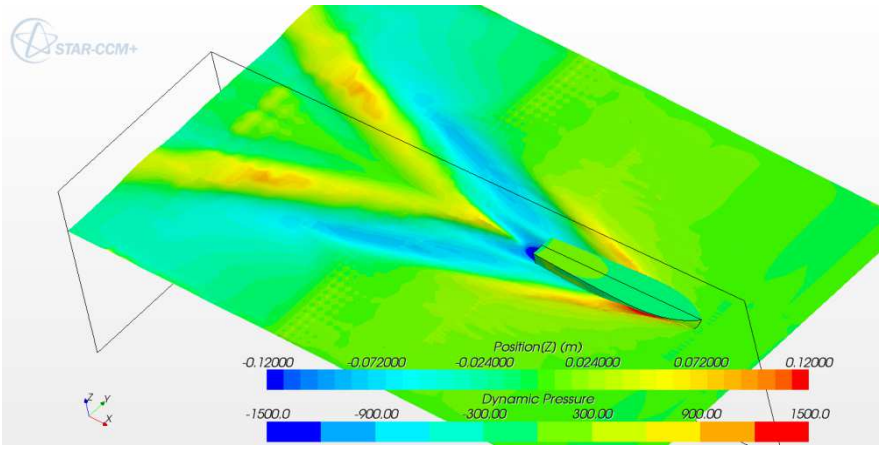

Fig. 4.26 - Wake of NPL 5.41 at Fr 0.79

Table 4.6 Comparison between NPL series data and CFD calculations

NPL 5.41					
V_M	**Fr**	**Fr_∇**	**10^3 C_R NPL**	**10^3 C_R CFD**	**C_R CFD / C_R Series %**
0.80	0.13	0.34	7.71	7.28	-6%
1.61	0.26	0.67	4.18	4.49	8%
2.41	0.39	1.01	5.14	5.59	9%
3.21	0.52	1.34	7.23	7.13	-1%
4.82	0.79	2.01	4.85	4.45	-8%

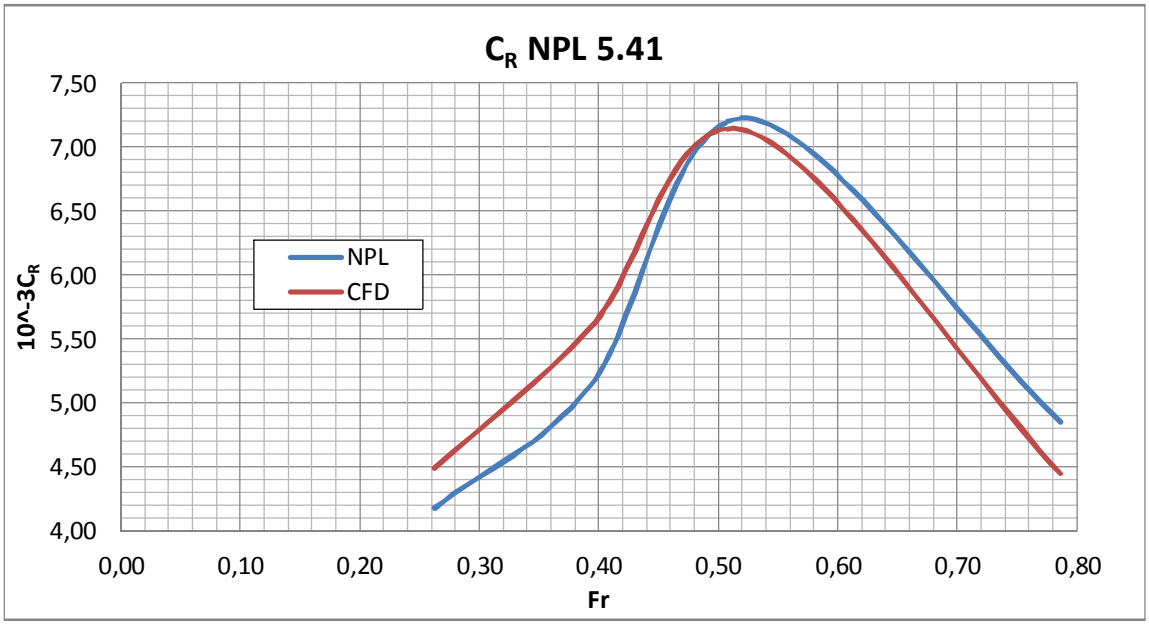

Fig. 4.27 - C_R comparison between NPL series data and CFD calculations

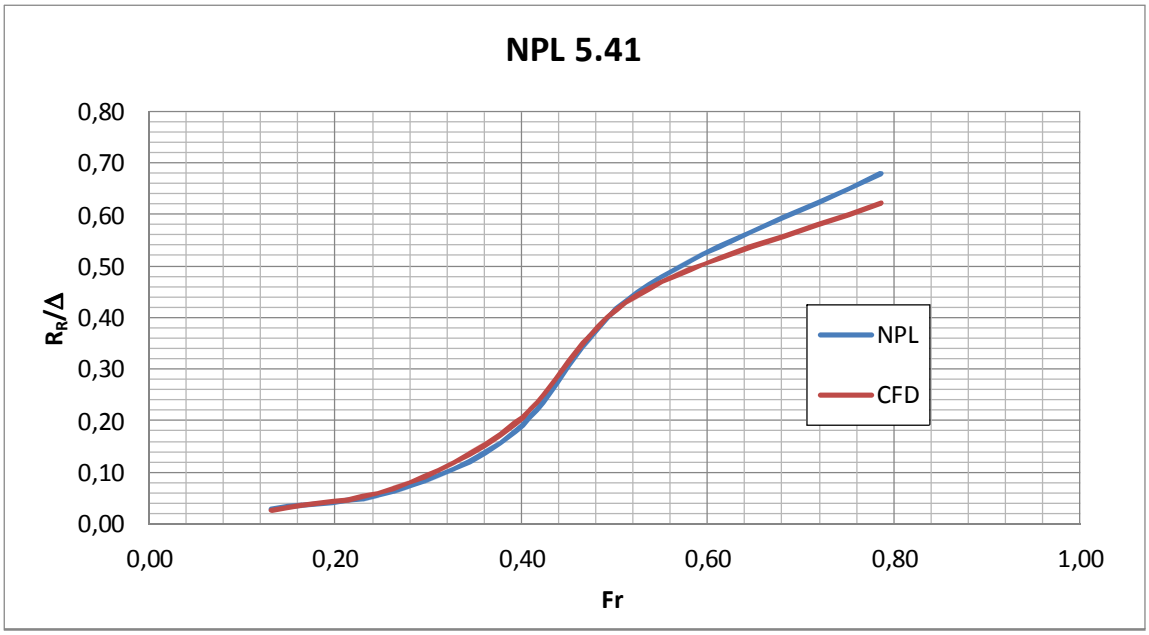

Fig. 4.28 - Comparison between R_R/Δ of the series and R_R/Δ of CFD (mod 5.41)

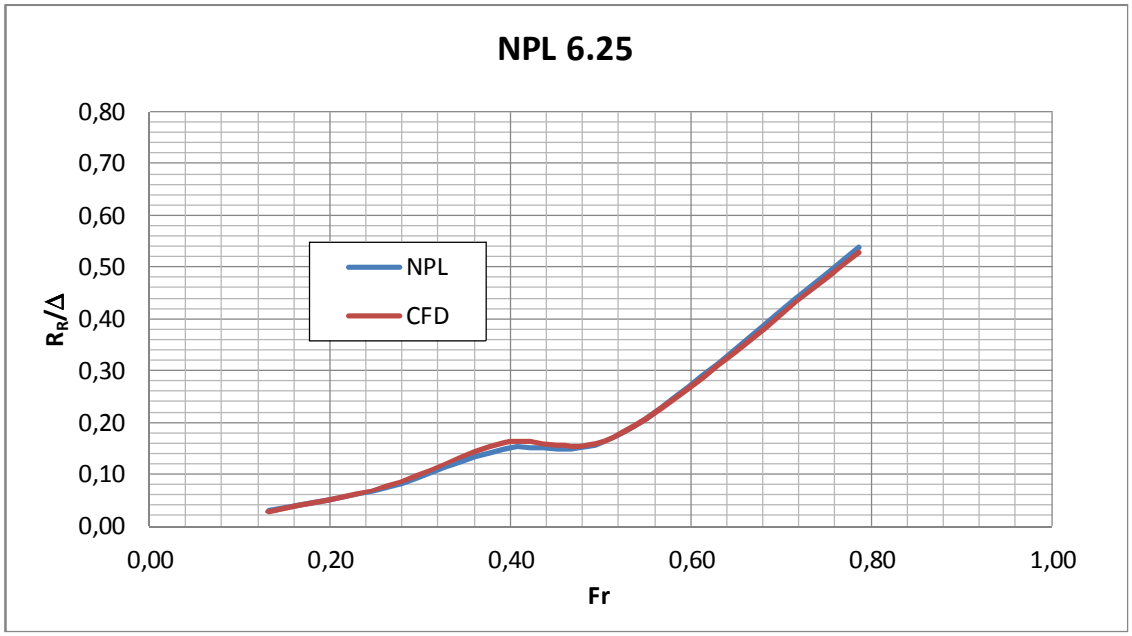

Fig. 4.29 - Comparison between R_R/Δ of the series and R_R/Δ of CFD (mod 6.25)

4.2.2 *MTC (Multi-Hull)*

A particular trimaran hull available in two version called MTC was used (see fig. 4.30). It's a semi-planing hull with a flat-bottom canoe body and two thin outriggers in the stern part. The two version has different thickness of outriggers.

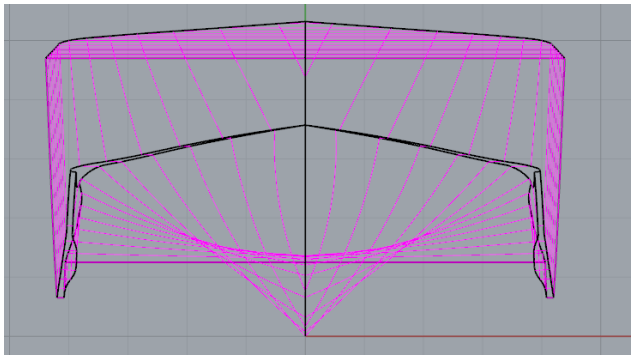

Fig.4.30 - Transversal section of MTC v1

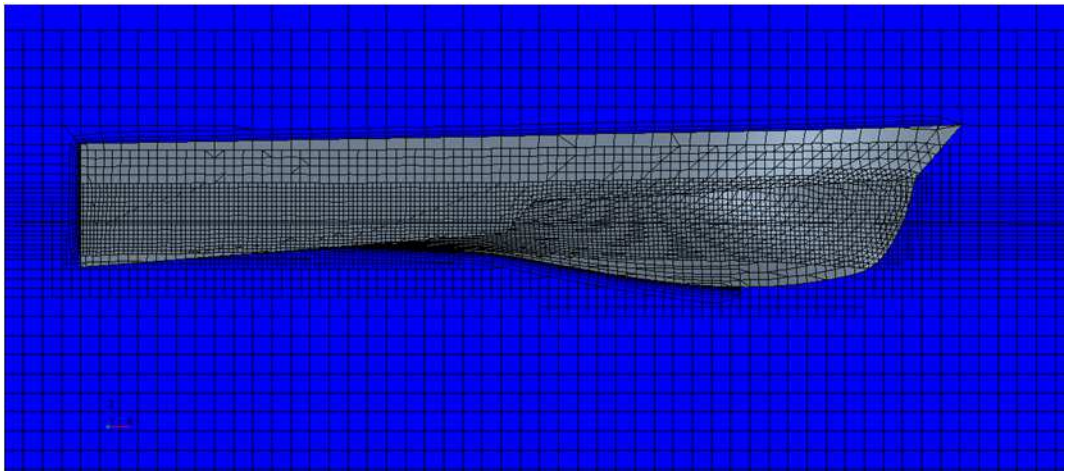

Fig. 4.31 - Volume mesh

Simulations with viscous method were carried out by the developed procedure to replicate tests performed in the towing tank. The calculations were performed on a scale model (λ=8.5) in order to directly compare the results without any scale. Some graphical extrapolation of the results can be seen following figures (fig. 4.31, 4.32, 4.33).

As can be noted in table 4.7 and in figure 4.34, the resistance trend line measured in CFD is fully validated, although worked with a coarse grid and then having lost some resolution on the absolute value of resistance (average error abt. 6.9%) [37].

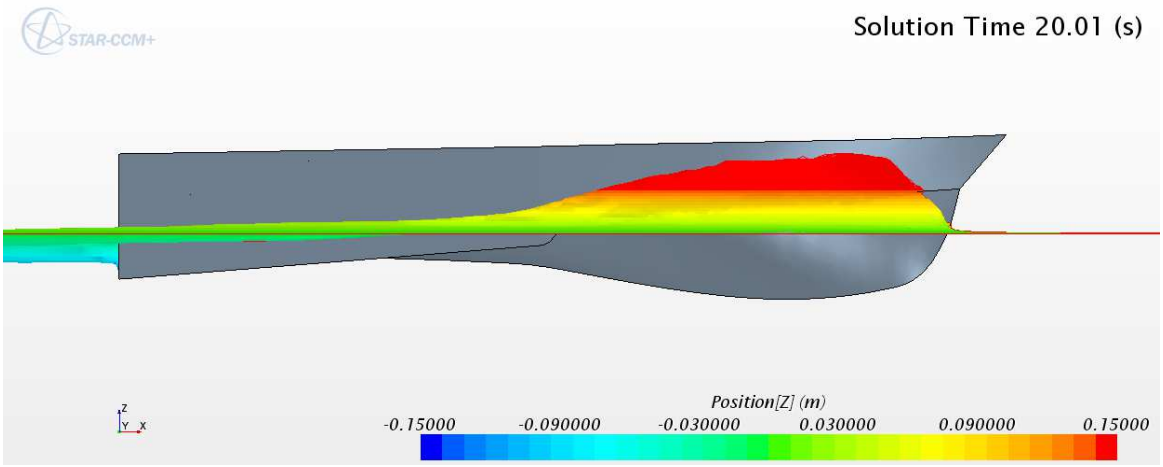

Fig. 4.32 - Wake profile of MTC v1 at 24kn

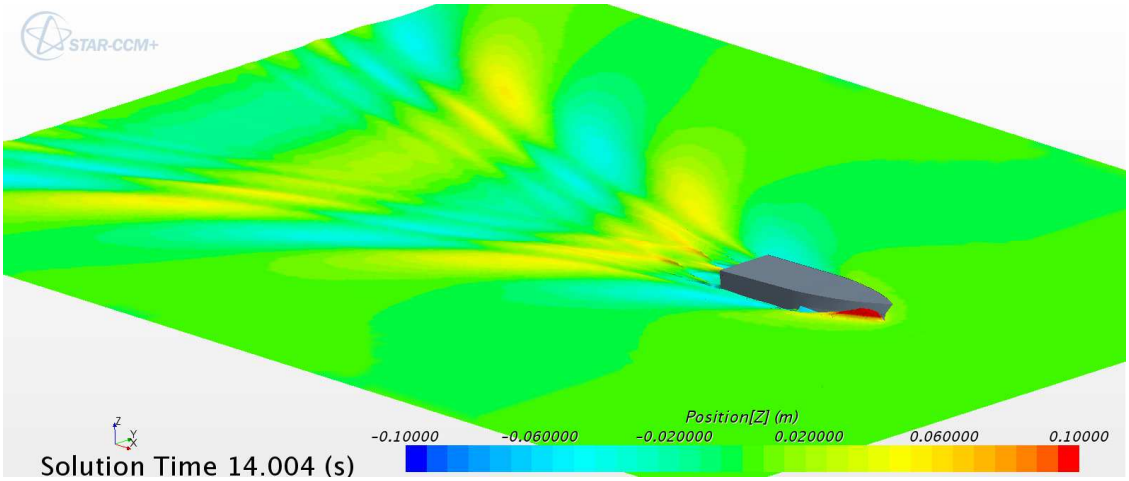

Fig. 4.33 - Perspective view of wake of v2 at Fr 0.55

Table 4.7 Comparison between RANS CFD and tank results.

V_M, m/s	V_S, m/s	Fr	Fr_V	R_{TM} CFD v1	R_{TM} tank v1	R_{TM} CFD / R_{TM} tank %
1.412	8.00	0.27	0.65	19.15	18.24	5.0%
2.117	12.00	0.41	0.97	68.83	64.73	6.3%
2.823	16.00	0.55	1.30	104.75	97.29	7.7%
3.529	20.00	0.69	1.63	124.40	115.33	7.9%
4.235	24.00	0.82	1.95	155.24	144.56	7.4%

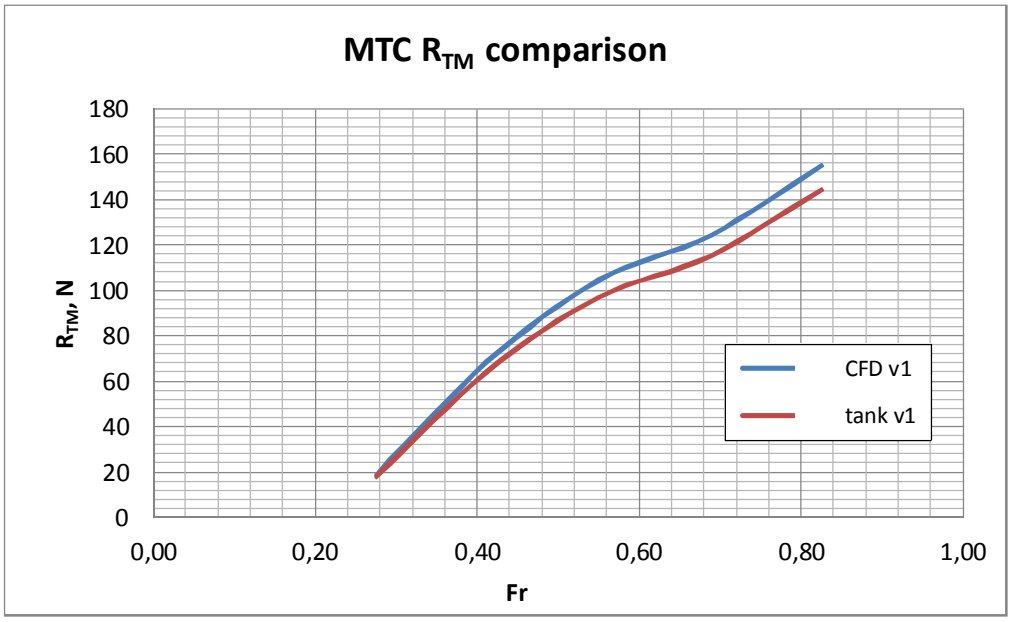

Fig.4.34 - MTC: Comparison between CFD and tank total resistance curves

Despite having worked with a coarse grid, standardizing the volume mesh through the method RANS we tried to densify the mesh thickness in the free surface area in order to capture with a good approximation also the waves generated by the hull, thus to compare them with those calculated with a BEM method. The BEM software used is a well-known in-house code of University of Genoa called "Nuovoswelem"[38],[39],[40],[41].

Some simulations were performed in the same conditions of immersion and trim, at relative speeds of *Fr = 0.41*, *Fr = 0.55* and *Fr = 0.69*, in order to measure three entities of the wake quite different from each other since at these speeds the hull comes into transition from displacement to planing.

Then several wavelength cuts have been carried out for both methodologies (see Fig 4.35) and, in particular, for each of the three speeds tested: one longitudinal cut at $y = 0.3L$ from the center line and three transverse cuts, respectively at $x = 0$, that is in correspondence of transom , $x = -0.5L$ and finally at $x = -L$.

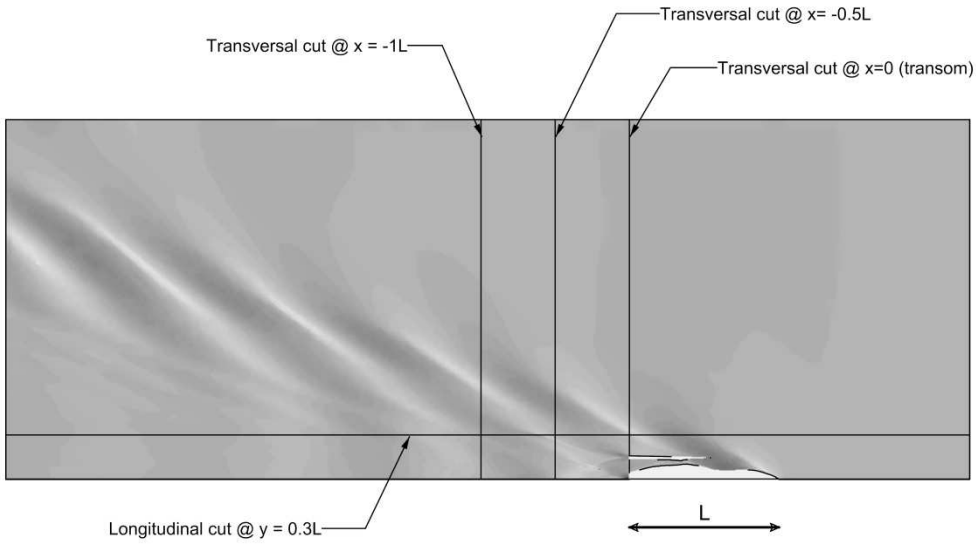

Fig. 4.35 - Transverse and longitudinal wave cuts position

From the accurate comparison obtained between the different wavelength cuts, it can be seen that the two methods, although based on completely different techniques and in spite of the different coarse grid adopted to significantly reduce the computation time in the RANS method, the wavelength cuts' geometry in some cases appear similar even if the RANSE grid computing it was not designed to capture such complex wave pattern. In particular is interesting to see the good capture of the macro peaks and the difference of the transom cut of the outriggers, due to the linear solution proposed by the BEM solver.

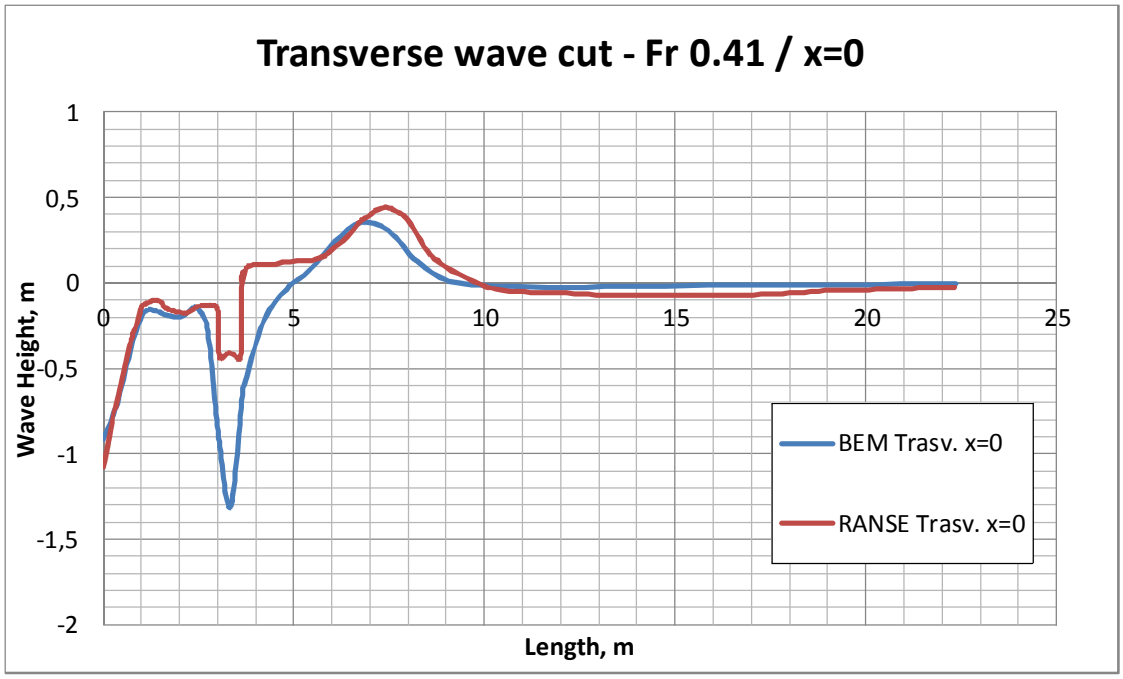

Fig. 4.36 - Transverse wave cut at Fr 0.41, x= 0.0 L

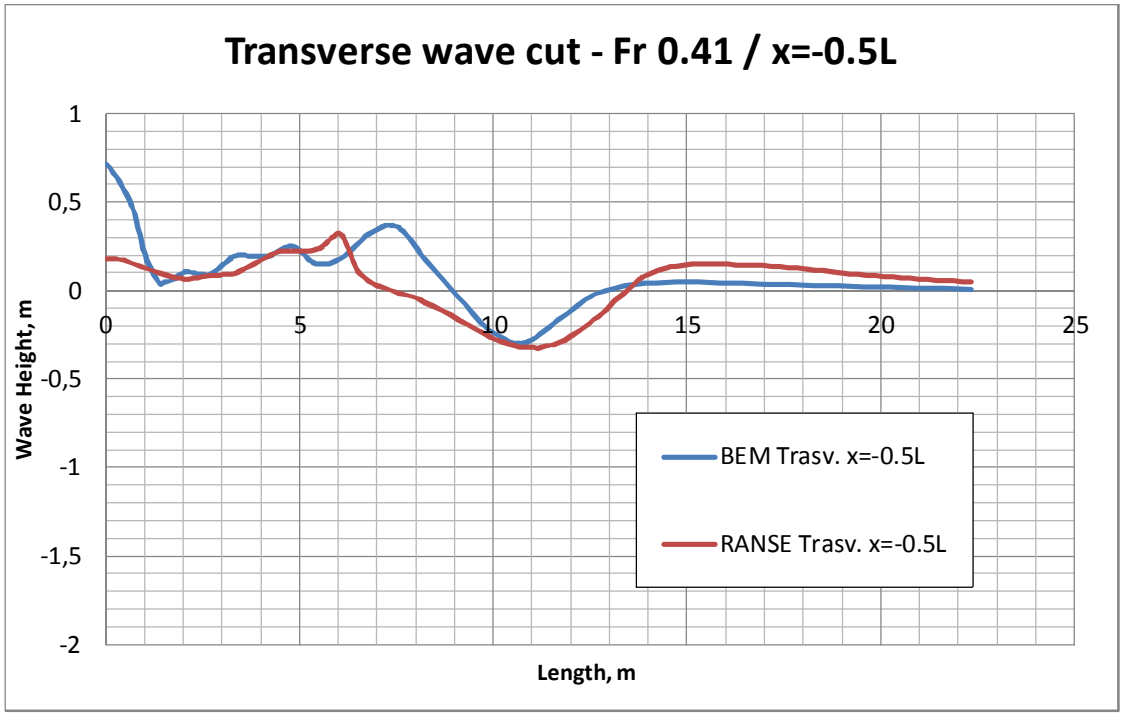

Fig. 4.37 - Transverse wave cut at Fr 0.41, x= -0.5 L

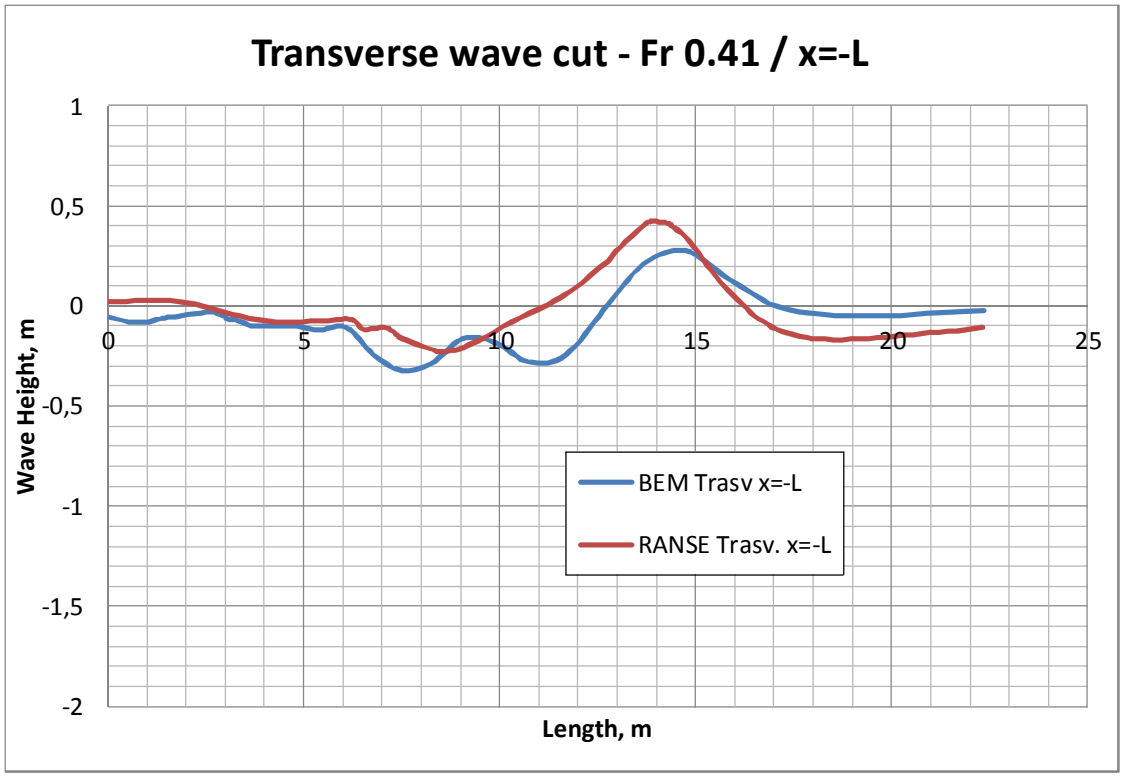

Fig. 4.38 - Transverse wave cut at Fr 0.41, x= - L

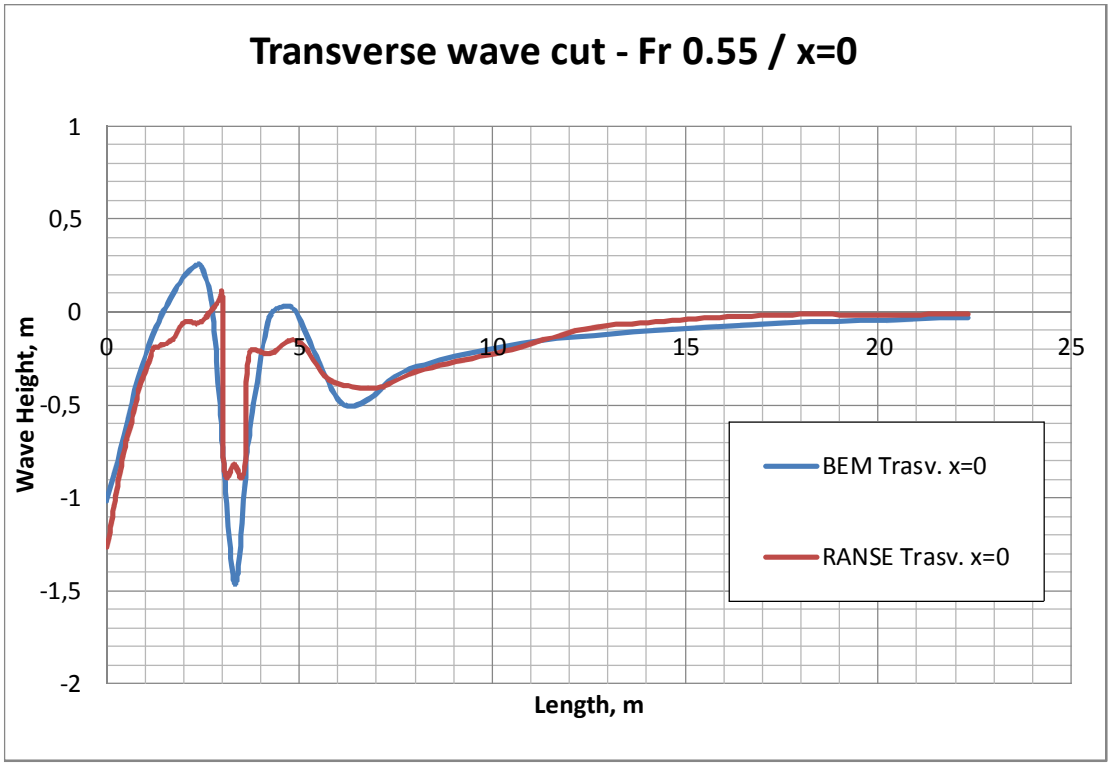

Fig. 4.39 - Transverse wave cut at Fr 0.55, x= 0.0 L

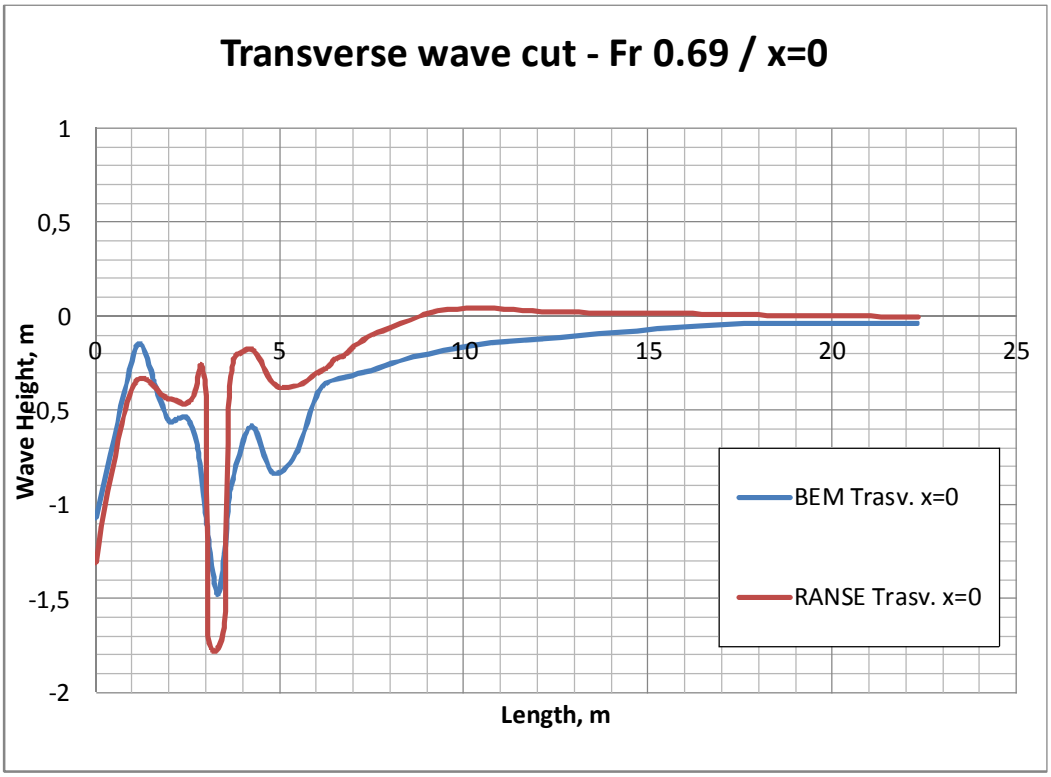

Fig. 4.40 - Transverse wave cut at Fr 0.69, x= 0

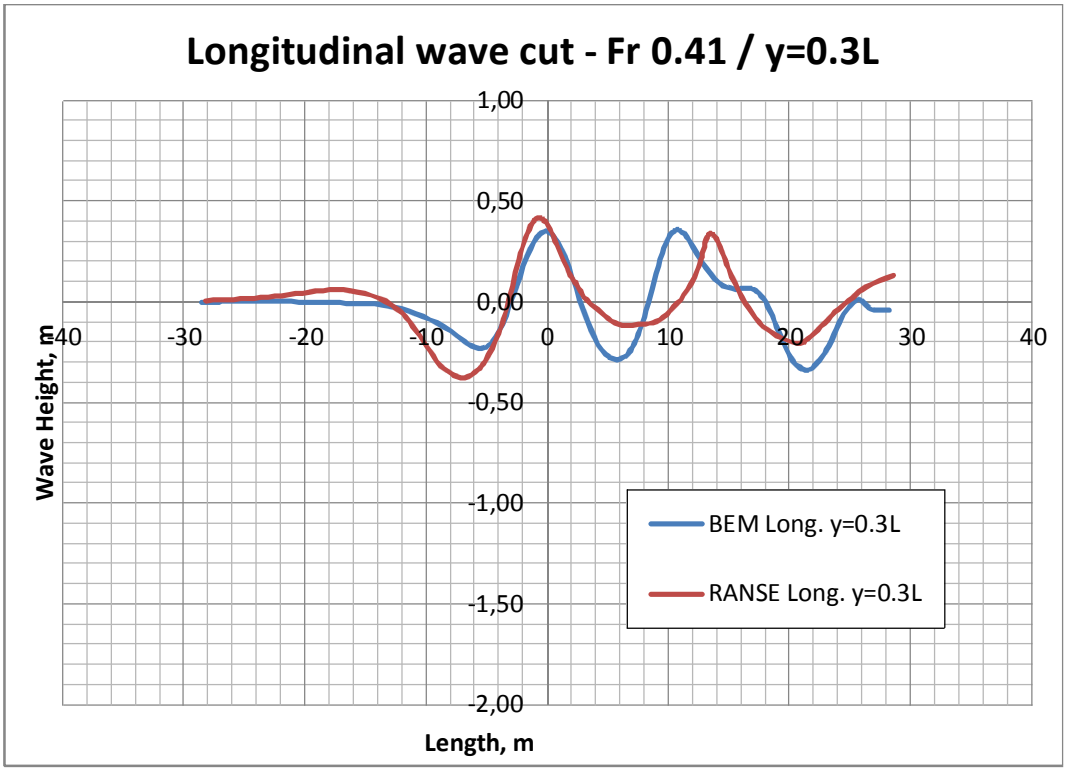

Fig. 4.41 - Longitudinal wave cut at Fr 0.41, y= 0.3L

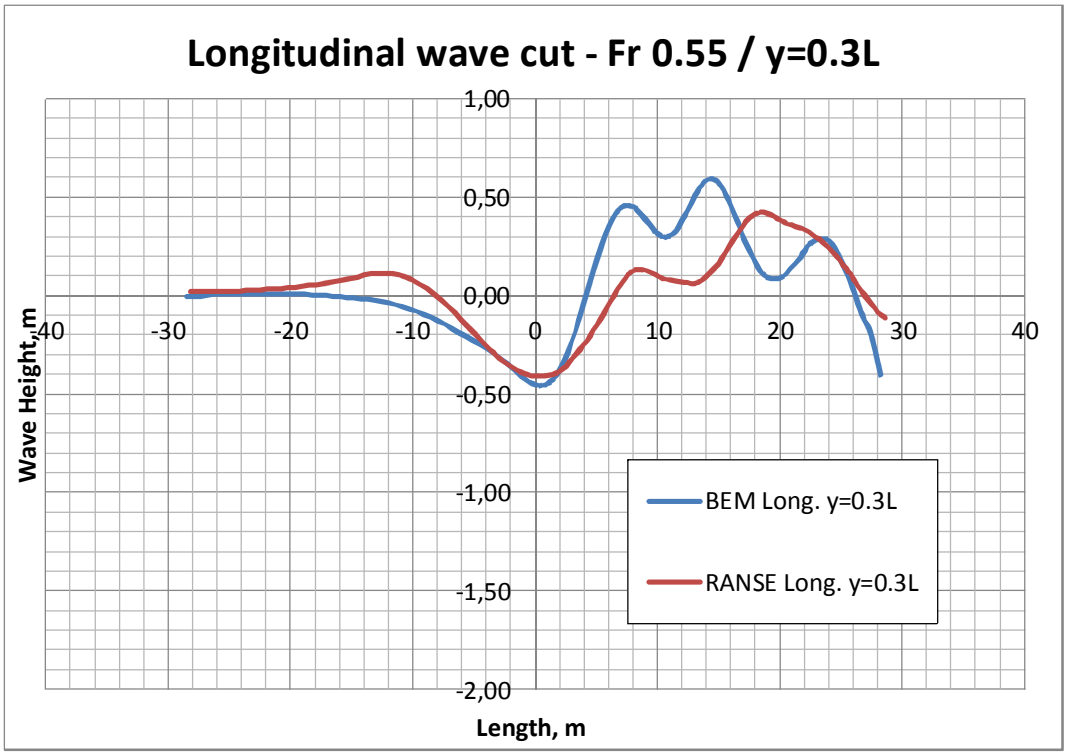

Fig. 4.42 - Longitudinal wave cut at Fr 0.55, y= 0.3L

It can be noticed that the RANSE methodology with low number of cells is able to capture not only the resistance fairly but also the transverse and longitudinal wave cuts, even if the hull in question generates extremely complex wake.

4.3 FAMILY 3 – HARD CHINE PLANING HULL

4.3.1 62 series test

Reductions of cells in simulations of hard chine planing hulls was tried by for the model 2.0 (fig. 4.43) of the well-known Series 62 [42]. In this case, performing simulations in the same scale of the experiments of the systematic series, a mesh utilizing little more than 70k cells has been obtained. Nevertheless, the CFD results are very similar with those from tank experiments with an average error of only 3.2% (table 4.8, fig.4.44) .

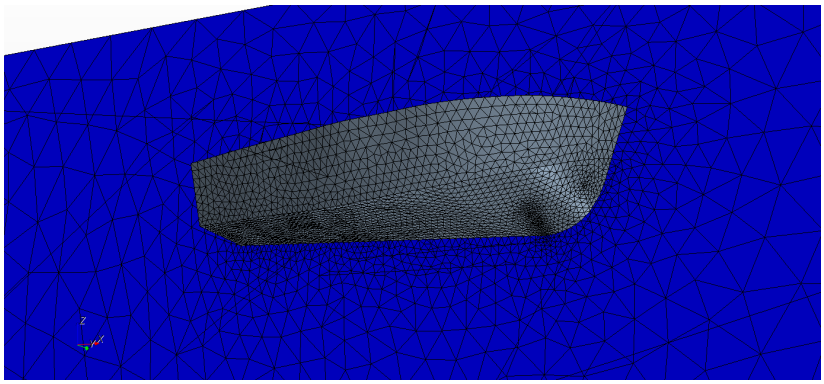

Fig. 4.43 - Surface mesh of 62 series hull – model 2.0

Table 4.8 Comparison between 62 series data and CFD calculations

62 - 2.0				
V_M	**Fr**	**10^3 C_R**	**10^3 C_R CFD**	**C_R CFD / C_R Series %**
0.80	0.13	7.71	7.49	-3%
1.61	0.26	4.82	4.94	3%
2.41	0.39	4.28	4.63	8%
3.21	0.52	2.89	2.91	1%
4.82	0.79	3.86	3.78	-2%

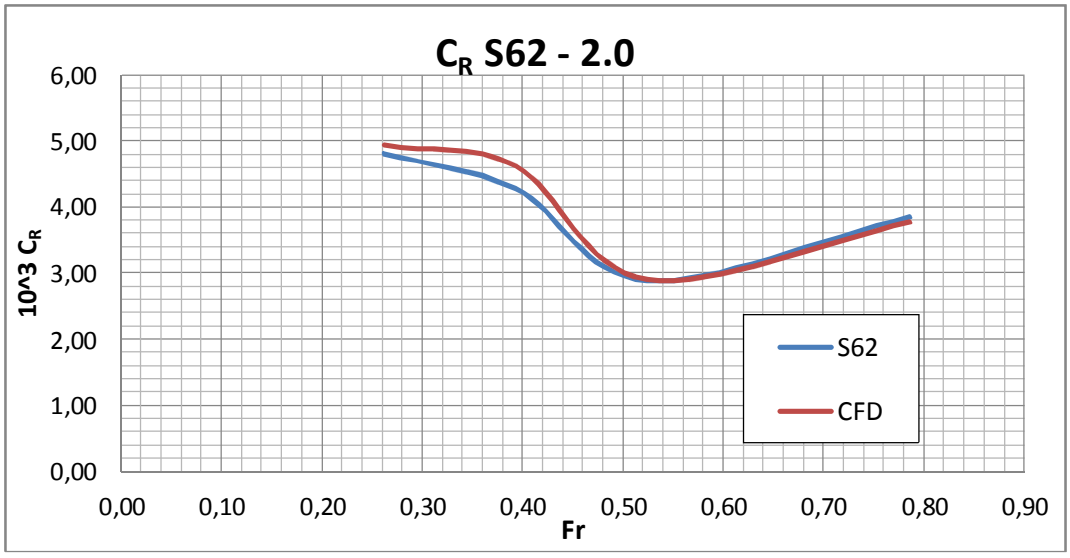

Fig. 4.44 - C_R comparison between 62 series data and CFD calculations

4.3.2 B42 hard chine hull

On the B42 hull(fig 4.45 and 4.46) several simulations have been performed trough the automated procedure with a number of cells of about 80,000. This is an hard-chine planning hull for a 12metre pleasure craft with more than 40kn of top speed. The results were excellent highlighting a difference of about 1.8% (see table 4.9 and fig. 4.47) compared with the resistance values measured in the towing tank (test performed at University of Trieste) [43].

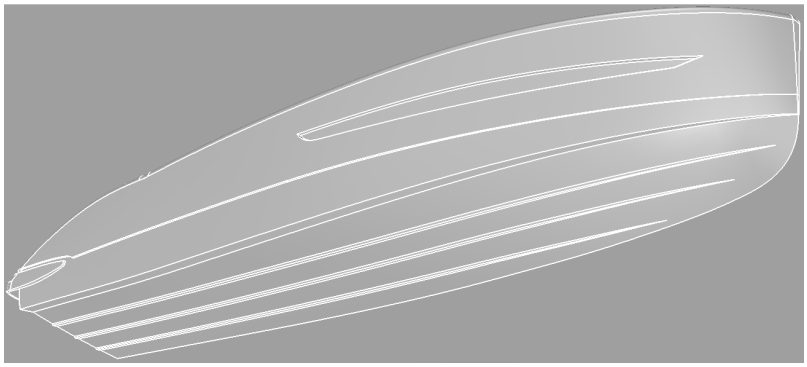

Fig. 4.45 - View of B42 hull

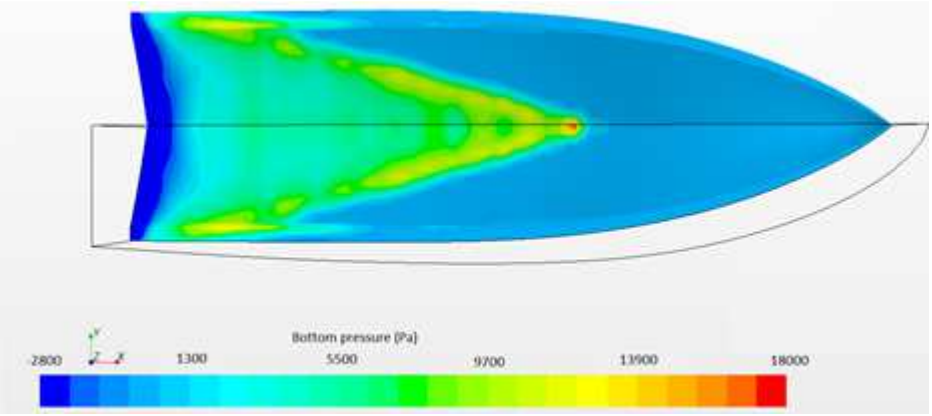

Fig. 4.46 - Dynamic pressures on the bottom trend of B42 hull at 38kn

Table 4.9 comparison between B42 tank tests and CFD calculations

V_M, m/s	Fr	R_{TM} tank, N	R_{TM} CFD, N	R_{TM} CFD / R_{TM} tank %
2.03	0.58	17.35	-	-
2.49	0.71	19.97	-	-
3.00	0.85	22.38	-	-
3.22	0.92	22.63	22.17	-2.0%
3.96	1.12	23.73	23.49	-1.0%
4.43	1.26	24.46	23.84	-2.5%
4.95	1.41	26.31	25.52	-3.0%
5.43	1.54	27.47	27.19	-1.0%
5.88	1.67	29.01	28.43	-2.0%
6.43	1.83	31.11	30.17	-3.0%
6.92	1.97	33.65	32.98	-2.0%
7.43	2.11	36.54	36.91	1.0%

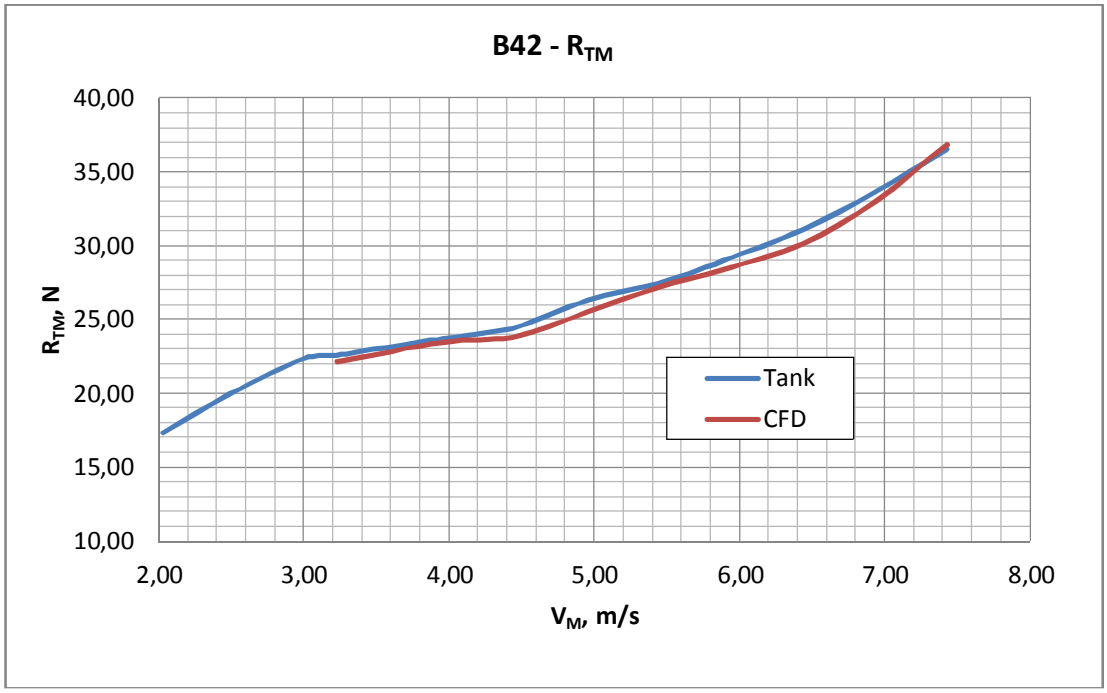

Fig 4.47 - B42 hull: Comparison between resistance measured in the tank and the one calculated in CFD

4.4 CONCLUSIONS

In order to prepare and to optimise the procedure, about 1.250 case studies on over 40 different hulls were performed in total. As we have seen from the cases selected and above displayed, the discrepancy between numerical simulation with a low number of cells and experimental data is always attributable to a few percent. In any case, the trend and the shape of the curve are always correctly predicted, thus ensuring a good final result, especially to make any comparative analysis. It was therefore considered appropriate and correct to use such kind of simulations to perform numerical multi-objective optimisations.

OPTIMISATION METHODS AND TOOLS

Optimisation is a section of applied mathematics, in particular of numerical analysis, which studies the theory and methods for the detection of maximum and minimum points of a mathematical function; so you can obtain a mathematical model able to traduce in mathematical terms a given problem (not therefore dealing of how such a model has been built, directly). The favored field of research of optimisation are some models expressed in terms of several variables functions, in which the optimal points are searched placing also constraints expressed by equations or disequations also in terms of higher order derivatives. Any optimisation problem can be expressed through the following form:

$$z = \begin{cases} \min f(x) \\ x \in X \subseteq \mathbb{R}' \end{cases} \tag{5.1}$$

where x is the vector of decisional variables of n components, X is the subset of Euclidean space R^n defined by the constraints and z is the objective function. Numerical optimising aim is therefore to identify the vector x (i.e., the values to be assigned to n decisional variables) that, respecting the constraints, minimizes the objective function value.

5.1 MULTI-OBJECTIVE OPTIMISATION

In most real-world problems it appears necessary finding a solution able to optimise various objectives simultaneously, objectives which are often competing each other. In this case, the problem to be faced is not simply searching for a maximum or a local minimum (or global) value for a given function: in a multi-objective optimisation problem you need to find a certain solution that could be optimal for all objective functions describing the problem, simultaneously [44].

Generally speaking, when you deal with a multi-objective optimisation problem, the optimal solution achieved is never unique (as in single objective optimisation), but you face with a set of equally optimal solutions compared to the given problem. Such set of solutions is called Pareto Optimal Set. It is then up to the figure of the Decision Maker the task of deciding which of the solutions found within Pareto Optimal Set is best suited to meet his needs (which may mean favoring a goal rather than another, or choose an intermediate value so that all objectives are optimized in the same way, and so on).

A mathematical problem of optimisation can be defined as the minimization or maximization of a real-valued function on a specified set.

The importance of this mathematical model obviously derives by the fact that several real problems are being addressed thanks to this model use. However, almost every real optimisation problem is marked by the simultaneous presence of several objectives, i.e real-valued functions to maximize and/or minimize, typically contrasting with each other.

5.2 MULTI-OBJECTIVE OPTIMISATION PROBLEM

Speaking of Optimisation for a given problem, means finding one or more solutions, so-called Feasible, corresponding to the extreme values of one or more objective functions. When an optimisation problem modeling a physical system requires a single objective function, the task of finding the optimal solution is called a Single Objective Optimisation. In order to extend the applicability of an optimization algorithm to different problems, natural and physical principles have been imitated so as to develop strong optimization algorithms.

The Evolutionary Algorithms and Simulated Annealing are two examples of such algorithms. When an optimisation problem requires the presence of more than one objective function, the problem of finding one or more optimal solutions is called Multi-objective Optimisation. Since the Multi-objective Optimisation requires more than an objective, it is logical to conclude that the Single Objective Optimisation is a special case of Multi-objective Optimisation. However,

there is a reason why you have to pay more attention to the Multi-objective Optimisation than a single one: most of real-world problems requires the simultaneous optimisation of a series of objectives sometimes competing. An optimal solution respect to a single objective requires a compromise with the others.

5.3 MULTI-OBJECTIVE DESIGN OPTIMISATION

In recent years multi-objective optimisation algorithms have been greatly used in the field of industrial design, often associating the optimisation software to parametric mathematical models of three-dimensional modeling and/or to simulation software able to evaluate the goodness of the solution itself. The multi-objective optimisation is mainly used in the following industries:

- Automotive: improved duct performance (pressure loss, flow uniformity, etc.), engine intake port, engine calibration, fuel injection system optimisation, crankshaft dynamics and FEM, catalyst performance, external aerodynamics (drag and lift optimisation, noise reduction, wing mirror design, etc.)
- Aerospace: fuselage optimisation, HVAC optimisation of cabin interiors, smoke dispersal and fire detection sensors position, optimisation and calibration of control systems
- Buildings: optimisation of building ventilation and thermal comfort, smoke dispersal and fire detection sensors position
- Heat exchangers: optimisation of heatsink pins, geometrical shape of finned condenser/evaporator, air charge cooler design, etc.
- Marine and Naval: ship hull hydrodynamics, robust design of rudder, propeller design, HVAC of cabin interiors
- Turbomachinery: improved pump efficiency, propeller performance, etc [45].

5.4 OPTIMISATION ALGORITHMS AND METHODS

5.4.1 Genetic Algorithm

This is a multi-point, evolutionary search method that performs global exploration of the design space while searching for an optimal solution. It does not require the calculation of solution gradients [46],[47],[48].[49].

A genetic algorithm is an heuristic method of research and optimisation, based on the Charles Darwin natural selection principle which governs biological evolution; is normally used for optimization of hull shape [50],[51].

During execution, the algorithm repeatedly changes a population consisting of a several number of solutions (individuals): at each iteration, it operates a random selection of the current population individuals, using them to create new elements of the population itself, which will replace an equal number of individuals already existing, and thereby establishing a new population for the following iteration (or generation).

This sequence of generations evolves towards an optimal solution of the problem assigned.

Genetic algorithms are applicable to the resolution of a wide variety of optimization problems. They are not suitable for classic algorithms, including those in which the objective function is discontinuous, non-derivable, stochastic, or strongly nonlinear.

According to the classical principles of natural evolution, each individual conveys part of his genetic heritage to their descendants; also, sporadically individuals with features not belonging to the original species gene pool born, giving rise thereby to genetic variations. At last, individuals - with the most suitable qualities to their living environment - have more opportunities to survive and to reproduce.

As said earlier, the translation and the extension of these principles, valid for biological systems, also to artificial ones is ascribed to John Holland, historically. After a long period of time, in which this work importance was not fully acknowledged, the genetic algorithms use has been consolidated in computer science, engineering, financial, and obviously in the field of social and natural sciences.

The implementation of a genetic algorithm fulfills the similarity with the existing natural systems, and it always involves some basic steps, which are listed below:

• a selection phase in which individuals to be reproduced , said parents, are identified. They contribute to the next generation of the solutions' population.

• a crossover phase or reproduction of the selected individuals, in which two parents are combined in order to form opportunely new individuals for the next generation.

• Lastly, a mutation phase, during which in a random way some changes are made to parents before they can generate new individuals, who will have a genetic heritage quite different from their parents'one.

In detail, the algorithm evolves through the following points:

• the algorithm begins generating, at random, an initial population;

• the algorithm creates a result a sequence of new populations, or generations. In each iteration, the individuals in the current population are used to create the next generation, and to this end further steps are performed:

- any member of the current population is estimated by calculating the corresponding value of fitness
- determining an appropriate order of such individuals on the basis of fitness values;
- the most promising individuals shall be selected as parents;
- starting from such individuals it is generated an equal number of next generation individuals; this can occur in two distinct modalities i.e. making random changes on a single parent - mutation - or appropriately combining a pair of parents' features - intersection.
- individuals thus generated replace parents, allowing the formation of the next generation
- finally, the algorithm stops when one of the criteria for arrest is satisfied.

A well-known theorem (due to Holland), ensures that, under certain circumstances, individuals with high fitness values tend to grow exponentially in the population through the mechanism of the crossing, thus ensuring the convergence of the genetic algorithm to an optimal solution. In his schema theorem, also called the fundamental theorem of genetic algorithms, he shows that a scheme (ie a particular combination of genes occupying a precise location within a chromosome) proliferates more quickly if, besides having a high fitness value, contains a small number of specific genes not far from one another. This, in fact, reduces the probability of destroying the scheme during the reproduction phase.

5.4.2 Simulated Annealing

This is a single-point algorithm that is capable of finding global optima but often finds a local optimal solution. It is not dependent on solution gradients. Is often used, in combination with the Genetic Algorithms, in hull shape optimization [52].

In fact, The Simulated Annealing is a strategy used to solve optimisation problems. This process seeks to find a global minimum in case of multiple local minima.

The concept of annealing derives from the science of metals, where it is used to describe the process of elimination of reticular defects from the crystals, through a procedure of heating followed by slow cooling. In this case a reticular defect corresponds to a wrong combination of

two objects (for example, a wrong connection of two neurons within a neural net).

Method of use:

• an initial temperature is arbitrary chosen:

- you examine the problem in order to identify possible solutions (50 to 100 solutions);
- for each possible solution the cost is computed;
- you take the ΔE_{max} ;
- at this point you take an initial temperature greater than the energy variation ($T_{initial} > \Delta E_{max}$) but of the same order of magnitude ;

• the temperature is lowered until it reaches a value close to 0;

• in the proximity of the minimum value of *T*, a strong enough (energy) minimum will be located;

• Repeating this cycle, the chance to find the same solution tends to 0. If you find two identical solutions for two different tests of the same problem it means that, probably, something hasn't been worked properly.

The temperature of the network is determined so that:

• If T is high: you can afford to do high steps and when you find a minimum you can try to go on finding out if it was only a local minimum;

• If T is low: you can still do high steps but there are less chances, so you then proceed to shorter steps;

• Fast T reduction: it involves the freezing of some thermal fluctuations;

• Very slow T reduction: it could imply the failure to achieve the calculation conclusion and then not finding a global minimum.

5.4.3 NLSQP – Non linear sequentic quadratic programming

This is a single-point, gradient based approach that typically exhibits good convergence toward the nearest local optimal solution.

The SQP method (also called the method of Lagrange projected, or Newton-Lagrange method), is a constrained optimisation method, NLSQP typically non-linear, which uses the so-called "merit" methods in order to obtain a quadratic convergence or at least super -linear one, using Newton or quasi-Newton methods, thereby overcoming the difficulty operating in a space of n + m dimensionS, with equalities and inequalities.

Precisely, you solve a sequence of quadratic programming problems, in which the Hessian of the objective function to minimize is the Hessian of the Lagrangian and the constraints are the

approximation of the actual constraints of first-order. The global convergence is obtained simultaneously minimizing a suitable merit function.

One difficulty of the SQP method is to require the existence of the second order derivatives (the Hessian matrix), and also that the same Hessian is positive definite. To overcome these difficulties you prefer using and a quasi-Newton method, introducing an approximation of the Hessian Bk which is defined positive.

Obviously, the method becomes locally super-linear, and if the starting solution is not quite near the minimum searched, the method does not converge.

To overcome this problem and to provide a global convergence, we introduce a merit function. This is a function that, together with the objective function, is simultaneously minimized.

It should also ensure a " decreasing slope condition ", achieved with a suitable line search.

5.4.4 RSM – Response surface methodology

This method searches a surrogate approximation model that is generated by fitting a chosen function to a set of evaluation data points.

The response surface methodology (RSM) is in fact a set of statistical and mathematical techniques widely used to determine the effect of some experimental parameters and to optimize various biotechnological processes. This technique allows to obtain level curves on the basis of linear effects, quadratic and interactional ones generated by two or more parameters, in order to calculate the system's optimal response. This technique has been proposed to investigate the optimisation of physical and chemical parameters in fermentation processes employing various microorganisms. The RSM explores the relationships between some experimental variables (independent variables) and one or more response variable (the dependent variable).

This method was introduced in 1951. The main idea of RSM is represented by the use of a sequence of experiments designed in such a way as to obtain an optimal response. To do so, a second degree polynomial model has been used (examples of RSM are visible in fig.5.1).

A simple way to estimate a first-order polynomial model is using an experiment designed according to a factorial design or fractional factorial. This is sufficient to determine which variable has an impact on the response variable affecting the final response of the process. Once taken into consideration only the significant variables, it is used for a more complicated experimental design (i.e. central composite design), which can be implemented in order to estimate a second degree polynomial model. This can be used to optimize (maximize, minimize, or reach a specific objective) the final response.

In order to develop new processes for the production of new molecules from yeast, the DBVPG Collection currently uses the RSM for the definition and validation of the best combination of variables able to optimize the selected responses.

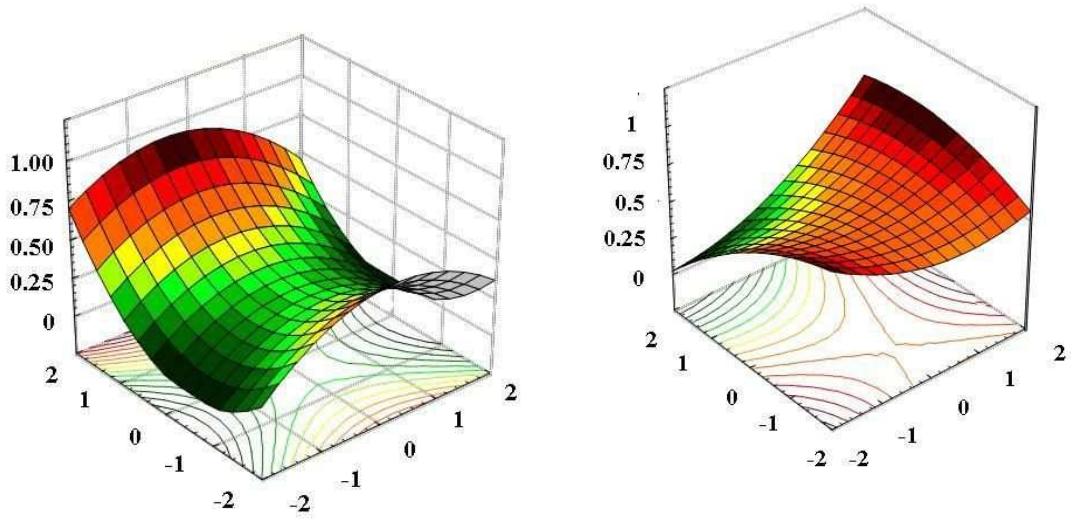

Fig. 5.1 - Examples of RSM response surfaces

5.5 SHERPA® "SIMULTANEOUS HYBRID EXPLORATION ROBUST, PROGRESSIVE AND ADAPTIVE" COMBINED ALGORITHM

Each of the multiple optimization systems has its upsides and downsides, so the choice of which to use is not always simple. Therefore, this analysis has been also evaluated the possibility of using a mixed algorithm, said SHERPA®, which includes all the previous ones. Today unfortunately SHERPA® is a proprietary algorithm, so it is only possible to know the operating principles but not the mathematical procedures in detail. What is certain and tested, is that it allows to achieve the optimum in a very strong way and in much less time.

The optimal design research is achieved by the "evaluations", i.e. optimization algorithms assessed on the results of the simulations and numerical analyzes.

A "evaluation" for example is a finite element analysis of a particular configuration. The total number of evaluations required, in order to find the optimal solution or a configuration to a specified level of performance, measures the efficiency of an algorithm.

Each evaluation requires a large amount of CPU time: that's why the potential use of the lowest

possible number of assessments is so significant; actually the CPU can take from a few hours to several days to make certain types of non-linear finite element simulation

In such kind of approach it becomes clear as the optimization of a project lies also in the impact of the time required to make the necessary assessments.

Each optimization algorithm adopts a different searching path for each run.

This implies that a specific level of design performance can be achieved thanks to a number of different evaluations from run to run.

An aspect not to be underestimated is that the same algorithm may not produce the same final results, after some runs: that is, each run may fall short in some way to find an optimal solution.

The factors, to which these differences depend, are the initial baseline design in a gradient based algorithm, the initial conditions of the search or the initial population of design in an evolutionary algorithm.

Potentially, all kinds of different starting conditions should make the optimization algorithm execution quite similar. This type of algorithm is called "robust" one. The robustness of an algorithm is an important feature to inspire reliability in the algorithm results and to approximate the valuations' number needed to identify a good design.

SHERPA adopts various research methods not in sequence and all at once during one single search. This approach exploits the best particular features of each method. It also minimizes the intervention of a method for the search if or when it is occurred not be effective.

A combination of global and local search methods is used. The number of different methods used each time is approximately within the range between two and ten.

While searching, each method includes tuning parameters automatically changing. Such modification is developed on the basis of the knowledge gradually gained by the design space nature. For the design space, this evolution of competence also determines when and how far each method is used.

More specifically, SHERPA is able to properly understand the design space and to adjust itself simultaneously in order to analyze all types of design spaces, also very articulated ones, efficiently. Of course, there is no certain that the described method is more effective for all kinds of problems compared to some other approach could be, or that such method will be able to achieve an overall optimum solution.

For many practical problems of technical design, the method SHERPA has however proven to work in a very effective and efficient way.

The method described, in addition to the robustness and efficiency, has other important advantages:

- Users need not spend time and effort trying to understand their design space before choosing a suitable algorithm for an optimization run. SHERPA will learn about the design space and employ the appropriate algorithms as it proceeds toward finding an optimized solution.
- Users do not need much, if any, expertise in optimization algorithms and applications, because SHERPA makes all of the decisions about which methods to use and how to tune them.
- Users can define a problem realistically, based on actual engineering or business costs and benefits, without feeling constrained by the capabilities of a particular search method. Problem definitions can be much broader and include a larger number of variables.

5.5.1 SHERPA - Simple Benchmark Problem [53]

In the overall resolution of the varying type and complexity numerous problems lies the actual level of performance of any optimization algorithm. Rather simple problems, as that considered here, would still be successfully solved by all the algorithms regarded for general use.

If, as shown in Figure 5.2, consider a cantilevered I beam subjected to a tip load: the task is to design a cross-sectional shape such that minimizes the mass and simultaneously also satisfies constraints on stress and deformation.

Mathematically, this is expressed as:

Minimize: $m\ (H, h_1, b_1, b_2)$ such that:

$$\sigma_{max} \leq \sigma_{all} \tag{5.2}$$

$$u_{max} \leq u_{all} \tag{5.3}$$

where (H, h_1, b_1, b_2) are the design variables, m is the mass of the beam, σ_{max} is the maximum bending stress, $5000=\sigma_{all}$ psi is the allowable bending stress, u_{max} is the maximum deflection, and $u_{all} = 0.1$ inches is the allowable deflection.

The variables may mutate in the following way:

$3.0 \leq H \leq 7.0$

$0.1 \leq h_1 \leq 1.0$

$2.0 \leq b_1 \leq 12.0$

$0.1 \leq b_2 \leq 2.0$

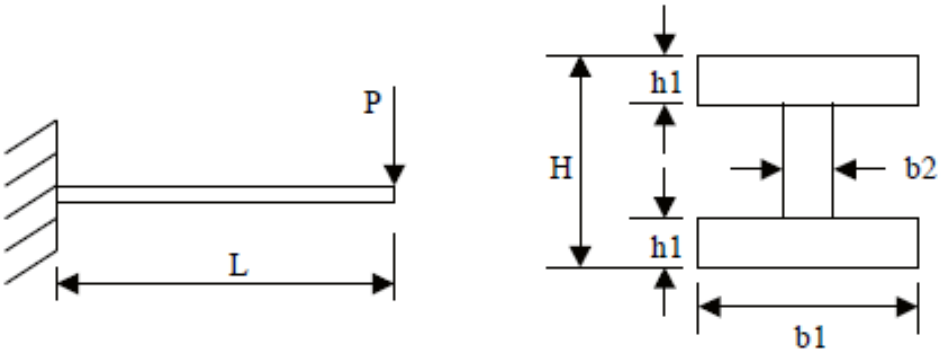

Fig. 5.2 - Cantilever beam with a tip load and cross sectional shape variables in the I beam.

Of the five types of algorithms investigated in this research, only four of them were chosen because they are the most commonly used today, and also because they can be found in most commercial optimization packages:

- GA – Genetic algorithm
- SA – Simulated annealing
- NLSQP – Non-linear sequential quadratic programming
- RSM – Response surface method
- SHERPA – Simultaneous Hybrid Exploration Robust, Progressive and Adaptive

Through the use of a specified number of evaluations, this study investigates the ability of each algorithm to find the optimal solution, known the lowest mass condition. Each algorithm was run fifty (50) times starting from various and random initial conditions and for a given number of eligible evaluations. The method has experienced the best solution found in each path. The average of these best solutions is first computed and then normalized by the known optimal solution. These results are shown in Figure 5.3. Figure 5.4 instead shows these calculated solutions' standard deviation. In order to optimize the study of this specific problem, the parameters in every single algorithm have been "harmonized" before performing the final runs. SHERPA is an exception because the parameters are automatically adjusted adaptively.

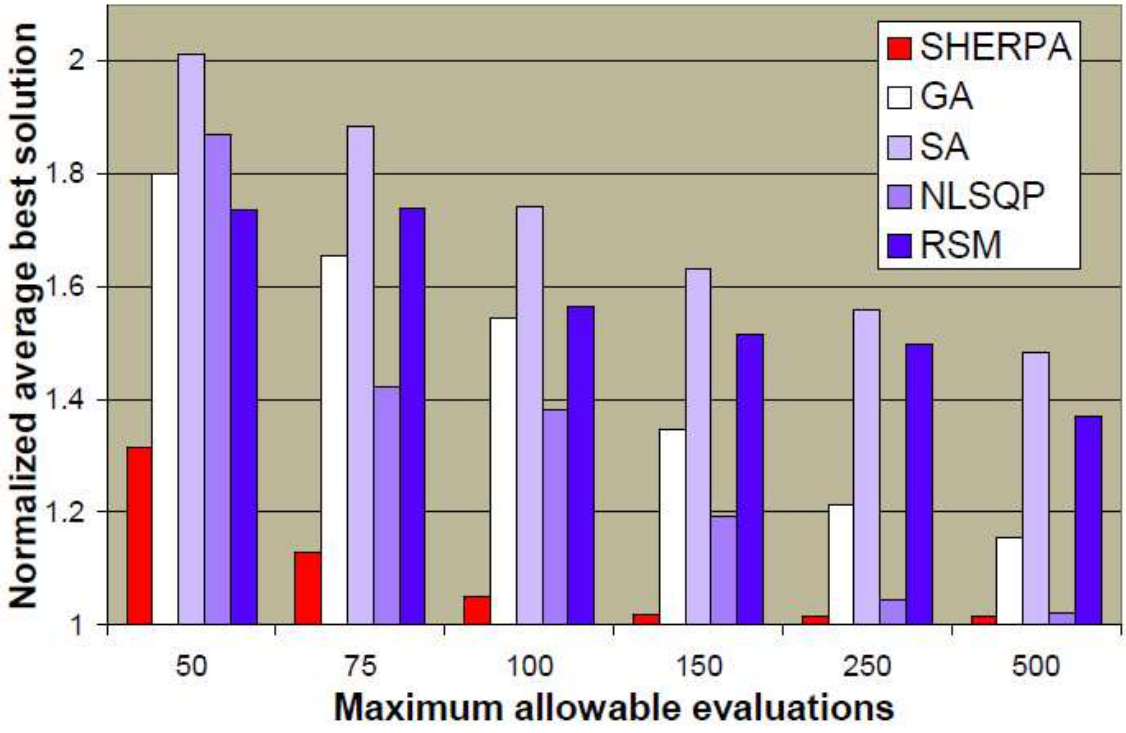

Fig. 5.3 - Average best solution found over 50 runs versus the number of allowable evaluations

(Courtesy of RED-Cedar)

All solutions are normalized by the known optimal solution.

To find nearly optimal solutions, SHERPA has needed of far fewer valuations than other algorithms. In fact, it can be said that SHERPA, for a given number of admissible evaluations, has found better designs than the other algorithms (Figure 5.3).

This means that SHERPA is much more efficient than the other algorithms related to this particular problem, even after the adjustment of their parameters to improve their performance.

Similar conclusions have been achieved for many other problems.

The results shown in Figure 5.4 indicate that the SHERPA method is also very robust for this problem: for all levels of assessments carried out, it has the least amount of changes in the final solutions found.

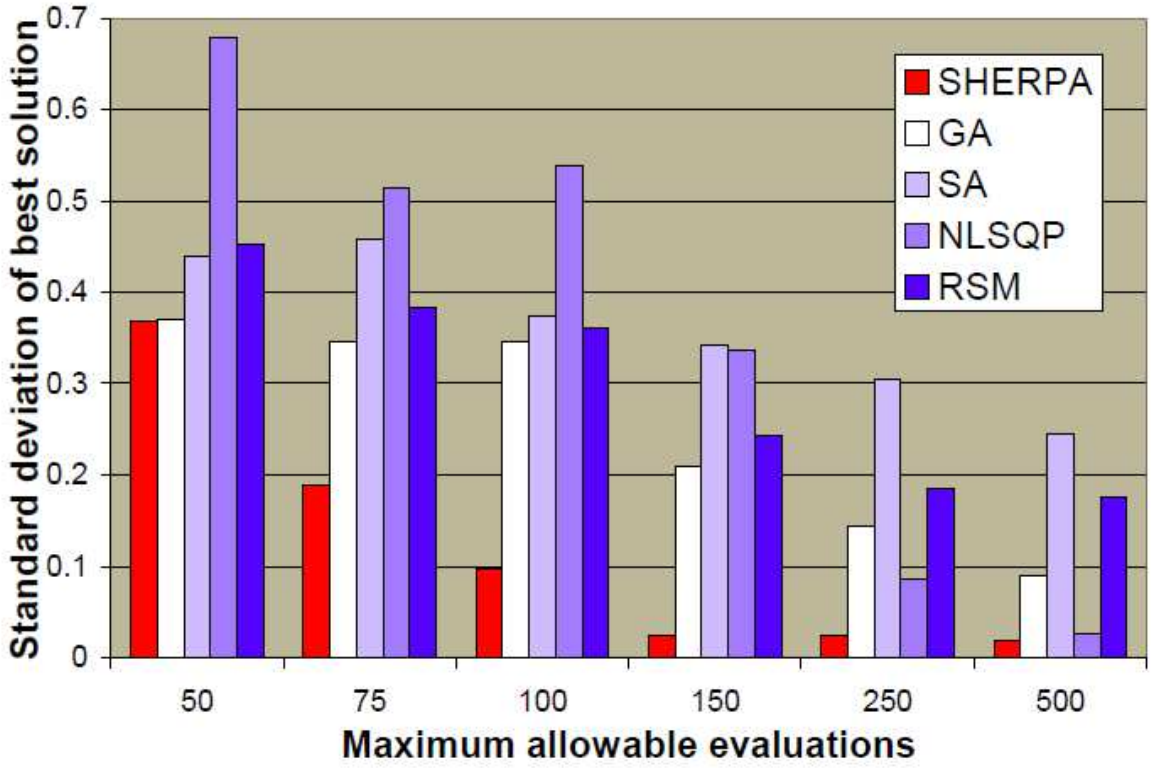

Fig. 5.4 - Standard deviation of the best solutions found over 50 runs versus the number of allowable evaluations (Courtesy of RED-Cedar)

STUDY OF A SEMI-PLANING HULL OPTIMIZED BY THE PRESENT PROCEDURE

6.1 CHOICE AND CONTROL OF OPTIMIZING PARAMETERS

6.1.1 Selection procedure and softwares

The standardized procedure of cells' reduction which has been developed, can be applied and rationalized for any viscous software solver. In the present research, Star CCM + v9.0 of CD-Adapco was always used. It was decided to use the SHERPA algorithm thanks to its strength and its ability to achieve the result in less time (in fact SHERPA analyzes the solutions trend and therefore it prevents the simulation of every case that results already losing on paper).

Once it has been decided to work with both Star-CCM + simulator and Sherpa algorithm, the choose of Heeds-Optimate of Red Cedar as optimization software was quite automatic: Optimate involves the use of SHERPA and through a plug-in it is integrated into Star-CCM +. Hence the idea of using a 3D modeler integrated environment Heeds-Optimate, in order to have

an optimization and verification system simulation, fully automated: the choice fell upon the Star-CAD CD-Adapco, since it's possible to manage it directly via Star-CCM +.
The parametrization of the hull shape is the first step in an automated procedure of optimization [54].
The hull to be optimised was then integrally molded in Star-CAD, defining parametric constraints able to change its geometry. This 3d model has also been introduced in Star-CCM + using standardized computing domains with low number of cells. At this stage, thanks to Heeds-Optimate [55],[56] a multitude of alternatives hulls have been created, by varying one or more geometric parameters of the established range from time to time. Then, Heeds provides to perform the various runs of Star-CCM + and it analyzes the results starting to build the solution's Frontier of Pareto.

6.1.2 Main objective: reducing total resistance

While setting optimization parameters, it was taken into account that the main idea was to modify the geometry of the bottom of a hull, in compliance with strict geometric-dimensional constraints, in order to reduce the total resistance and not only the wavy contribution as typically done till today. This is possible thanks to the viscous solver which, through the k-epsilon turbulence model, can evaluate changes in shear strength.
It was therefore decided to create a parametric hull whose optimized version could produce less resistance at two different speeds (cruise and maximum).
Though multiobjective programming of HEEDS-Optimate was possible to generate an objective function adapted to minimize the total resistance as at cruising speed V_{CR} as at the maximum speed V_{MAX}.

$$z = min(R_{T\_V_{CR}}, R_{T\_V_{MAX}}) \tag{6.1}$$

The SHERPA algorithm, after generating a high number of random solution, starts to analyze them individually evaluating the resistance for each speed.
In a second phase shall select designs having lower resistance than the initial one at either speed and, carrying out an analysis of the trends allows which of the changes contributes simultaneously to the reduction of the resistance at both speed and can continue with an integrated process of optimization.

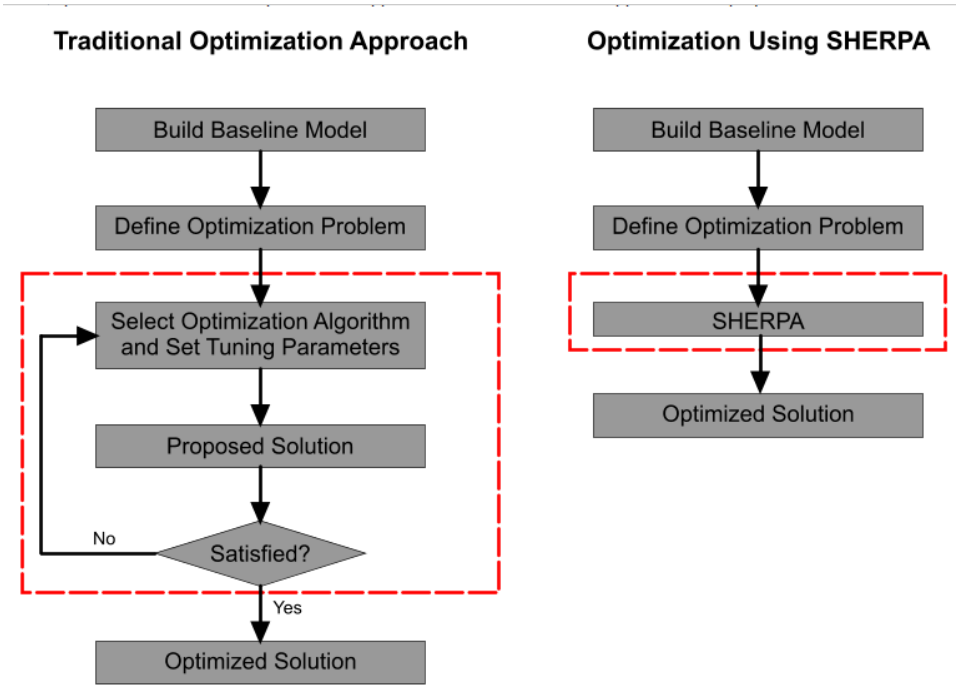

Fig. 6.1 - Traditional optimisation process with SHERPA (courtesy of RED-Cedar)

6.2 MOTHER HULL

6.2.1 The hull: HPH24

The hull used for optimisation test, known as HPH24 (fig. 6.2), is a semi-planing chine one, with a blade bulbous bow. The initial parameters of the hull were chosen according to the best design practices supported by classic hydrodynamic theories [57],[58], in order to obtain an initial hull with a well-designed and congruent shape. The hull has been remodeled in a Star-CAD environment in order to parameterize the spline curves on which the bottom of the hull and the bulb are both built.

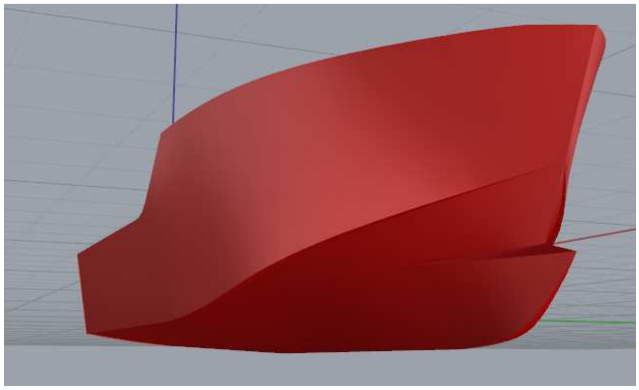

Fig 6.2 - Perspective view of the mother hull

The main parameters of the hull are the following:

L_{OA} = 24.00m

L_{OS}=L_{WL}=23.40m

B_{MAX}=6.70m

B_{WL}=6.2m

Δ=85t

LCB=40%L_{WL}

$L_{bulb\_overbow}$=0.52m

Subsequently, the HPH24 hull has been meshed through the procedure developed above (computational domain around 250k cells, see in fig. 6.3 the volume mesh). The simulations were performed in 1:15 scale to speed up the computation time (reduction of the timestep and the number of cells). The scale factor has been chosen to subsequently build an appropriate model to be tested at Trieste's towing tank.

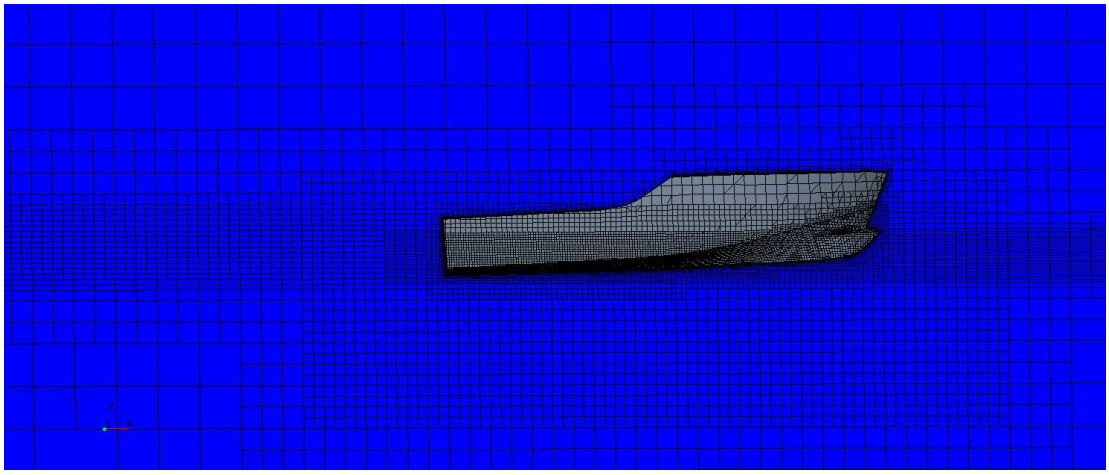

Fig. 6.3 – HPH24 hull volume's mesh

6.2.2 Blade bulbous bow: why

All variants of the hull have a blade bulbous bow (fig. 6.4). At the outset, the bulb overall length - obtained not only considering the protruding portion, but also the part integrated into the stem - that has been calculated using statistics based on similar boats.

The bulbous bow performs a dual role: on one hand it increases the draft length and , being surface-piercing, it contributes to lower the Froude number and, consequently, the wave resistance itself; on the other hand the bulbous bow always acts to reduce the wave resistance, helping to break down the wave crests generated by the forward quarters of the ship.

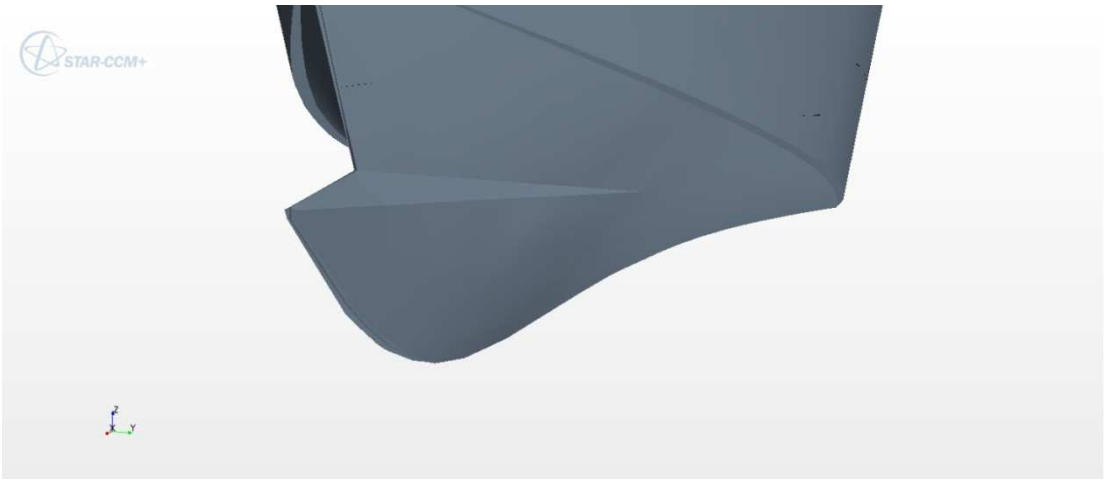

. *Fig. 6.4 - 3D view of the blade bulbous bow in question*

Not commonly such kind of bulbous bow are found in fast boats, since at high speeds and because of the trim angle, the bulb would tend to come out from the water becoming no bearing and even problematic in case of slamming.

In this study case, a chine bulb with reduced transverse area has been performed, mainly to exploit the first feature, i.e. the Froude number reduction, particularly at medium-low speed.

Transverse sections of ∇ kind, favor the entrance of the wave in case of moderate slamming and they also support the bow at higher speeds. In fact, because of the high lift given by the stern quarters, it would tend to go in bow-down too easily.

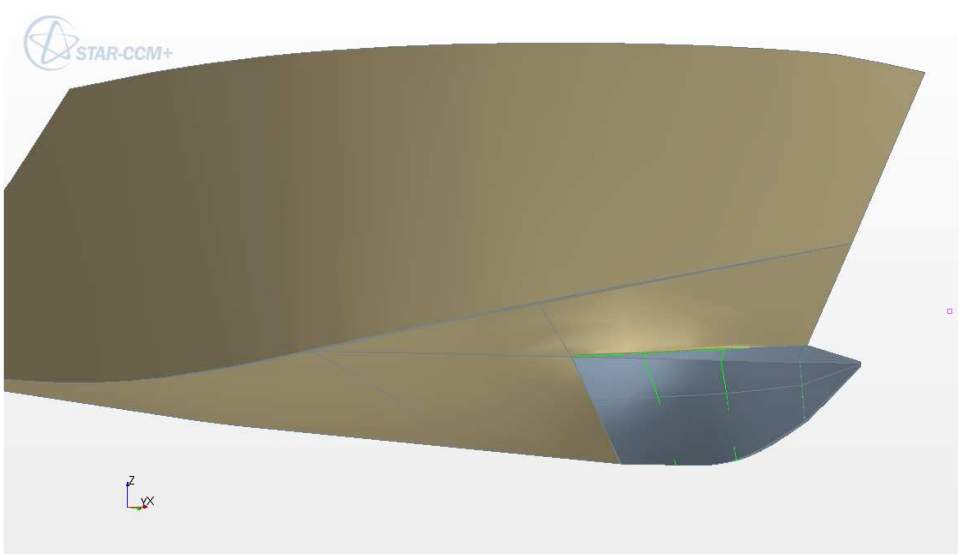

Fig 6.5 - Parameterisation of the bulb in Star-CAD environment

This configuration has been chosen in order to get a boat sailing at always low trims in all operating speeds. Concerning the effect of suitable antiphase wave formation creation, as long as the bulb is sufficiently immersed, you have in particular:

• Generation of hollows at the bow (bow depressions, fig. 6.6):

The application of a bulb, by reducing an hypothetical fluid flow section, decreases the pressures around the hull. This pressure reduction lowers the crests of the forward wave train;

• Overlapping wavy components:

The hull without bulb and the bulb itself are both considered to be independent parts which, advancing into the fluid at the same speed, produce two different wavy trains independently. The combination of the two wavy formations produces a wavy component having such kind of magnitude less than the one produced by the bare hull.

• Reduction of whirling components:

The application of a bulb reduces the formation of shoulder and keel vortices created by the fluid streamlines movement around the hull. Consequently, the result is a benefic effect for both relatively slow hulls with rounded shapes and for the most thin and fast ones, as in the present study case.

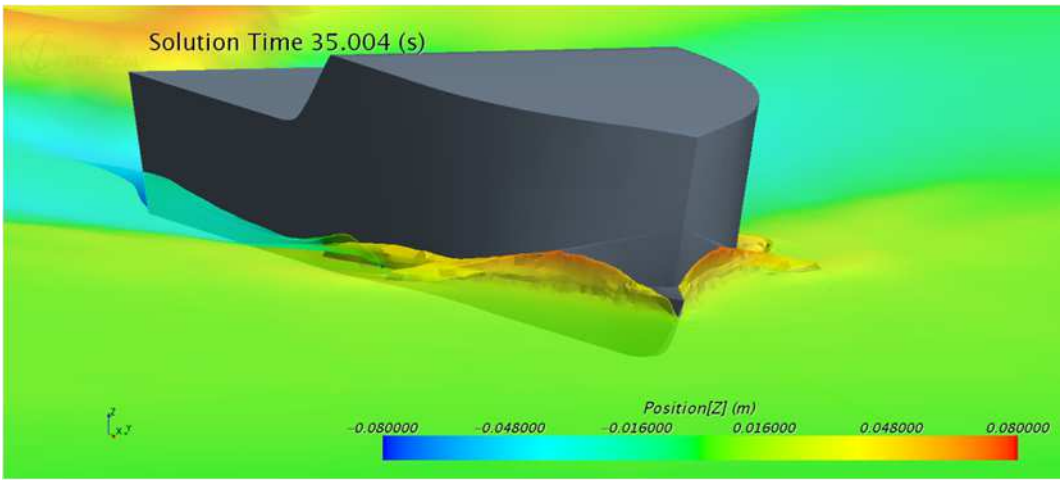

Fig. 6.6 - HPH24 in navigation at 16kn, particular of the bulb action

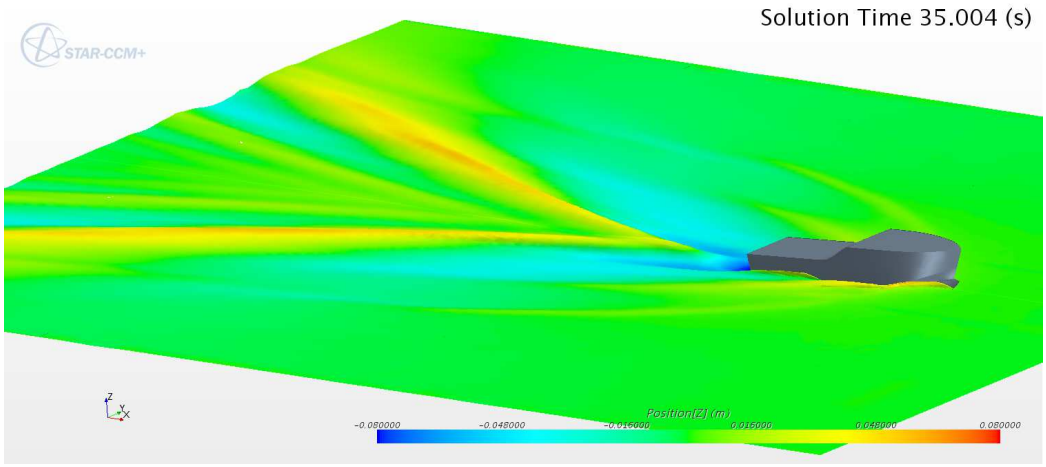

Fig. 6.7 - HPH24 in navigation at 24kn

6.3 OPTIMISATION PARAMETERS AND CONSTRAINT

6.3.1 Modeling 3D parametric hull and bulb

The bottom of the hull has been parameterized subdividing it into 10 frames, each one equipped with four control points; the end points were constrained, leaving the optimizer the opportunity to move only the 2 intermediate points (fig. 6.8).

The bulb was instead subdivided into two surfaces: The first surface, flat one, has been constrained to the hull bottom and the to the other surface of the bulb itself. Instead, the second surface has been split into 4 frames, each equipped with three points. The three points of the astern frame of the bulb are forced to be coincident with the 3 control points lower of the forward frame of the bottom (fig. 6.9 and 6.10).

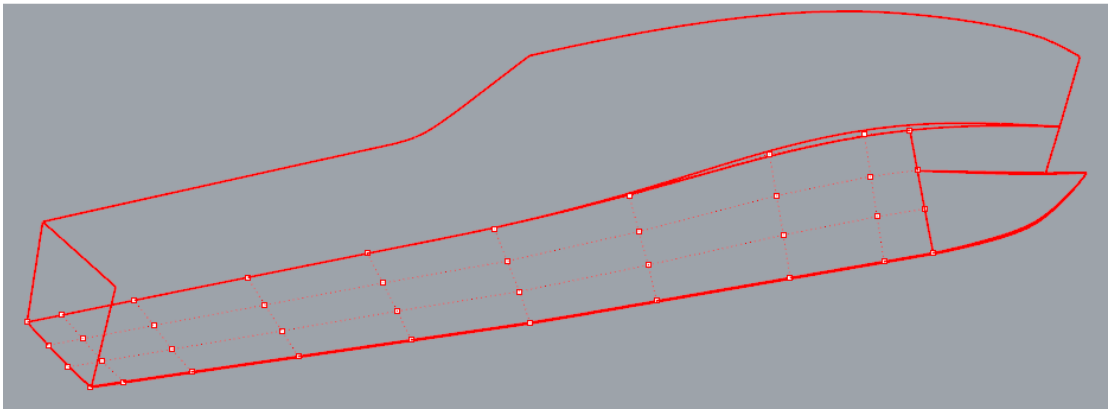

Fig. 6.8 - Control points on the hull bottom

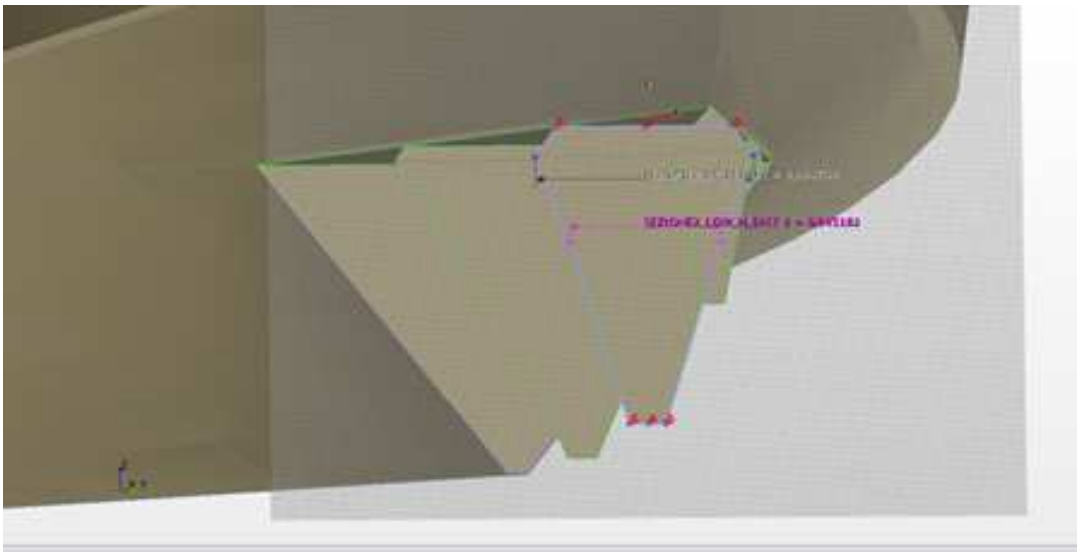

Fig. 6.9 - Bulb control sections setting

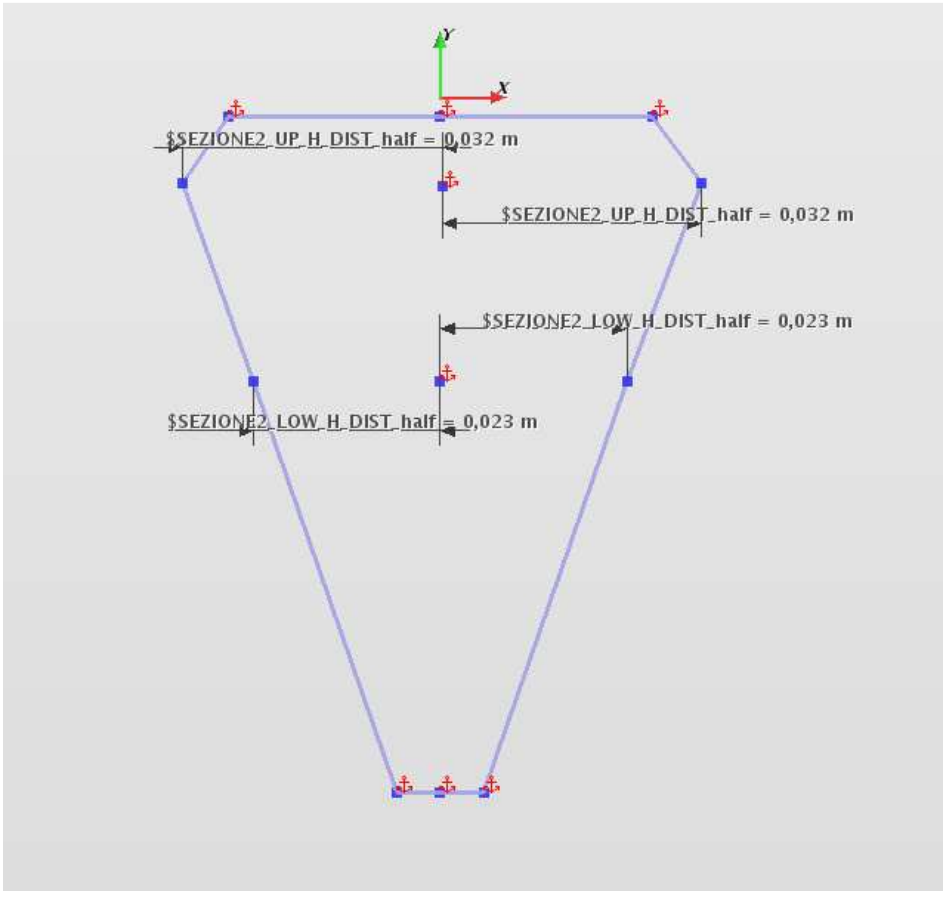

Fig. 6.10 - Parameterisation of bulb sections

6.3.2 Constraints

In order to comply with the shapes' unfolding , to get some printable surfaces without undercuts, to take into account of potential requirements of nautical interior installation and furnishing lay-out, as well as to create a hull volume with its center compatible with the the boat's weights castle, strict constraints have been set:

Water lines: each Y_m frame may fall towards the mizzen axis up to 5% of its initial Y_i extension and away maximum of 15%.

$$0.95Y_i \leq Y_m \leq 1.15Y_i \quad (6.2)$$

Centre of buoyancy: may fluctuate around to the starting position up to 5% of L

$$37.5\%L_{OS} \leq LCB_m \leq 42.5\%L_{OS} \quad (6.3)$$

Displacement: may fluctuate around 5% to the initial value

$$0.95\Delta_i \leq \Delta_m \leq 1.05\Delta_i \quad (6.4)$$

Bulb: its length variation may fluctuate at maximum around 2% of L vessel

$$0.98\ L_{bulb\_i} \leq L_{bulb\_m} \leq 1.02L_{bulb}i \quad (6.5)$$

6.3.3 Parameters analysis

The hull developed was modeled by inserting 26 modification parameters (as discussed below) and therefore having to minimize the resistance under two different conditions (speeds), the optimisation to be performed is actually a double objectives one. The only downside is that the simulation software is scheduled to simulate the behavior at one speed a time. Therefore it was necessary to prepare two different setups, one for each speed. Heeds, randomly generates eligible basic hulls, and it starts to execute the various runs of Star-CCM + analyzing the results. If a specific combination of changes should lead to increasingly worse results, Heeds "understands" that the way is the right one and it avoids to start the simulations that will give bad results probably, thus allowing to save several tens of hours of calculation.

In broad terms, the flow optimisation run by Heeds-Optimate works like this:

• Analysis of the number n of parameters (in this case n = 26)

• Analysis of the number m of objectives (in this case m = 2)

• Analysis of the constraints for each parameter and the discretization step of the single constraint

• Generating a Q number of alternative designs (in this case it has been imposed an executable runs limit equal to

2Q = 11 * m * n = 572 runs

286 daughters hulls available, because each hull is tested twice at different speeds)

• Trend analysis of results for similar designs waste of falling design

• Convergence optimality in W runs, with

5 * m * n≤W≤6 m * n

in this case taken place in 271 runs (the winning run 246).

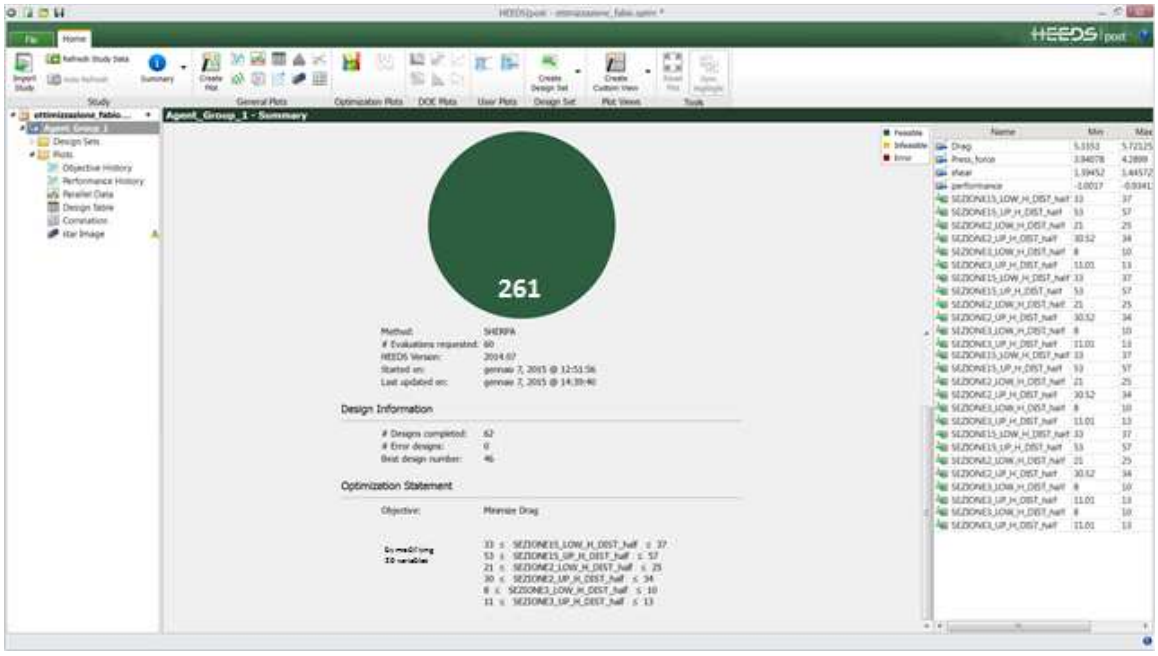

Fig 6.11 - Summary of HEEDS post-processing

Not all variants randomly generated are good, in fact, despite being geometrically congruent with the constraints required, they may lead to diverge the CFD simulation. In this case Heeds shall discard them.

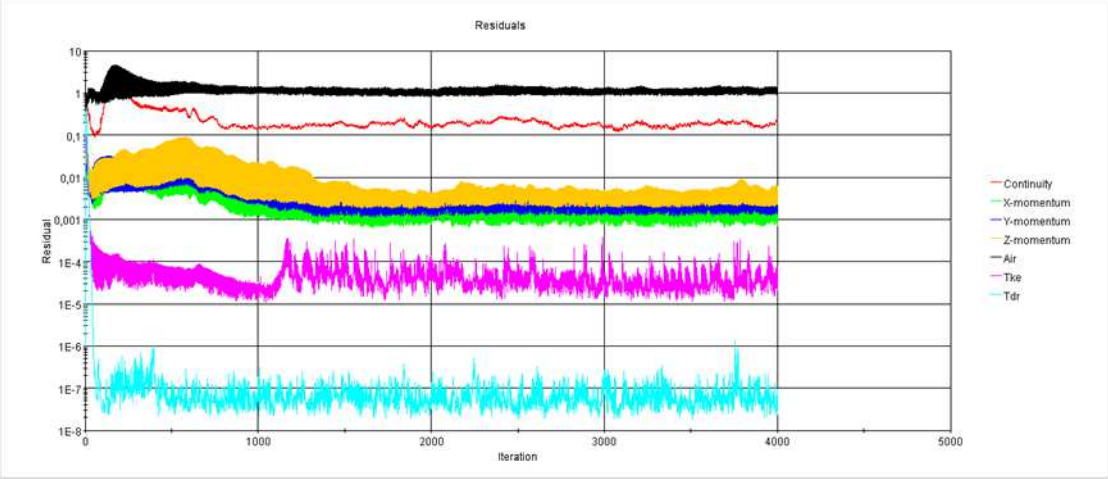

Fig. 6.12 - Typical Residual analysis to evaluate the convergence

If you are measuring forces, as in the present case, it doesn't necessarily mean the value converges perfectly - only considering the low number of cells - since it could present several harmonic oscillations. In this case it is necessary to create a Field Function that makes the average value of the force in a given time, at least equal to 2 times the duration of the single oscillation. This will be the average value that Heeds-Optimate will consider.

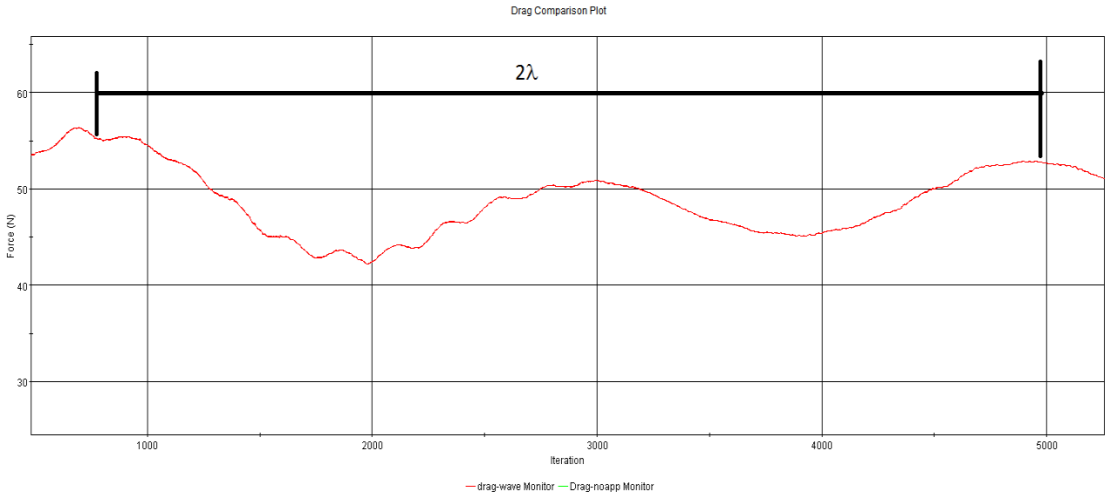

Fig 6.13 – Numerical oscillation of the forces measured

6.3.4. Objectives and expected results

The dual objective required was the reduction of the total resistance, at two different speeds, 16kn and 24kn, i.e. cruising speed and maximum speed.

As specified in paragraph 6.3.3, the parameters set are n = 26, the objectives m = 2 and then the cases generated by Heeds-Optimate have been Q = 11/2 *m*n = 286, with an expected number of runs (two for each speed) equal to 2Q = 572, while the convergence towards the optimum was achieved in W = 271 runs (winning the 246 run), observing the expected parameters equal to 5*m*n ≤W ≤ 6 *m*n.

Performing calculations on 12 cores workstation, the results have been obtained in about **680 hours of computing time**, drastically reducible using suitable computing centers for the only optimization.

Heeds-Optimate stopped on reaching the dual objective, providing the final result of the hull lines capable of providing:

• 4% reduction in resistance to 16kn (cruising speed);

• 2% reduction in resistance to 24kn (top speed).

In the figures 6.14, 6.15, 6.16 and 6.17 you can see the changes made by the optimization.

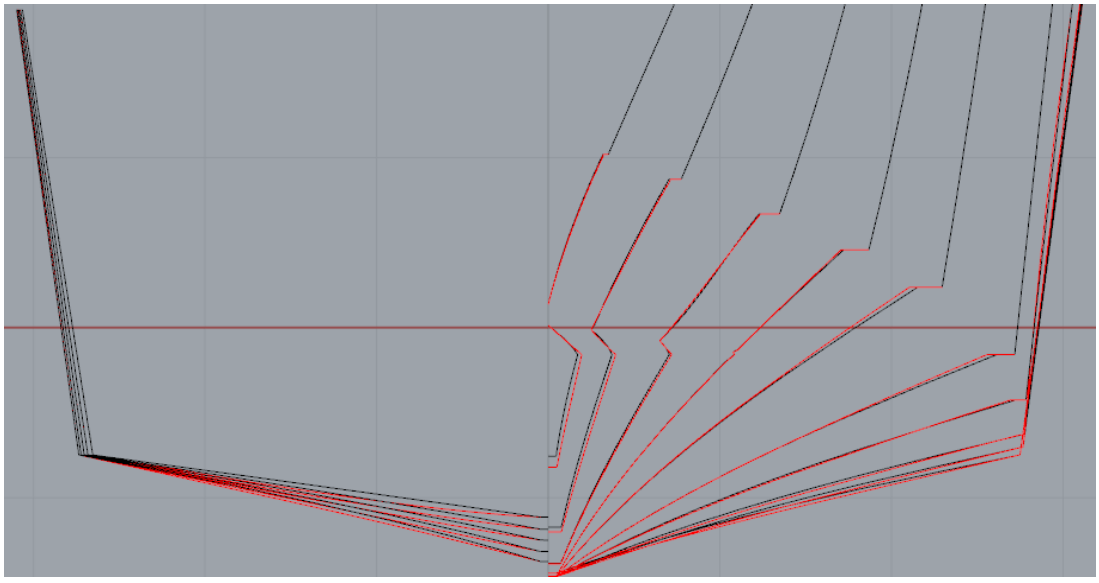

*Fig 6.14 - Comparison between the mother hull (**black**) and the final hull (**red**): transverse sections*

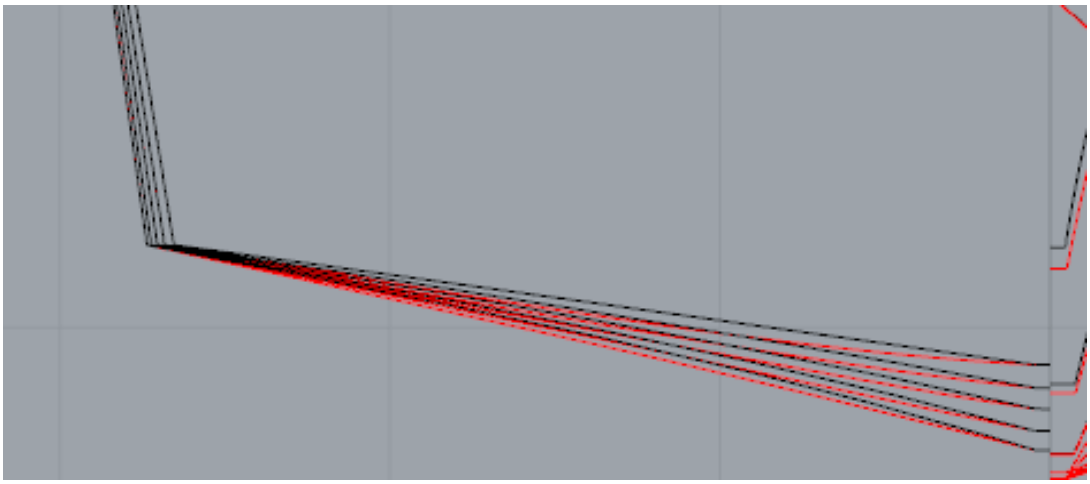

*Fig 6.15 - Comparison between the mother hull (**black**) and the final hull (**red**): transverse sections – bottom stern zone*

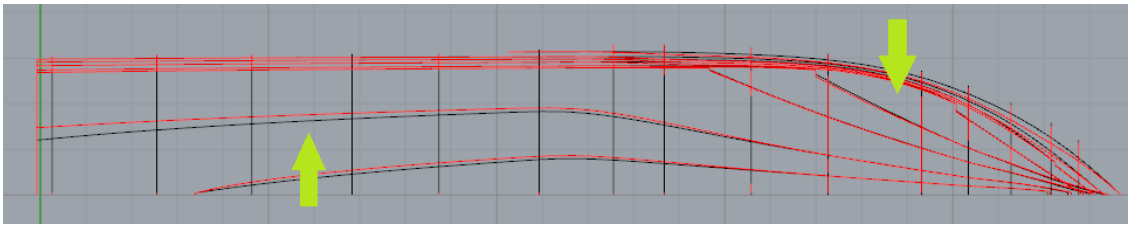

*Fig 6.16 - Comparison between the mother hull (**black**) and the final hull (**red**): water lines*

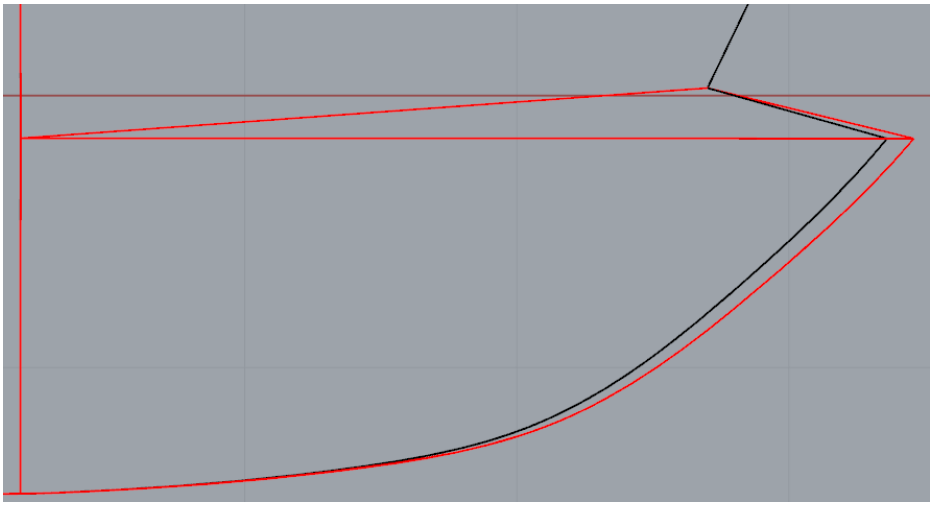

*Fig 6.17 - Comparison between the mother hull (**black**) and the final hull (**red**): bulb length*

As can be seen from figures the chosen hull has more volume in the stern and less volume in the bow, offset by a bulb's greater length that helps to reduce the center of buoyancy recession.

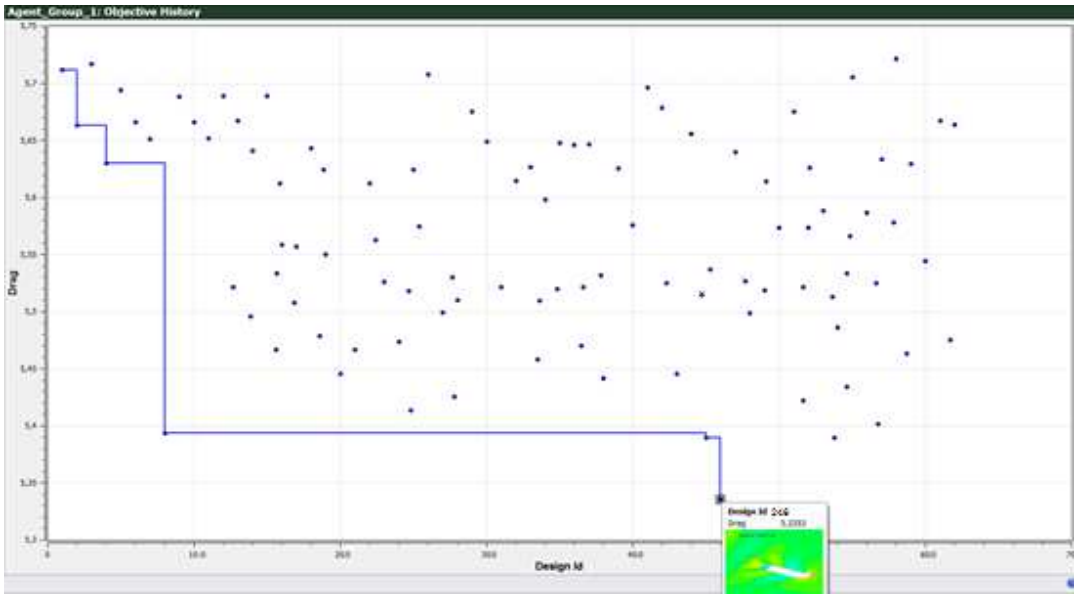

Fig 6.18 - Solutions' space generated by Optimate and related optimality frontier

At the end of the optimization it has been carried out the simulation of each point of the resistance curve of both the initial hull and the final one. In the fig. 6.18 it's possible to see the solutions' space generated by Optimate and the related optimality frontier.

It is noted that the final hull has smaller resistance and trim values throughout the whole speed range, except in the very low ones, where, as expected, the hull worsens having the center of buoyancy more backlog (see table 6.1 and fig. 6.19).

Regarding the trim angle (fig. 6.20) it's interesting to see that in the final hull the values are smaller, this due to the more lift carried out by the new bottom sections.

Table 6.1 Comparison between initial and final resistance

V_S, kn	Fr	R_{TM} init, N	R_{TM} final, N	R_{TM} final / R_{TM} initial %	Trim angle init, deg	Trim angle final, deg
12	0,41	11,82	12,38	5%	0,10	-0,20
16	0,55	24,32	23,43	**-4%**	2,67	1,74
20	0,69	28,38	27,51	-3%	3,22	1,90
24	0,82	33,13	32,30	**-2%**	3,35	1,66
28	0,96	37,56	37,18	-1%	3,77	1,45

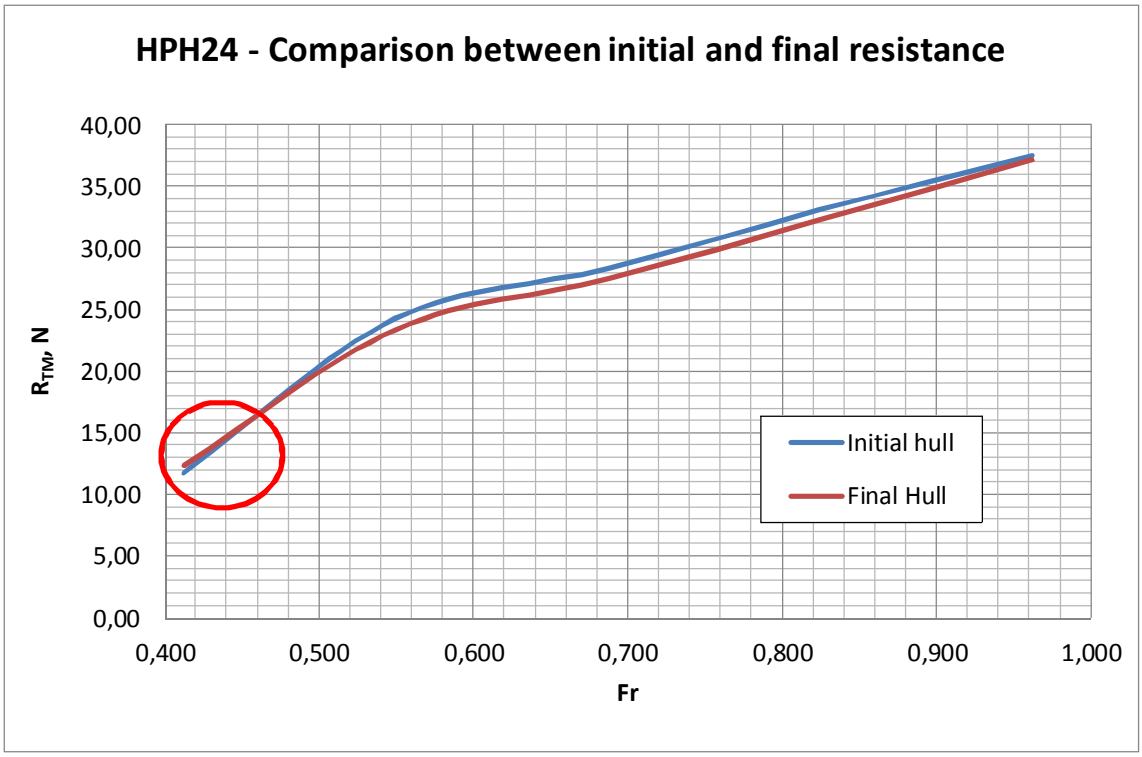

Fig. 6.19 - Comparison between total resistance curves of the two hulls (initial and final one)

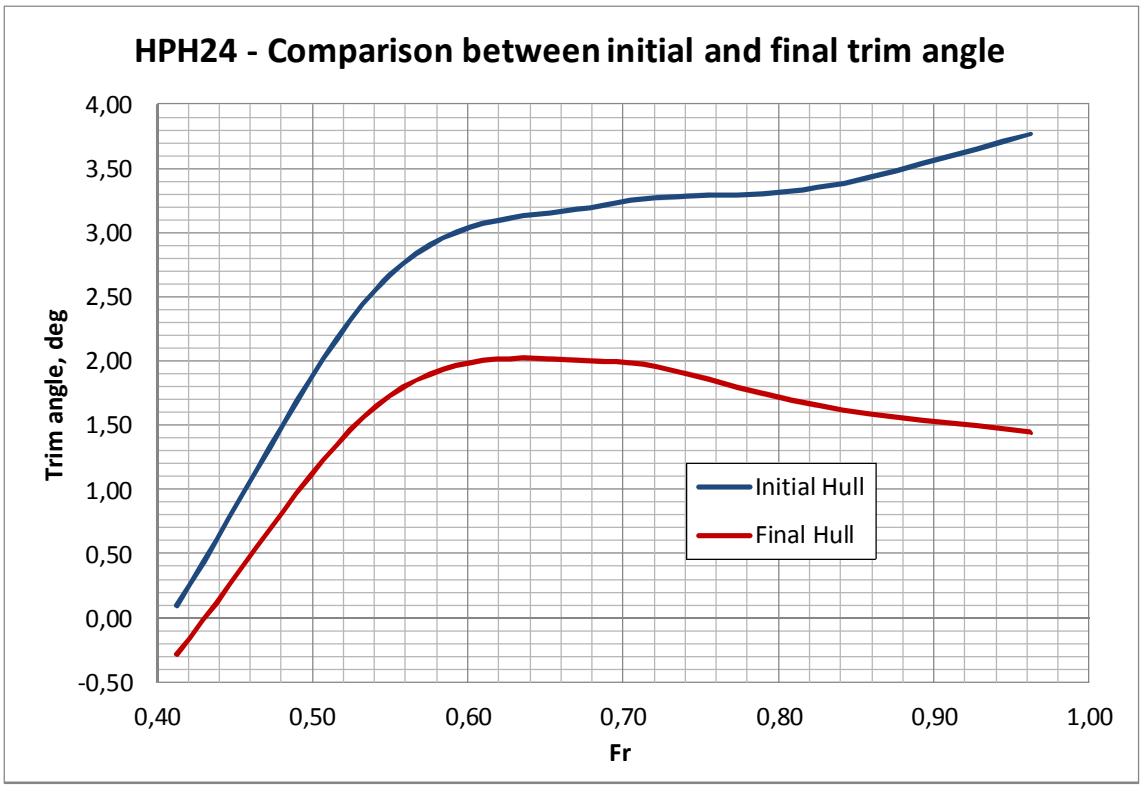

Fig. 6.20 - Comparison between trim angle curves of the two hulls (initial and final one)

Finally, by analyzing separately the only pressure resistance (for the most part made up of wave resistance), in order to assess the real added value of such kind optimization compared to an hypothetical classical optimization through BEM method, it can be noticed that while the total resistance at medium to high speeds is always lower in the final hull, it is not properly in this 1way for the friction resistance (see table 6.2 and fig. 6.20 and 6.22).

In fact, the final hull navigates to a very small trim and with a greater heave, and therefore, while generating different (and apparently more) wave formation in the bow, it appears to have a bigger wetted surface than the initial hull, in particular in the bow zone, earning in increasing of friction a part of what has been reach by the bow wave formation, due to the antiphase wave generated by the blade bulbous bow.

These insights are supported by the observation of the wave profile generated by the initial and final hulls (fig. 6.23, 6.24, 6.25 and 6.26), as well as the pressure field on the bottom, which is also much more regular in the optimised hull (fig. 6.27 and 6.28).

Table 6.2 Pressure and Friction Resistance Comparison

V_S, kn	Fr	R_P init, N	R_P final, N	R_F init, N	R_F final, N
12	0,41	8,816	9,363	3,001	3,018
16	0,55	19,346	18,573	4,974	4,854
20	0,69	21,331	20,340	7,045	7,171
24	0,82	23,112	22,131	10,013	10,169
28	0,96	25,204	24,126	12,351	13,053

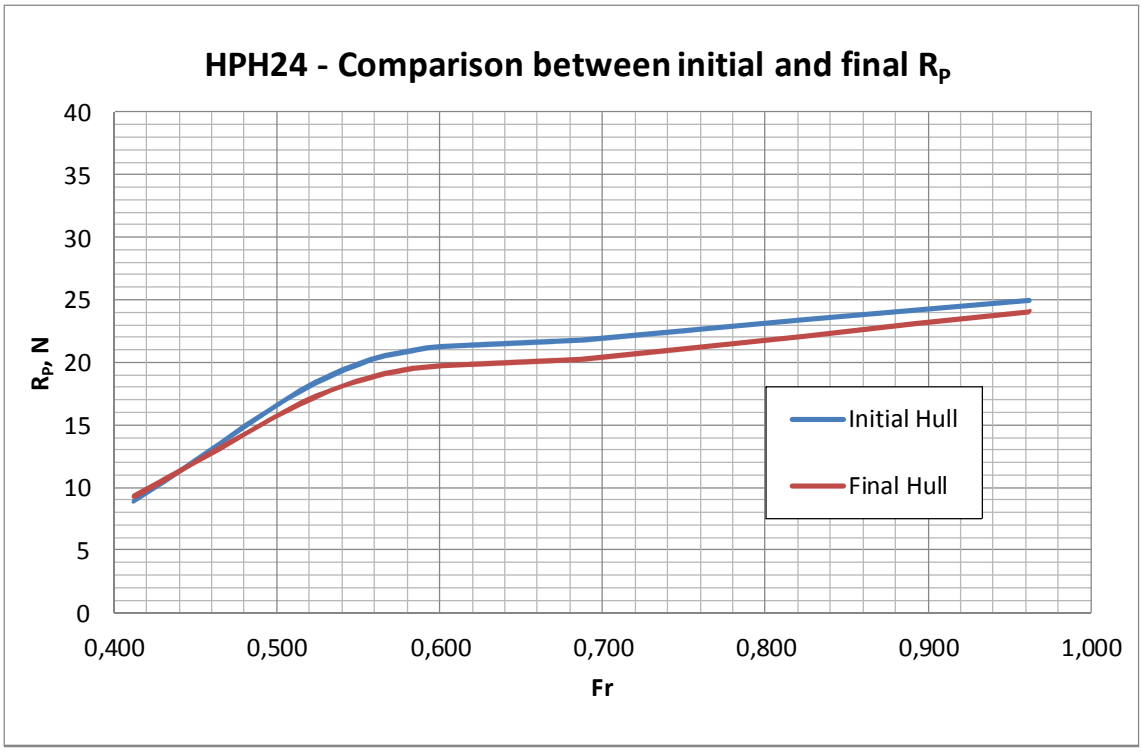

Fig. 6.21 - Comparison between initial and final pressure resistance

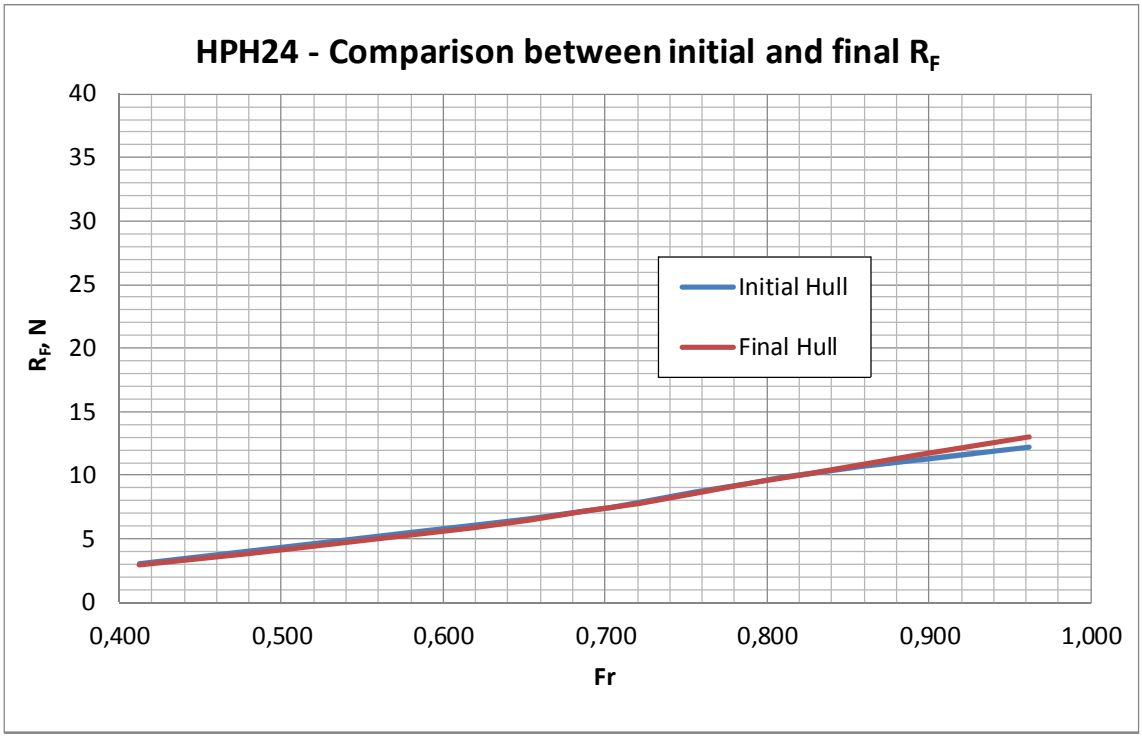

Fig. 6.22 - Comparison between initial and final friction resistance

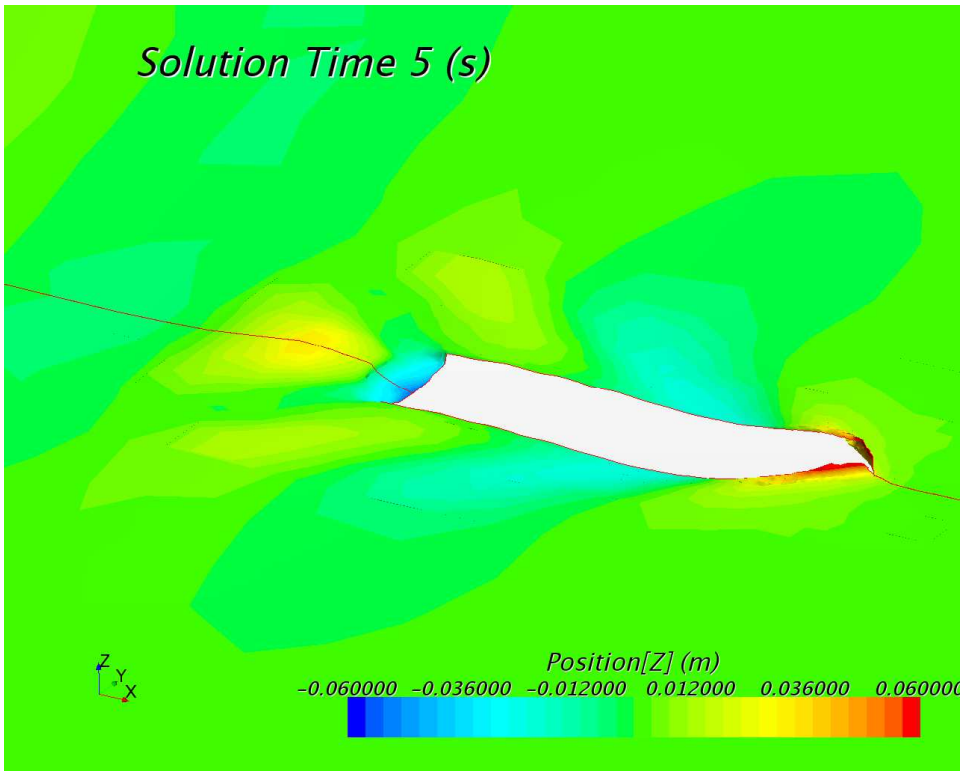

Fig. 6.23 - Wave pattern at 16kn – mother hull (id-1)

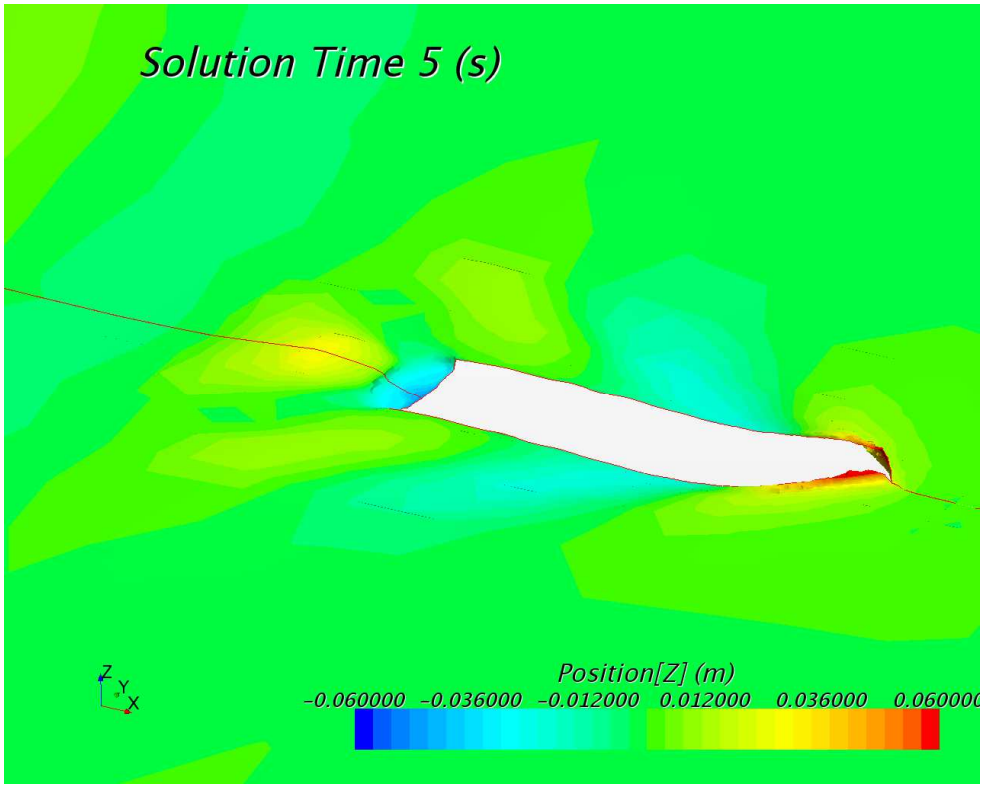

Fig. 6.24 - Wave pattern at 16kn - optimised hull. (id-246)

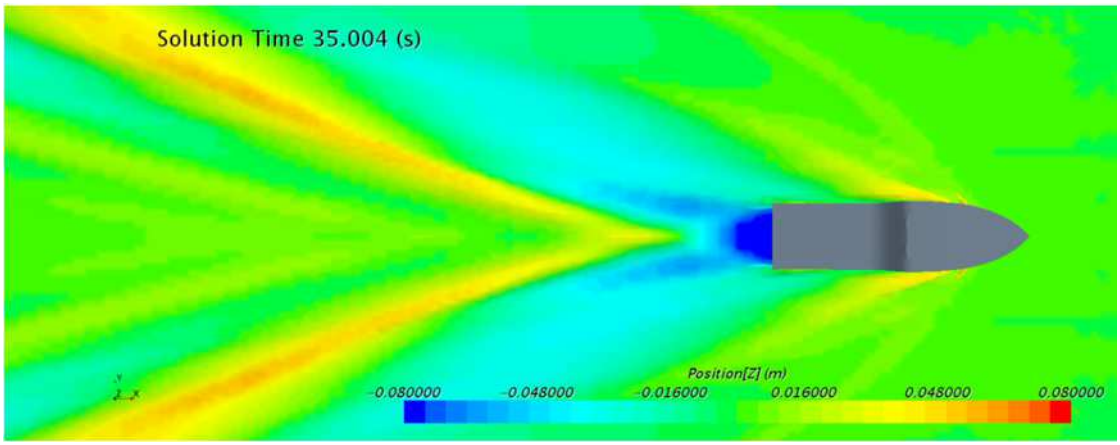

Fig. 6.25 - Wave pattern at 24kn – mother hull (id-1)

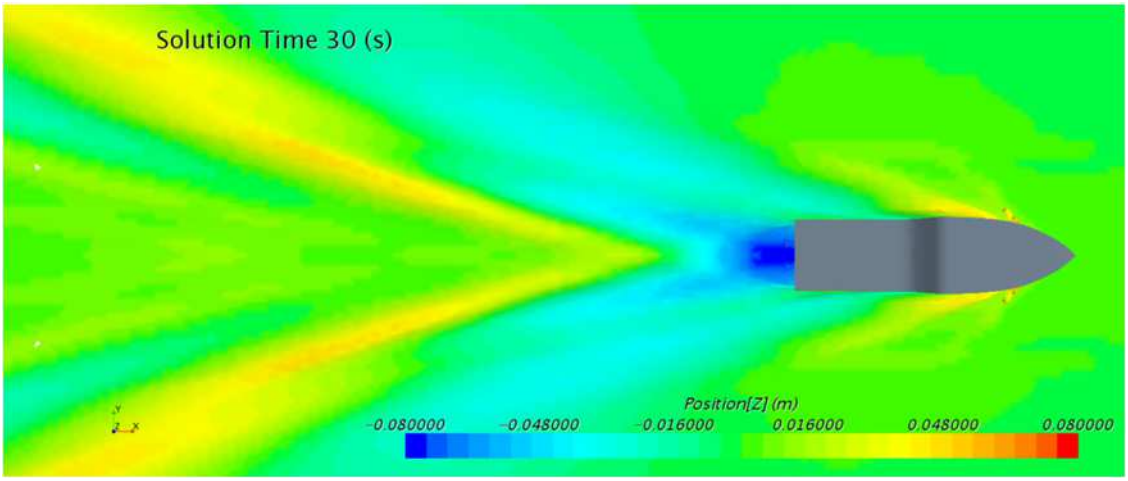

Fig. 6.26 - Wave pattern at 24kn – optimised hull (id-246)

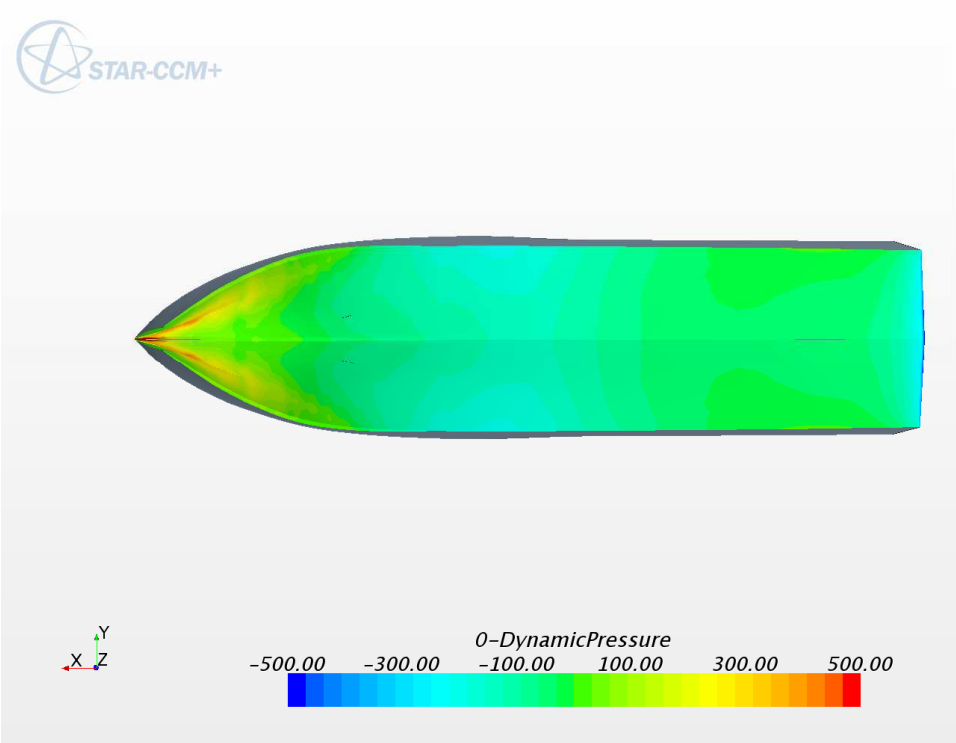

Fig. 6.27 - Dynamic Pressure at 16kn – mother hull (id-1)

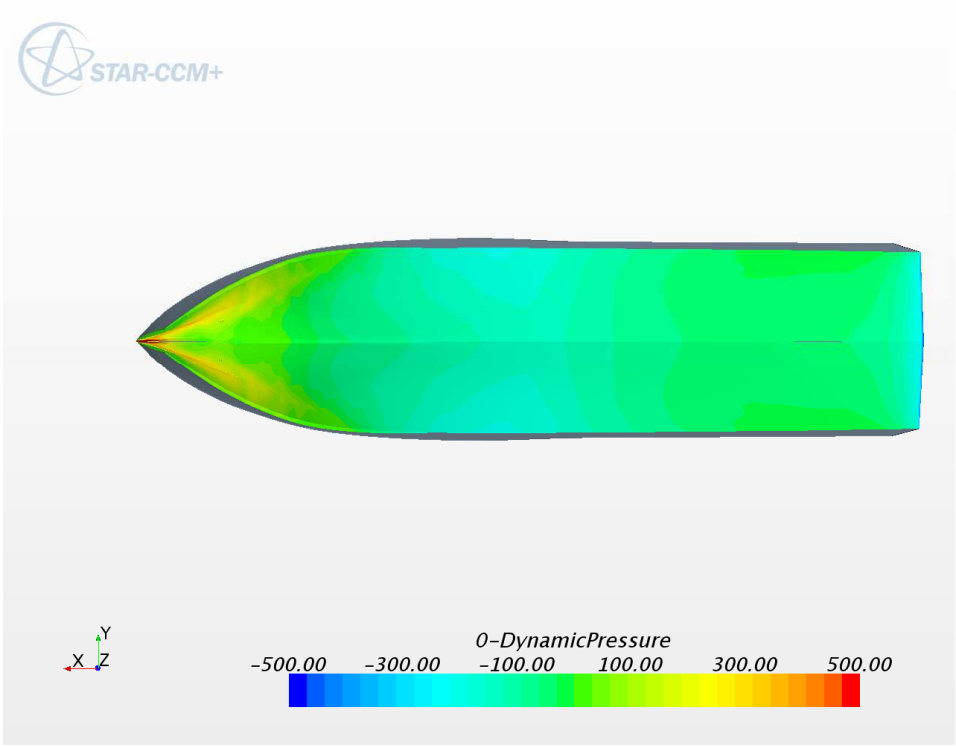

Fig. 6.28 - Dynamic pressure at 16kn – optimised hull (id-246)

6.4 CONCLUSIONS

It was seen that in less than 680 hours of calculation with a traditional 12 core server, (using a computing 100 core center, time would be reduced to about 80 hours), you can obtain a morphological optimisation of the hull based on minimizing total resistance at two different speeds, the results of which are also valid, in absolute terms, to calculate the vessel necessary power in order to reach the predetermined speed, unthinkable with a classic BEM solver.

Extremely interesting is also the diagram of the correlation provided by Heeds-Optimate (fig. 6.29), which indicates how each measured parameter (pressure, forces and anything else regarded as necessary) varies according to one of the input parameters' variation. This is extremely useful to understand how much it is worth or not insisting upon a particular area of the hull to reach a good result, while avoiding wasting time and energy in making changes that account for a few millesimal points.

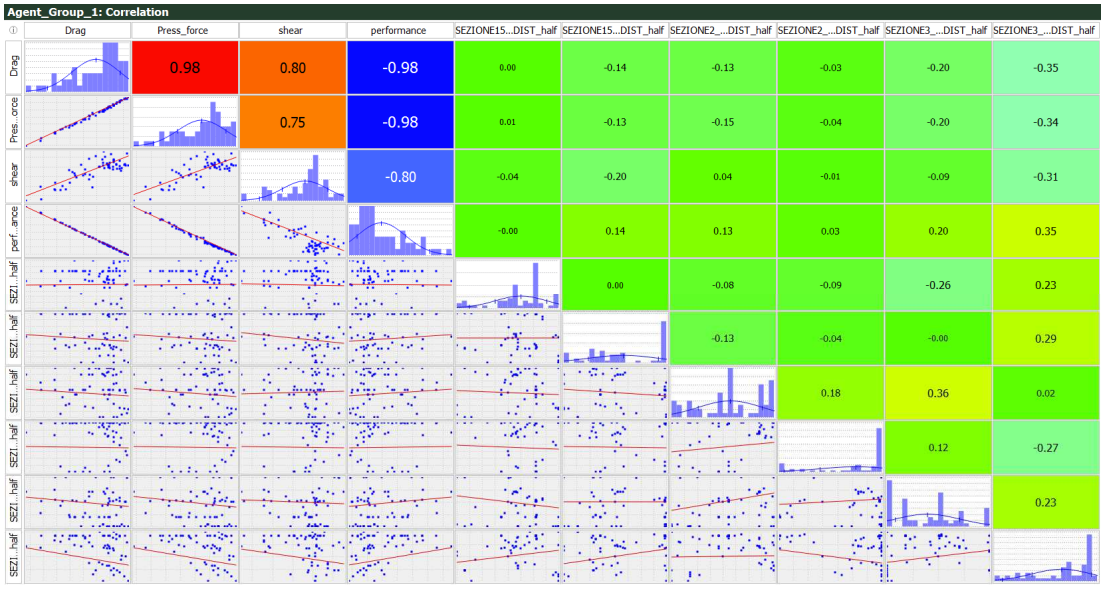

Fig. 6.29 - Diagram of correlations between input and output parameters

COMPARISON BETWEEN NUMERICAL ANALYSYS AND EXPERIMENTAL TESTS

In order to validate the results of the optimization, it was decided to build a 1:15 scale model (see fig. 7.1, 7.2 and 7.3) of the final optimized hull to perform Towing Tank Tests at the University of Trieste [59]. The scale factor is the same used during CFD simulations. Thereby, it becomes possible to compare the results obtained without the scale effect troubles, directly.

Fig. 7.1 - profile view of the HPH24 scale model

Fig. 7.2 - view of the bottom of HPH24 scale model

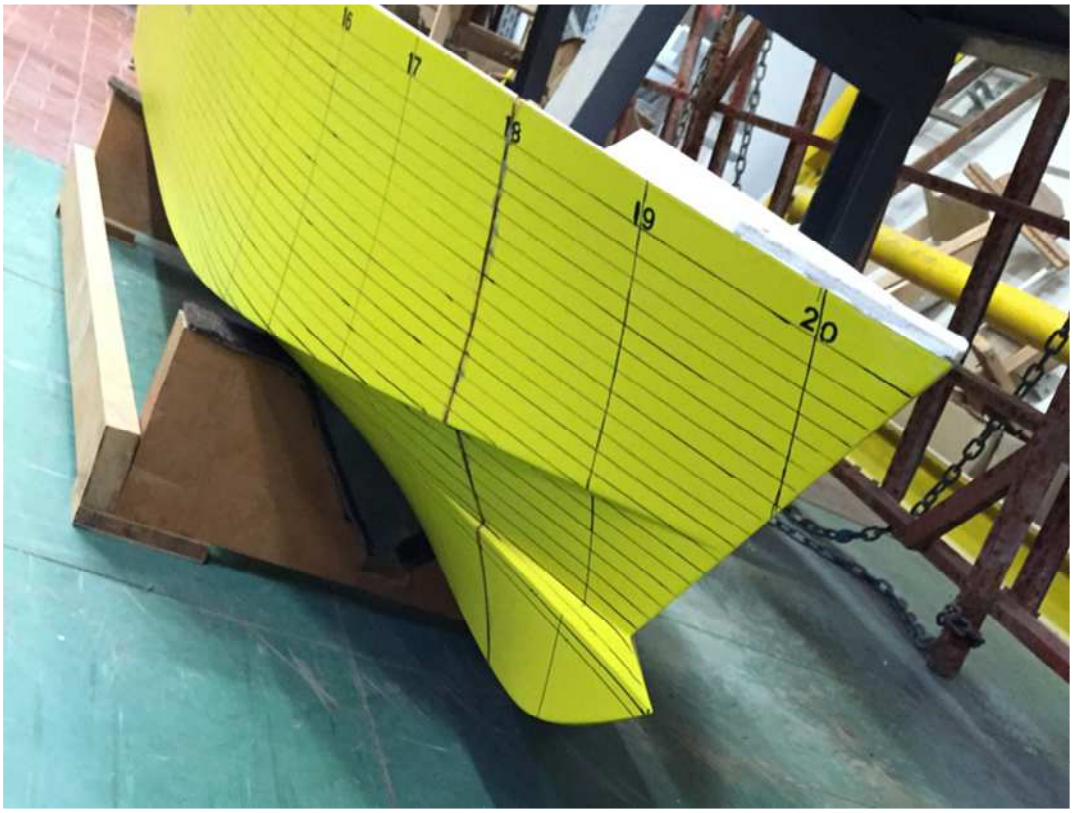

Fig. 7.3 - HPH24 scale model with waterlines and sections

As can be seen from the table 7.1 and the figure 7.5 and 7.6, towing tank tests' results confirm, with an absolute error of about 2%, what had been numerically calculated. In fact both the resistance values and HPH24 hull optimized trim's ones are confirmed.

Fig. 7.4 - Tank test of HPH24 at Fr 0.2

Table 7.1 Resistance comparison between CFD analysis and towing tank tests

$V_{M,}$ m/s	V_S, m/s	Fr	R_{TM} CFD	R_{TM} tank	R_{TM} CFD / R_{TM} tank %
1.59	12	0.41	12.38	12.13	0.02
2.13	16	0.55	23.43	23.19	0.01
2.66	20	0.69	27.51	27.10	0.02
3.19	24	0.82	32.30	31.59	0.02
3.72	28	0.96	37.18	36.55	0.02

Table 7.2 Dynamic trim angle comparison between CFD analysis and towing tank tests

$V_{M,}$ m/s	V_S, m/s	Fr	CFD Trim angle, deg	Tank trim angle, deg	Delta angle, deg
1.59	12	0.41	-0.28	-0.18	0.10
2.13	16	0.55	1.74	1.86	0.12
2.66	20	0.69	2.01	2.16	0.15
3.19	24	0.82	1.66	1.86	0.20
3.72	28	0.96	1.45	1.60	0.15

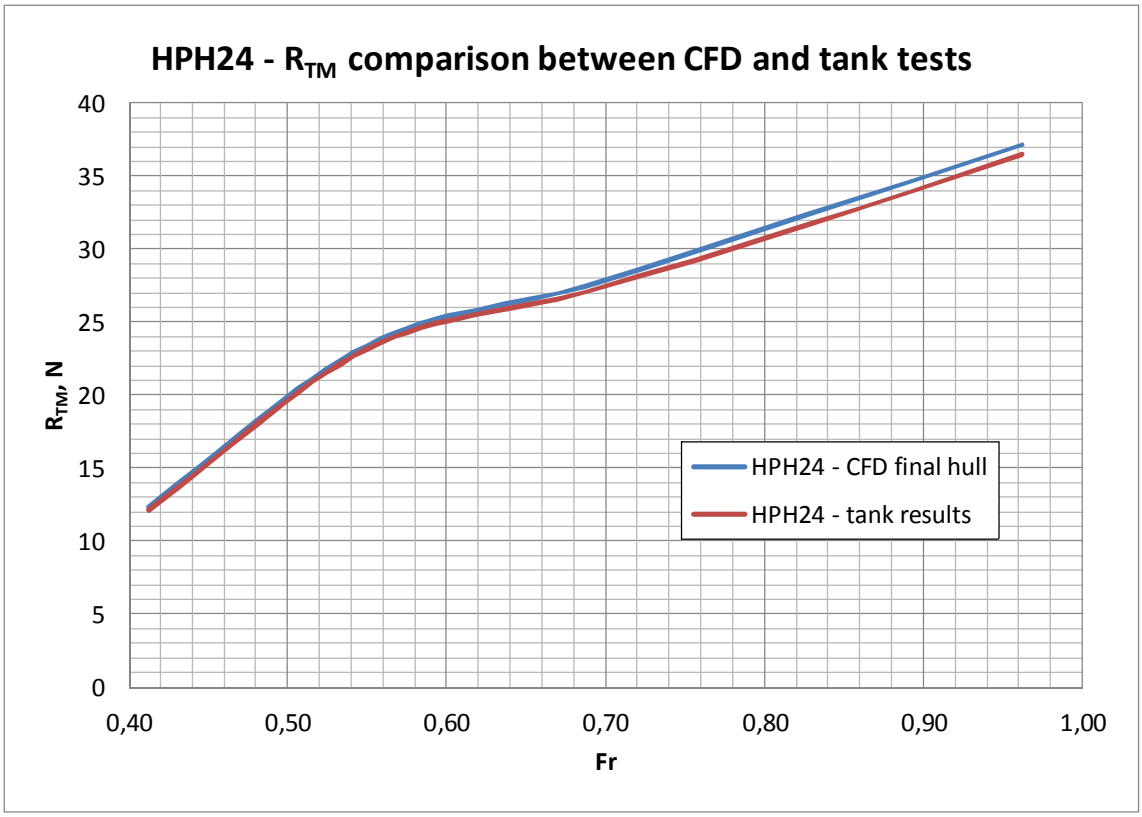

Fig. 7.5 - Resistance comparison between CFD analysis and towing tank tests

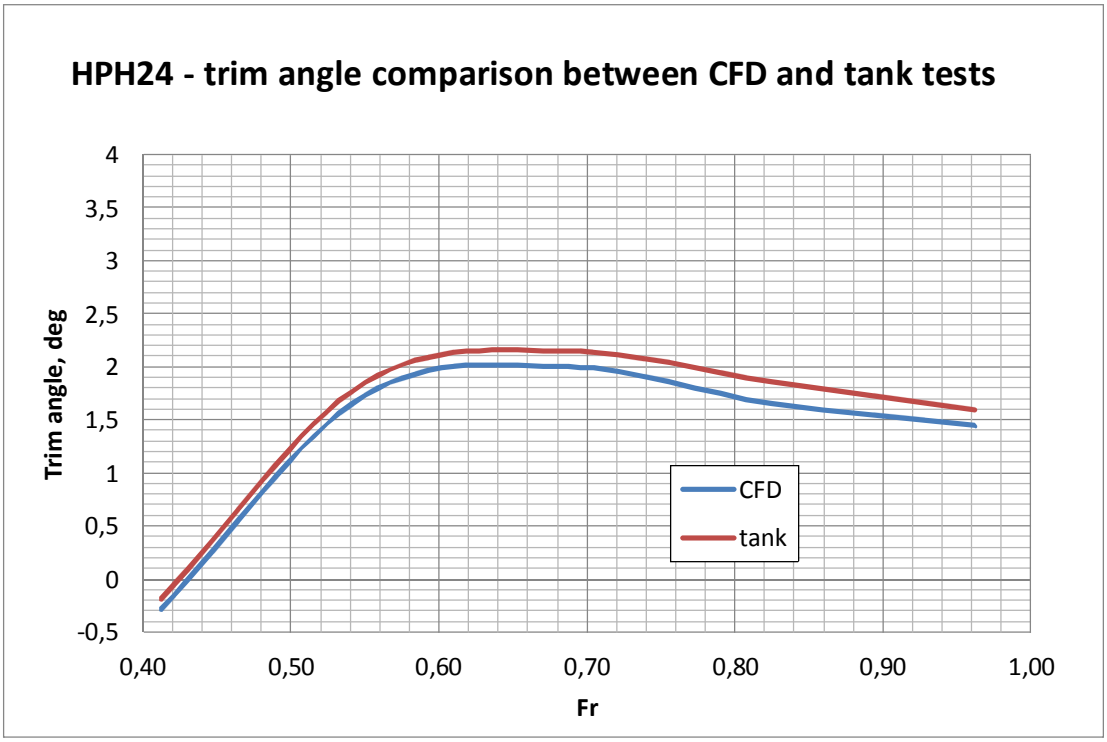

Fig. 7.6 - Dynamic trim angle comparison between CFD analysis and towing tank tests

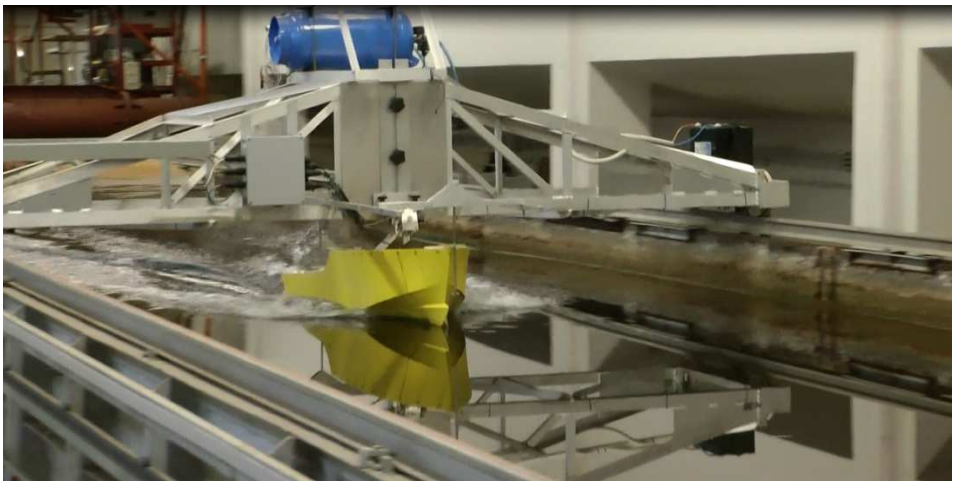

Fig. 7.7 - Tank test of HPH24 at Fr 0.7

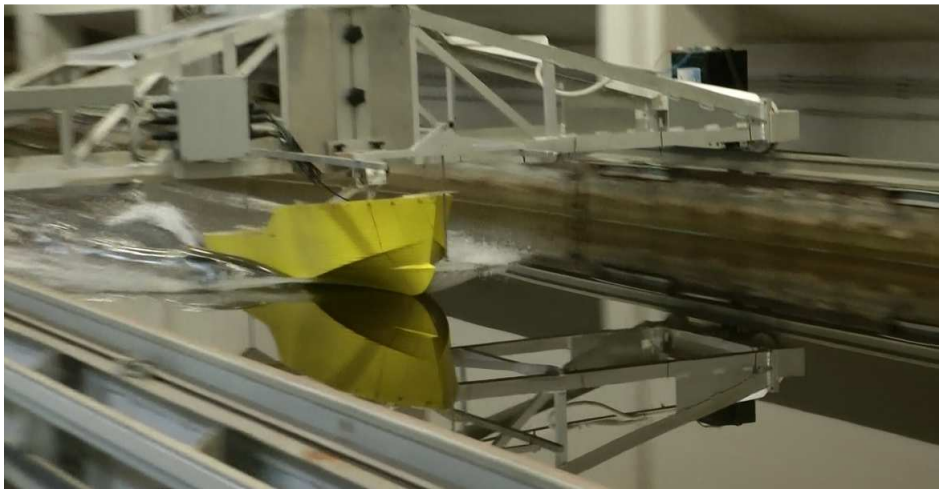

Fig. 7.8 - Tank test of HPH24 at Fr 0.8

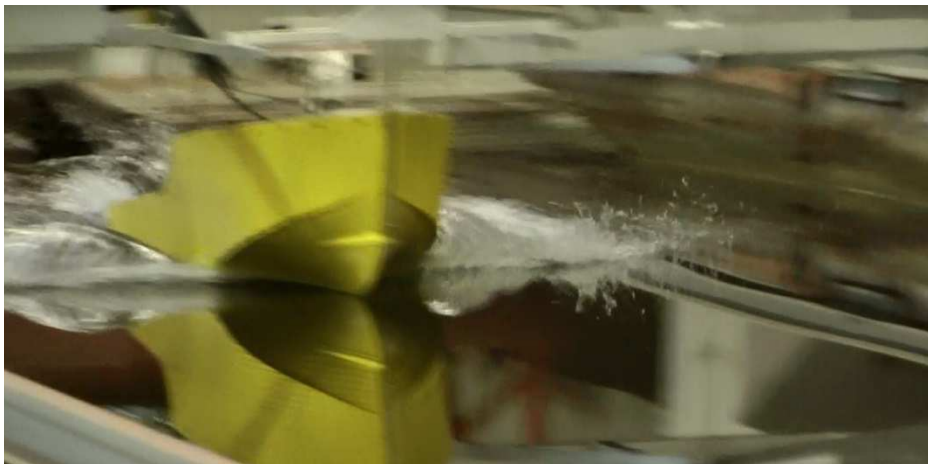

Fig. 7.9 - Tank test of HPH24 at Fr 1.0

CONCLUSIONS

Aim of this work was searching for a method that could be reasonably fast and reliable to optimise the hull shape, in order to minimize the total resistance.

It was therefore decided to work with RANSE simulation codes in order to evaluate total resistance and, having a large amount of calculations to be faced, it was proceeded to investigate and to standardize a computing procedure with low number of cells, as to be able to ensure a good approximation of the absolute result in reasonable computation time. The CFD software chosen was Star-CCM + by CD-Adapco.

A standardization process of meshing with low number of cells has been developed and proven. After a series of analysis and investigations, it was considered possible to divide the potential hulls to be tested in three different families, each of which relating with geometries of the same kind and sailing in the same range of Froude numbers. In this case, by comparing the hull relative speeds to the morphology will typically have, it was possible to develop 3 only standard setup, with a drastic reduction of the number of computing elements than those normally used in literature.

The use of simulations with coarse mesh for comparative analysis is already known and used; in this case the innovation lies in having been able to develop standard set-up suitable for any hull relating to the family in question. The procedure was then proven and validated through numerous case studies, comparing the obtained results with those available in literature as well as with the results of numerous towing tank tests.

Then, it was evaluated the possibility to use this kind of fast RANSE simulations to perform multi-objective optimization calculations. After evaluating several options, it was decided to go on with the parameterization of the hull using Star-CAD. The procedure to search several

alternatives and the best optimisation has been performed using the software Heeds-Optimate by RED Cedar, using the hybrid algorithm called SHERPA (see chapter 5).
Such kind of procedure, applied on a particular semi-planing hull with a blade bulbous bow, led to the possibility of performing an optimization based on the total resistance reduction at two different speeds, whose results have been subsequently validated by tank tests.
This work demonstrates that it's possible to perform multi-objective optimizations using the support of viscous CFD solvers without increasing computing time and costs.

Implicitly, it has been shown that it is possible to standardize a "coarse grid" able to ensure a good simulation result in less time, without having to run simulations with several millions of elements and without having to run grid-independence assessments and custom mesh refinements, each time.

The use of this methodology, both in the case of optimisation or simple comparative simulation, allows the designer to be able to evaluate his hull behavior characteristics, such as the analysis of the total resistance, in a reasonable timeframe.
Typically in fact, hull morphological optimisations are developed with the aid of fast BEM simulators, which in a short calculation time are capable to assess the wave resistance of the boat.
Furthermore, the use of a RANSE software allows the designer to get a myriad of information in addiction and particularly the information about the total resistance value in absolute terms at a given speed, allowing to make more accurate analysis and to achieve a better end result.
By using the procedure developed in the present thesis it will be able to work with CFD RANSE at low cost, drastically reducing the computation time and especially allowing to carry out the work on traditional workstation without having to rely on the computing centers.
Whilst wanting to use a computer center equipped with hundreds of processors, the optimization results of the total resistance based on two distinct speeds would require little more than 80 hours of calculation, which is a completely reasonable time.
A procedure like this, on one side, allows the opportunity to work on the total resistance or other physical quantities expressed by the RANSE solver, on the other side - thanks to its speed and its simplicity of use - enables the approach to the CFD also for small boats' designers who, due to lack of time and budget, could not approach to a so refined hulls designing technology, up to now. There are few examples in literature that confirms this way [60].

In the near future the widespread use of optimization techniques, or even just comparative and analysis ones on hulls for large and small boats, will be able to significantly contribute to save engine power installed on board (i.e. by reducing the total resistance), allowing both economic fuel savings and, above all, a strong toxic emissions reduction in the atmosphere.

As a first approach to such kind of issue - for simplicity, technical support and result's warranty - it was decided to use only commercial software, also because a connection interface with each other was already provided.
Nevertheless, in the near future such kind of procedure can be implemented and standardized also using an open source set of codes.

BIBLIOGRAPHY

[1] BRIZZOLARA, VIVIANI, VERNENGO, et al., "Automatic Hull Form Optimization in the Context of the Preliminary Ship Design", *FAST Conference 2011*. Honolulu, Hawaii, 2011

[2] HARRIES, "Parametric design and hydrodynamic optimization of ship hull forms". Mensch & Buch Verlag, 1998.

[3] BILIOTTI, BRIZZOLARA, VERNENGO et al., "Automatic Parametric Hull Form Optimization of Fast Naval Vessel". *Proceedings of HIPER Conference 2010*, pp. 261-273, Melbourne, Florida.

[4] VERNENGO, "Parametric Hydrodynamic Optimization of Ship Hull Forms based on CFD Techniques: Theory and Application", *PhD Thesis*, University of Genoa, 2012

[5]BRIZZOLARA, VIVIANI, VERNENGO et al., "Automatic Hull Form Optimization in the Context of the Preliminary Ship Design". *FAST Conference 2011*. Honolulu, Hawaii.

[6] VERNENGO, BRIZZOLARA, "Automatic Computer Driven Optimization of Innovative Hull Forms for Marine Vehicles". *ACACOS Conference 2011*. Venice, Italy.

[7] CAMPANA, PERI, TAHARA, STERN, "Shape optimization in ship hydrodynamics using computational fluid dynamics", *Computer methods in applied mechanics and engineering* 196, pp. 634–651, 2006

[8] VASUDEV, SHARMA, BHATTACHARYYA, "A multi-objective optimization design framework integrated with CFD for the design of AUVs", *Methods in Oceanography* 10 pp.138–165, 2014

[9] SHENG-ZHONG LI, FENG ZHAO, QI-JUN NI, Bow and Stern Shape Integrated Optimization for a Full Ship by a Simulation-based Design Technique, *Journal of Ship Research* Vol. 58, No. 2, pp. 83–96, 2014

[10] PERCIVAL, HENDRIX, NOBLESSE, "Hydrodynamic optimization of ship hull forms". *Applied Ocean Research*, Vol. 23, pp. 337-355. 2001

[11] JANSON, LARSSON, "A method for the optimization of ship hulls from a resistance point of view", *21st symposium on Naval Hydrodynamics*, Trondheim, Norway, 1996

[12] SOONHUNG HAN, YEON-SEUNG LEE, YOUNG BOK CHOI, "Hydrodynamic hull form optimization using parametric models", *Journal of marine and science technology* vol.17, pp.1–17, 2012

[13] VAN MANEN, VAN OOSSANEN, "Principles of Naval Architecture", Second Revision, vol.2, cap.V, E.V. Lewis, 1988

[14] INTERNATIONAL TOWING TANK CONFERENCE, "ITTC symbols and terminology list, version 2011, 2011

[15] HEGGERT, "Further from resistance experiments", *Society of Naval Architects and Marine Engineering (U.S.)*, 1939

[16] HAVELOCK, "The calculation of wave resistance", *Proceeding of the royal society of London*, 1934

[17] HESS, SMITH, "Calculation of non-lifting potential flow about arbitrary three dimensional bodies", *Journal of Ship Research*, Vol.8, No.2, 1964

[18] DAWSON, "A Pratical Computer Method for Solving Ship Wave Problems", *Proceedings of 2nd International Conference on Numerical Ship Hydrodynamics*, University of California, 1977

[19] FERZIGER, PERIC, "Computational Methods for Fluid Dynamics", 3rd Edition, Springer, 2002

[20] HIRT, NICHOLS, "Volume of Fluid (VOF) Method for the Dynamics of Free Boundaries", *Journal Of Computational Physics*, n.39, pp.201-225, 1981

[21] LAX, MILGRAM, "Parabolic equations in contributions to the theory of partial differential equations", *Annals of Mathematics Studies*, n.33, pp.167-190, Princeton University Press, 1954

[22] BABUSKA, “Error-bounds for finite elemet method”, *Numerische Mathematik*, vol.16, pp.322-333, 1970

[23] CD-Adapco (2014) STAR-CCM+ User Guide, version 9.04.

[24] AGRUSTA, ZOTTI, “Evoluzioni e tendenze idrodinamiche nello sviluppo idrodinamico delle modern carene veloci”, *Proceeding of SEA-MED 2012 – Innovazione e Nautica Sostenibile*, University of Messina, 2012

[25] AGRUSTA, BRUZZONE, ESPOSITO, ZOTTI, “CFD simulations to evaluate the ship resistance; development of a systematic method with use of low number of cells”, *Proceedings of SORTA 2014*, University of Rijeka, 2014

[26] AGRUSTA, BRUZZONE, ESPOSITO, ZOTTI, “Computational simulations with low cell number for displacement hulls and planning boats: a rational approach”, *Proceeding of HYDRONAV 2014*, Wroclaw University of Technology, 2014

[27] AGRUSTA, BRUZZONE, ESPOSITO, “2ª Relazione semestrale attività di ricerca”, *Internal Report*, University of Genoa, 2013

[28] AGRUSTA, BRUZZONE, ESPOSITO, “3ª Relazione semestrale attività di ricerca”, *Internal Report*, University of Genoa, 2014

[29] TAHARA, WILSON, CARRICA, STERN, "RANS Simulation of a Container Ship Using a Single Phase Level Set Method with Overset Grids and Prognosis for Extensions to Self-Propulsion Simulator" *Journal Marine Science and Technology*, Vol. 11 No. 4, pp. 209–228, 2006.

[30] PENSA, “Test Report 118 – Carena 1113–SL42, *Towing Tank Tests Report*, University of Naples Federico II, 2012

[31] ZOTTI, “Risultati delle esperienze di rimorchio carena C12–448 – AP1–40”, *Towing Tank Tests Report*, University of Trieste, 2012

[32] ZOTTI, “Risultati delle esperienze di rimorchio carena C12–449 – AP2–40”, *Towing Tank Tests Report*, University of Trieste, 2012

[33] PENSA, “Test Report 105 – Carena 1100–SL36, *Towing Tank Tests Report*, University of Naples Federico II, 2011

[34] BAILEY: "The NPL High Speed Round Bilge Displacement Hull Series", *Maritime Technology Monograph*, n.4, RINA, 1976

[35] RADOJCJC, RODIC, KOSTIC: "Resistance and Trim Predictions for the NPL High Speed Round Bilge Displacement Hull Series", *International Symposium on Power, Performance and Operability of Small Craft*, RINA, 1997

[36] SAHOO, DOCTORS, RENILSON: "Theoretical and Experimental Investigation of Resistence of High-Speed Round-Bilge Hull Forms, *Proceedings of FAST99*, Seattle, 1999

[37] AGRUSTA, BRUZZONE, ESPOSITO, ZOTTI, "Comparison between RANS simulations with low number of cells and BEM analysi for a high speed trimaran hull", *Proceedings of HIPER 2014,* University of Athens, 2014

[38] BEGOVIC, BERTORELLO, BRUZZONE, CASSELLA, ZOTTI, "High Speed Trimarans Validations on Numerical Results by Geosim Tests", *Proc. Of the 6th International Conference on Fast Sea Transportation FAST 2001*, vol II, pp.285-294, Southapthon, 2001.

[39] BRUZZONE, CASSELLA, PENSA, SCAMARDELLA, ZOTTI, "On the Hydrodynamic Characteristics of a High Speed Catamaran with Round Bilge Hull: Wave Resistance and Wave Pattern Experimental Tests and Numerical Calculations", *Proceedings of FAST '97*, Sidney Australia, 1997.

[40] BRIZZOLARA, BRUZZONE, CASSELLA, SCAMARDELLA, ZOTTI, "Wave Resistance and Wave Patterns for High Speed Crafts. Validation of Numerical Results by Model Tests", *Proc. of 22nd Symposium of Naval Hydrodynamics*, pp.69-83, Washington D.C,1998.

[41] BRUZZONE, CASSELLA, COPPOLA, RUSSO KRAUSS, ZOTTI, "Power Prediction for High-Speed Catamarans from Analysis of Geosim Tests and from Numerical Results", *Proc. of the 5th International conference on Fast Sea Trasportation*, Seattle, 1999.

[42] CLEMENT, BLOUNT: "Resistance tests of systematic series of planing hull forms", *SNAME Transaction* n.71, 1963

[43] ZOTTI, "Risultati delle esperienze di rimorchio carena C11–440 – B42", *Towing Tank Tests Report*, University of Trieste, 2011

[44] NELDER, MEAD, "A Simplex method for function minimization". *Computer journal*, Vol.7, pp. 308-313, 1965.

[45] GOLDBERG, “Genetic Algorithms in Search, Optimization & Machine Learning”. Addison-Wesley, 1989.

[46] DEB, “Multi-Objective optimization using evolutionary algorithms”. John Wiley & Sons, Chichester, 2001.

[47] LAMPINEN, ZELINKA, “On stagnation of Differential Evolution algorithm”. *Proceedings of sixth international conference on soft computing*, pp. 76-83, Brno, Czech Republic, 2000.

[48] ROBIC, BOGDAN. “DEMO: Differential Evolution for Multi-objective Optimization”. *Report of Dept. of Intelligent Systems*, Jozef Stefan Institute, Slovenia.

[49] ABBASS, SARKER, “The Pareto Differential Evolution Algorithm”. *International Journal on Artificial Intelligence Tools*, World Scientific Publishing Company, Vol. 11(4), pp. 531-552, 2002.

[50] DEJHALLA, MRSA, VUKOIC, „Application of genetic algorithm for ship hull form optimization“, *International Shipbuilding Progress*, vol.48, pp.117-134, 2001

[51] BAGHERI, GHASSEMI, “Genetic algorithm applied to optimization of the ship hull form with respect to seakeeping performance”, *Transactions of Famena*, vol.XXXVIII-3, 2014

[52] MISHRA, “Performance of the Barter, the Differential Evolution and the Simulated Annealing Methods of Global Optimization on Some New and Some Old Test Functions”. *MPRA* Paper No. 639, 2006.

[53] “SHERPA – An Efficient and Robust Optimization/Search Algorithm”, Red Cedar Technology, WP1023, Rev 05.08

[54] LACKENBY, “On the Systematic Geometrical Variation of Ship Forms”. *Trans. INA*, Vol. 92, 1950, pp. 289-315.

[55] CD-Adapco (2014) Optimate User Guide, version 9.04.

[56] “Using Optimate with Star-Ccm+”, *Proc. Of Star SEA Conference 2012*, Singapore, 2012

[57] SAUNDERS, “Hydrodynamics in Ship Design”. SNAME, Vol.1, pp.326-327, 1957. 210

[58] EGGERS, SHARMA, WARD, “An Assessment of Some Experimental Methods for Determining the Wave making Characteristics of a Ship Form”. *Transaction SNAME*, Vol. 74, 1967, pp. 112-157.

[59] ZOTTI, “Risultati delle esperienze di rimorchio carena C454–14 – HPH24”, *Towing Tank Tests Report*, University of Trieste, 2011

[60] CIMOLIN, SERRA, VATTERONI, “Optimization of the hull resistance for the Azimut 95’ yacht with CFD”, *Proceedings Of HSMV*, Naples, 2014